Proceedings of the

2nd International Symposium on Vibrations of Continuous Systems

The Sunstar Hotel
Grindelwald, Switzerland
11-16 July 1999

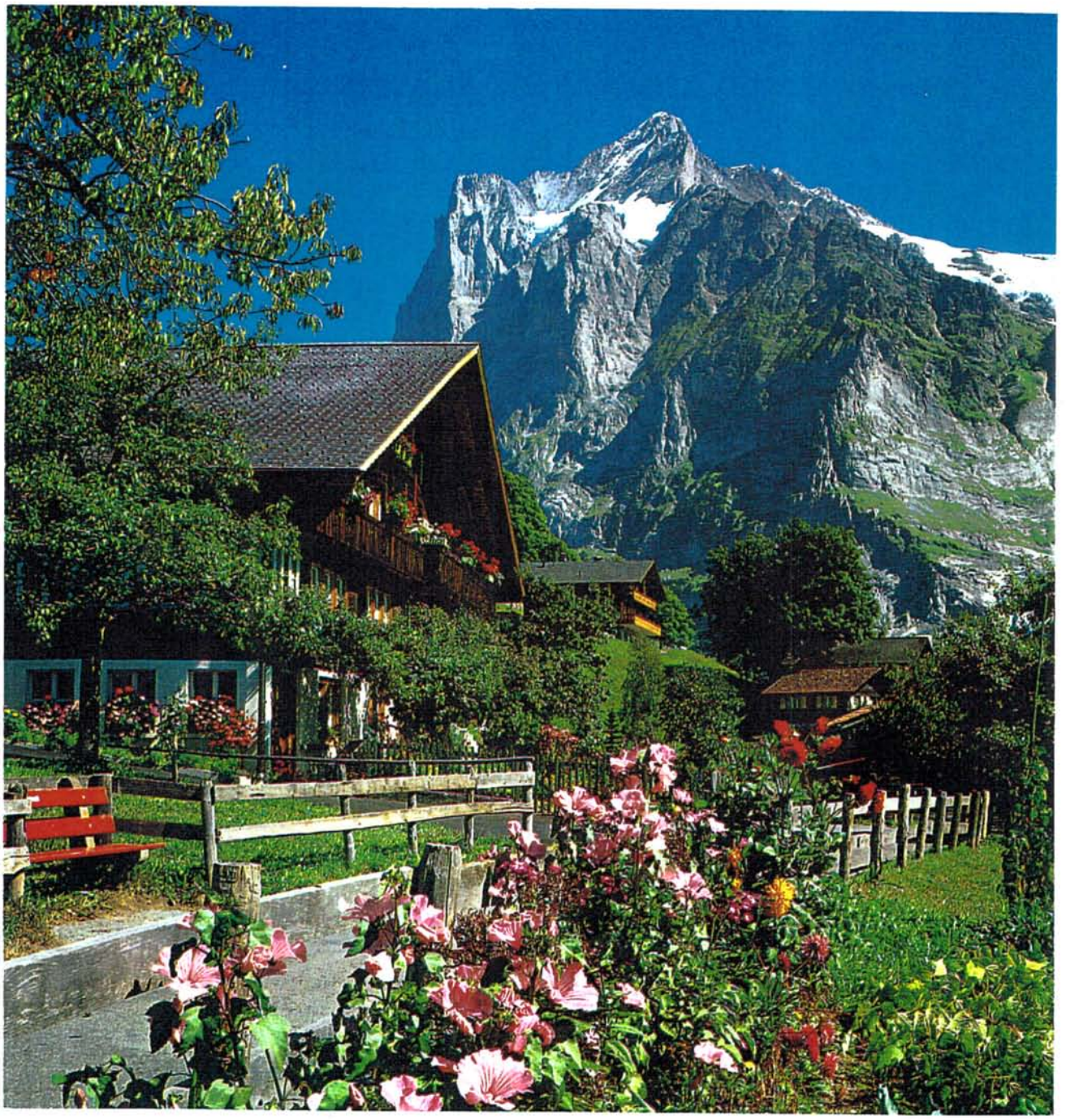

Preface

The International Symposium on Vibrations of Continuous Systems is a forum for leading researchers from across the globe to meet with their colleagues and present both old and new ideas on the field. Each participant has been encouraged to either present results of recent, significant research or to reflect on some aspect of the vibration of continuous systems ***which is particularly interesting, unexpected or unusual****. This latter type of presentation--of which there are several in the program--was proposed to encourage participants to draw on understanding obtained through--in many cases--decades of research.*

The location chosen for the 2nd Symposium is one of the most beautiful villages in Europe. Nestled in the Bernese Alps, Grindelwald offers spectacular views without even leaving the village. Because of the location, mornings of the Symposium have been kept free to permit hiking, sightseeing and mountain climbing.

This Proceedings contains short summaries of the presentations to be made at the Symposium. An accompanying addendum is a collection of short biographical sketches submitted by many of the participants.

Editor
Mark S. Ewing

Reviewing Editors
Charles W. Bert
Stuart M. Dickinson

General Chairman
Arthur W. Leissa

Contents

Contents

Contents

Controversial Aspects of Free Vibration of Shear-Deformable Beams

Charles W. Bert
School of Aerospace and Mechanical Engineering
The University of Oklahoma, Norman, OK 73019-0601

Introduction

The motivation for this paper was the recent work of Hutchinson[1] on circular plates. By comparison with an exact series solution, he showed that the appropriate value of the shear coefficient (K) in Mindlin plate theory depends not only on Poisson's ratio (ν) but also the vibration mode and the geometry (thickness-to-diameter ratio). The objective here is to study the various suggestions for K appropriate for a prismatic beam of solid rectangular cross section.

Theories for the Shear Coefficient

The first theory to include both transverse shear deformation and rotatory inertia was due to Bresse[2] in 1859. However, the concept of a shear coefficient was introduced by Timoshenko[3] in 1922. Originally[3] he proposed the value of 2/3, but one year later,[4] he proposed 0.889 based on Filon's photoelastic experiments.[5] Based on elementary shear theory, Goens[6] proposed 5/6 (≈ 0.833).

Apparently, the first to include the effect of Poisson's ratio on K was Olsson,[7] who obtained $K=(5/6)(1+\nu)/[1+(5/8)\nu]$. This can be generalized to $K=(5/6)(1+\nu)/(1+a\nu)$. Using static analysis, Cowper[8] and Kaneko[9] obtained $a=11/12$ and $5/6$, respectively.

Mindlin[10] developed two different dynamic expressions for K: an explicit one, $K=\pi^2/12\approx 0.822$, based on thickness-shear waves and an implicit one,

$$16(1-\alpha K)(1-K)=(2-K)^4,$$

based on short-wavelength flexural waves. Since K thus obtained did not depend on the aspect ratio (width/depth) of the cross section, the same value could be used for plates as well as beams. Later Mindlin found that the value of 0.822 agreed with experiments on quartz plates. Hutchinson[11] and Wittrick[12] independently obtained $K=5/(6-\nu)$. Kaneko[9] compared various predictions with experimental data for $0.13<\nu<0.38$ and found his expression ($a=5/6$) gave the best agreement. In a very important study, Hutchinson and Zillmer[13] used an exact series solution of the dynamic elasticity equations and worked backward to find K to match frequencies. The coefficient K thus obtained depended upon ν, mode number, and width/depth and depth/length ratios.

Since there is current interest in foam materials with negative Poisson's ratios, in Table 1, values of K are given for the entire theoretical range (-1 to $+0.5$) for isotropic materials.

Table 1. Values of shear coefficient K

		Poisson's ratio, ν				
Theory	Ref.	-1	-0.5	0	0.3	0.5
Olsson	7	0	0.606	0.833	0.912	0.952
Cowper	8	0	0.769	0.833	0.850	0.857
Kaneko	9	0	0.714	0.833	0.866	0.882
Mindlin (II)	10	0.475	0.600	0.764	0.860	0.913
Hutchinson	11	0.714	0.769	0.833	0.877	0.909

Jensen[14] concluded from an extensive finite-strip-method solution that if a consistent formulation for K as proposed by Cowper[8] or Stephen[15] is used, then very high accuracies in the natural frequencies can normally be expected even for wavelengths of the same magnitude as the transverse dimension of the beam. He also emphasized that no reduction in the moment of inertia due to shear lag effects must be included since this effect is implicitly included in consistent formulations of K.

Finally, it should be mentioned that equations alternative to the Timoshenko equations are the Love equations (Love[16] and Abramovich and Elishakoff[17]). Also, an extensive survey of Timoshenko beams was presented by Laura et al.[18]

The Second Frequency Spectrum

Although not discovered by Timoshenko himself,[3,4] a second frequency spectrum was implied in the work of Goens,[6] who obtained two solutions to the differential equations of motion, one involving both trigonometric and hyperbolic functions and the other just trigonometric functions, which suggested a change in vibration mode above a certain frequency. Anderson,[19] Traill-Nash and Collar,[20] and Dolph[21] interpreted the mode change as a second frequency spectrum. There was little or no mention of this second spectrum in experiments with the exception of the work of Barr[22] who noticed two frequencies with the same number of nodal points in vibration of free-free beams. Experimentally, Downs[23] found a deflectionless mode having the frequency $\omega = a(KG/\rho I)^{1/2}$, where $A \equiv$ area, $G \equiv$ shear modulus, $I \equiv$ area moment of inertia, and $\rho \equiv$ density. Strangely the very high K value of 1.04 was associated with the experiment.

Using a finite element model, Abbas and Thomas[24] explained the behavior of different frequency curves on the basis of coupling of various independent modes. They concluded that many of the earlier investigations were interpreted incorrectly and that there is no separate second frequency spectrum except in the case of a hinged-hinged beam. Further work in this area was undertaken by Bhashyam and Prathap,[25] Levinson and Cooke,[26] Stephen,[27] and Prathap.[28]

Higher-Order Theories

Due to the poor ability of the Timoshenko beam analysis (Cowper[29]) to predict moments and shear forces, and thus stresses, very accurately, several higher-order theories have been proposed. Two-parameter theories were introduced by Aalami and Atzori[30] and by Stephen and Levinson.[31] Other higher-order theories were presented by Levinson,[32] Bickford,[33] Heyliger and Reddy,[34] Leung,[35] and Senthilnathan and Lee.[36] Since the shear stress distribution at high frequencies (wave length $\approx$ beam depth) is not parabolic (Prescott[37]), even the higher-order theories are very inaccurate in this instance.

References

1 Hutchinson, J.R., *Proc., Int. Sympos. Vibration of Continuous Systems*, Estes Park, CO, 1997, 24-26.

2 Bresse, J.A.C., *Cours de Mécanique Appliquée*, Mallet-Bachelor, Paris, 1859.

3 Timoshenko, S.P., *Phil. Mag.*, ser. 6, 41, 742-746 (1921).

4 Timoshenko, S.P., *Phil. Mag.*, ser. 6, 42, 125-131 (1922).

5 Filon, L.N.G., *Phil. Mag.*, ser. 6, 23, 1-25 (1912).

6 Goens, E., *Annalen Phys.*, 11, 649-678 (1931).

7 Olsson, R.G., *ZAMM*, 15, 245 (1935).

8 Cowper, G.R., *ASME J. Appl. Mech.*, 33, 335-340 (1966).

9 Kaneko, T., *J. Phys.*, ser. D, 8, 1927-1936 (1975).

10 Mindlin, R.D., *ASME J. Appl. Mech.*, 18, 31-38 (1951).

11 Hutchinson, J.R., *ASME J. Appl Mech.*, 51, 581-585 (1984).

12 Wittrick, W.H., *Int. J. Solids Structures*, 23, 441-464 (1989).

13 Hutchinson, J.R. and Zillmer, S.D., *ASME J. Appl. Mech.*, 53, 39-44 (1986).

14 Jensen, J.J., Danish Center for Appl. Math & Mech., Rept. No. 238 (1982).

15 Stephen, N.G., *Int. J. Solids Structures*, 17, 325-333 (1981).
16 Love, A.E.H., *A Treatise on the Mathematical Theory of Elasticity*, 4th. ed., Dover, NY (1944). See pp. 430-431.
17 Abramovich, H. and Elishakoff, I., *J. Sound Vib.*, 137, 516-522 (1990).
18 Laura, P.A.A., Maurizi, M.J., and Rossi, R.E., *Shock Vib. Digest*, 22 (11), 3-10 (1990).
19 Anderson, R.A., *ASME J. Appl. Mech.*, 20, 504-510 (1953).
20 Traill-Nash, P.W. and Collar, A.R., *Quart. J. Mech. Appl. Math.*, 6, 186-222 (1953).
21 Dolph, C., *Q. Appl. Math.*, 12, 175-187 (1954).
22 Barr, A.D.S., *Proc., 9th Int. Cong. Appl. Mech.*, 7, 448-458 (1956).
23 Downs, B., *ASME J. Appl. Mech.*, 43, 671-673 (1976).
24 Abbas, B.A.H., and Thomas, J., *J. Sound Vib.*, 51, 123-137 (1977).
25 Bhashyam, G.R. and Prathap, G., *J. Sound Vib.*, 76, 407-420 (1981).
26 Levinson, M. and Cooke, D.W., *J. Sound Vib.*, 84, 319-326 (1982).
27 Stephen, N.G., *J. Sound Vib.*, 80, 578-582 (1982).
28 Prathap, G., *J. Sound Vib.*, 90, 443-445 (1983).
29 Cowper, G.R., *J. Eng. Mech. Div., Proc. ASCE*, 94, 1447-1453 (1968).
30 Aalami, B. and Atzori, B., *AIAA J.*, 12, 679-685 (1974).
31 Stephen, N.G. and Levinson, M., *J. Sound Vib.*, 67, 293-305 (1979).
32 Levinson, M., *J. Sound Vib.*, 74, 81-87 (1981).
33 Bickford, W.B., *Developments in Theoretical and Applied Mechanics*, 11, 137-150 (1982).
34 Heyliger, P.R. and Reddy, J.N., *J. Sound Vib.*, 126, 309-326 (1988).
35 Leung, A.Y.T., *J. Sound Vib.*, 142, 527-528 (1990).
36 Senthilnathan, N.R. and Lee, K.H., *ASME J. Vib. Acoustics*, 114, 495-497 (1992).
37 Prescott, J., *Phil. Mag.*, ser. 7, 33, 703-754 (1942).

VIBRATION OF STRUCTURES USING BOUNDARY CHARACTERISTIC ORTHOGONAL POLYNOMIALS IN THE RAYLEIGH-RITZ METHOD

R.B. Bhat
Professor of Mechanical Engineering
Concordia University, Montreal, Canada

Vibration of plate type structures of various configurations and boundary conditions have been extensively studied over the past several years. Excellent reviews of such studies are available in Leissa (1969, 1977, 1981, 1987). Closed form solutions are available for some simple cases and boundary conditions in Timoshenko and Woinowsky (1959), Gorman (1975, 1982), Soedel (1981), Meirovitch (1967, 1986).

The Rayleigh-Ritz method is a very powerful technique that has been used by various researchers to predict the natural frequencies and mode shapes of vibrating structures, Leissa (1969). The method requires a linear combination of assumed deflection shapes that individually satisfy at least the geometrical boundary conditions. Expressions for the maximum kinetic and potential energies are obtained in terms of the arbitrary constants in the deflection expression. By equating the maximum potential and kinetic energies an expression for the natural frequency can be formed. Applying the condition of stationarity of natural frequencies at the natural modes, the variation of natural frequencies with respect to the arbitrary constants is equated to zero to obtain an eigenvalue problem. Solution of this eigenvalue problem provides the natural frequencies and mode shapes.

One Dimensional Boundary Characteristic Orthogonal Polynomials(BCOP) :

The BCOP were first proposed by Bhat (1985) to study vibration of rectangular plates in the Rayleigh-Ritz method. The first member of the BCOP set is constructed so as to satisfy all the boundary conditions, both geometric and natural. The higher members of the set $\{\phi_k(x)\}$ are then constructed using the well-known three term recurrence relation as given in Chihara (1978) as,

$$\phi_{k+1}(x) = (d_k x + e_k)\phi_k(x) + p_k \phi_{k-1}(x), \quad k = 0,1,2,.., \tag{1}$$

where the coefficients $d_k, e_k, p_k,\ k = 0,1,2,...$ can be found out using the orthogonality property. It can be easily verified that the higher members of the set satisfy the geometrical boundary conditions. The method is described in the Appendix of Bhat (1985) for a rectangular plate with four types of boundary conditions at the edges. After the publication of this paper a series of research work has been done using this method to analyze vibration problems of various types of structural members with variety of conditions and applications.

Two Dimensional BCOP :

As proposed by Bhat (1987), the two dimensional orthogonal polynomials were constructed by orthogonalizing the k-th polynomial with all the (k-1) polynomials previously constructed, unlike the one dimensional BCOP where a three term recurrence

relation is available to generate them. Very recently Bhat et al. (1998) have proposed a recurrence scheme for the generation of two dimensional BCOP involving three classes of polynomials. The polynomials are first organised into following classes forming a pyramid given by

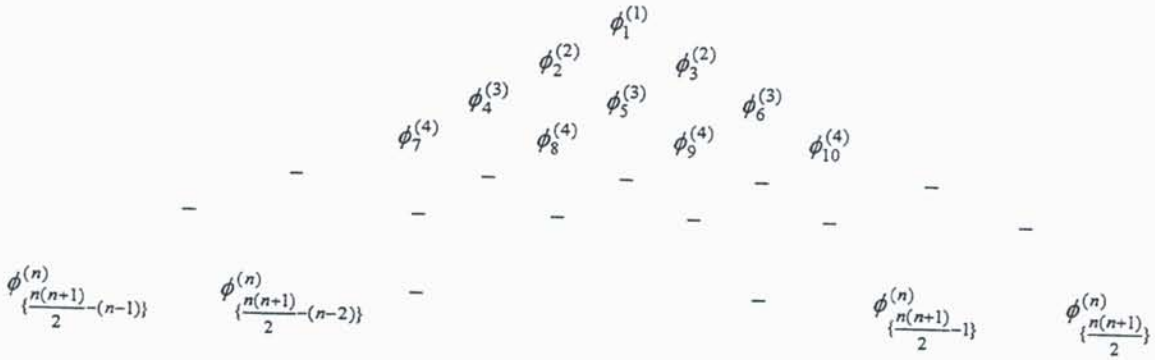

where, superscript in $\phi_i^{(j)}$ denotes the class number j to which it belongs.

Now, in general, class j will have j orthogonal polynomials, and those can be generated by the recurrence scheme given by Bhat et al. (1998).

Condensation in Rayleigh-Ritz Method :

A mass condensation scheme is proposed here in order to reduce the order of the eigenvalue problem in the Rayleigh-Ritz method,

$$(-\omega^2 M + K)_{n\times n}\{C\} = \{0\}, \tag{2}$$

Identifying the required order of eigenvalue problem as mxm, m<n, it is possible to express the M and K matrices as

$$[A]_{n\times n} = \begin{bmatrix} A_{m\times m} & A_{m\times(n-m)} \\ A_{(n-m)\times m} & A_{(n-m)\times(n-m)} \end{bmatrix} \tag{3}$$

with $$\{C\} = \begin{Bmatrix} C_m \\ C_{(n-m)} \end{Bmatrix} = \begin{Bmatrix} a \\ b \end{Bmatrix}, \text{ say.}$$

The condensation is done from (2) and (3) as follows,

$$\begin{bmatrix} (K_{11} - \omega^2 M_{11}) & (K_{12} - \omega^2 M_{12}) \\ (K_{21} - \omega^2 M_{21}) & (K_{22} - \omega^2 M_{22}) \end{bmatrix} \begin{Bmatrix} a \\ b \end{Bmatrix} = \begin{Bmatrix} 0 \\ 0 \end{Bmatrix} \tag{4}$$

Ignoring the inertia terms in the second row of equations

$$\{b\} = [K_{22}^{-1} K_{21}]\{a\},$$

$$\{C\} = \begin{Bmatrix} 1 \\ K_{22}{}^{-1} K_{21} \end{Bmatrix} \{a\}$$

Finally we have the mxm condensed eigenvalue problem,

$$\begin{Bmatrix} 1 \\ K_{22}{}^{-1} K_{21} \end{Bmatrix}^T [K - \omega^2 M] \begin{Bmatrix} 1 \\ K_{22}{}^{-1} K_{21} \end{Bmatrix} = \{0\} \qquad (5)$$

Example : Consider a cantilever beam with 2 term shape functions in the form of two BCOP given by $\phi_1 = x^2$ and $\phi_2 = 5x^2 - 6x^3$. With only one term we get $\omega_1 = 4.4721$. If two terms are considered then we have $\omega_1 = 3.5331$ and $\omega_2 = 34.443$. Using the present Condensation scheme and reducing it to a single coordinate, we have $\omega_1 = 3.5328$.

References :

1. Leissa A.W., 1969, *Vibration of Plates,* NASA SP160, Washington, D.C. : U.S. Government Printing Office.
2. Leissa A.W., 1977, "Recent Research in Plate Vibrations, 1973-1976 : Classical Theory," Shock and Vibration Digest, Vol. 9, No. 10, 13-24.
3. Leissa A.W., 1981, "Plate Vibration Research 1976-1980 : Classical Theory," Shock and Vibration Digest, Vol. 13, No.9, 11-22.
4. Leissa A.W., 1987, "Recent Studies in Plate Vibrations : 1981-1985, Part I, Classical Theory," Shock and Vibration Digest, Vol. 19, No.2, 11-18.
5. Timoshenko S. and Woinowsky K.S., 1959, *Theory of Plates and Shells*, McGraw-Hill Book Co., Inc., New York.
6. Gorman D.J., 1975, *Free Vibration Analysis of Beams and Shafts*, New York, John Wiley.
7. Gorman D.J., 1982, *Free Vibration Analysis of Rectangular Plates*, Amsterdam : Elsevier, North-Holland.
8. Soedel W., 1993, *Vibration of Shells and Plates*, Marcel Dekker, Hong Kong.
9. Meirovitch L., 1967, *Analytical Methods in Vibrations*, Mcmillon Co., New York.
10. Meirovitch L., 1986, *Elements of Vibration Analysis*, McGraw-Hill Book Co., 2nd Ed., New York.
11. Bhat R. B., 1985, "Natural Frequencies of Rectangular Plates Using Characteristic Orthogonal Polynomials in Rayleigh-Ritz Method," J. Sound and Vib., Vol. 102, No. 4, 493-499.
12. Bhat R. B., 1987, "Flexural Vibration of Polygonal Plates Using Characteristic Orthogonal Polynomials in Two Variables," J. Sound and Vib. Vol 114, No.165-71.
13. Bhat R.B., Chakraverty S. and Stiharu I., 1998, "Recurrence Scheme for the Generation of Two Dimensional Boundary Characteristic Orthogonal Polynomials to Study Vibration of Plates," J. Sound and Vib., Vol. 216, No.2, 321-327.

VIBROACOUSTIC MODELLING OF A SIMPLIFIED FUSELAGE

L. Cheng and J. Missaoui
Department of Mechanical Engineering, Laval University, Quebec, Canada, G1K 7P4

1. Simulation Model

Structures based on cylindrical shell have been widely used as a simplified aircraft fuselage model to understand the fundamental phenomena either on the dynamic behavior or the noise transmission into the fuselage cabin. A more realistic model requires the consideration of the floor. Compared to the cylindrical shells, the addition of the floor introduces more complex mechanical coupling. On top of this, the acoustic space inside the cabin no longer has a simple regular cylindrical shape. Due to both structural and acoustic modifications, most methods based on modal decompositions can no longer be used. More powerful and efficient simulation models must therefore be developed and aimed to give some physical insight into the system and to offer a flexibility in the design process. This paper summarizes our research work in this filed over the past few years.

A structural model has been developed on the free and forced vibrations of a shell-floor system as shown in Figure 1. The mechanical coupling between sub-structures was modelled using artificial springs. A virtual set of distributed spring system is introduced at the structural junction for every permitted degree of freedom. Physically, by allowing different values of the spring stiffness, various connections can be simulated. Mathematically, the use of artificial springs at the junctions replaces the geometrical conditions (continuity of the motion) by corresponding dynamic conditions (strain energy of the springs). As a result, the choice of the trial functions is simplified, since the later has only to verify the geometrical boundary conditions at the non-connected regions. The whole system is characterized using the classical Hamilton's principle, which needs the calculation of the kinetic and the strain energies of the combined system, as well as the work done by the external driving forces. The resulting Hamiltonian is then substituted into the Lagrange's equations to yield the governing equations of motion.

As far as acoustic modelling is concerned, an Integro-Modal approach for computing the acoustic properties of cavities of arbitrary shape has been developed. The approach was based on a discretization of the total cavity into mixed sub-cavities of either regular or irregular shape, interconnected by virtual elastic membranes. As illustrated in Figure 2, the cavity investigated can be divided into a regular (Figure 2(b)) and an irregular (Figure 2(c)) sub-cavities. The junction between the two sub-cavities is replaced by a vibrating membrane. Continuity of both the pressure and the pressure gradient at the boundaries of the interconnected regions was ensured by considering membranes with zero mass and stiffness. The modal characteristics of regular sub-cavities are obtained analytically while the irregular sub-cavities are treated using a modal expansion over the mode shapes of their regular bounding cavities. The internal pressure in each sub-cavity is obtained by using a modal basis of the bounding sub-cavity or envelope.

A complete vibroacoustic formulation of the shell-floor-cavity configuration has then been carried out by coupling the structural and acoustical models. Firstly, the cavity of the shell-floor system is discretized into N sub-cavities, the Integro-Modal solution is obtained using either a direct method (requiring no calculation of the acoustic modes of the real cavity) or an indirect one (with modal synthesis of the real cavity). With the last method, the system to be solved is of reduced size, since modal characteristics of the whole cavity (natural frequency, generalized mass and mode shape) should

be calculated a priori using the Integro-modal approach. Secondly, the vibroacoustic parameters are chosen to characterize the structural and acoustical responses of the system. In fact, at each excitation frequency, the motion of each sub-structure is characterized by the quadratic velocity for the shell and the floor. For the cavity, an average quadratic pressure is defined to quantify the noise level.

2. Structural-acoustic analysis

Various shell-floor connections are firstly simulated. The comparison with other available approaches shows that, with the proper assignation to the spring stiffness, the formulation allows an accurate simulation of the rigid attachment using high values of spring stiffnesses. A modal analysis shows three types of modes: floor dominated, shell dominated and coupled modes in which the two sub-structures vibrate with comparable levels. As far as the effect of the spring stiffness in different directions is concerned, the mode is most sensitive to the direction in which the impedance mismatch is most strong between the shell and the floor. The in-plane motion of the floor seems to be negligible for lower-order modes, except for antisymmetric ones which include the horizontal rigid body motion. At low and middle frequency range, the floor is strongly coupled to the shell with comparable vibration level. With the increase of the frequency, the coupling is weaken and the shell which is directly excited is more active than the floor.

The Integro-Modal formulation is shown to be general and flexible enough to handle different cavity configurations and can be easily extended to a vibroacoustic study. The proposed formulation permits the use of irregular-shaped sub-cavities, thus making the approach more powerful using fewer number of sub-cavities. Efficiency and the accuracy of the approach have been demonstrated by comparison with results presented in the literature.

The previously established methods (Artificial Spring technique and the Integro-Modal approach) were finally combined into a complete vibroacoustic model. Experiments were carried out to assess the established model. Although further improvements are still needed, numerical predictions seem to agree reasonably well with experimental data (Figure 3 to Figure 6). Numerical analyzes were performed to highlight the structural (Figure 7) and acoustic effects (Figure 8) of the floor on the sound field. It was noted that in any case, shell vibration plays an important role in the sound radiation into the cavity. When the excitation is applied to the shell, the floor becomes a very weak sound radiator. In this case, the effect of the floor is limited to a change in the shape of the cylindrical acoustic cavity, leading to significant differences in terms of sound level compared to what would have been predicted using a purely cylindrical shell configuration. Using the present configuration, analyzes of the modal radiation efficiency (Figure 9) were also performed and revealed a possible cancellation process between cells of opposite phase in circumferential direction (Figure 10).

3. Conclusion

Theoretical and numerical study of structural, acoustic and vibroacoustic behavior of a shell-floor-cavity system have been presented. The validation of the vibroacoustic model was achieved by comparison with laboratory experimentations. Vibro-acoustic parameters have been used to discuss the acoustic, structural effects of the cabin floor and joint condition on the noise level. The proposed model seems to be powerful and accurate enough to simulate most dominate phenomena encountered in such structure.

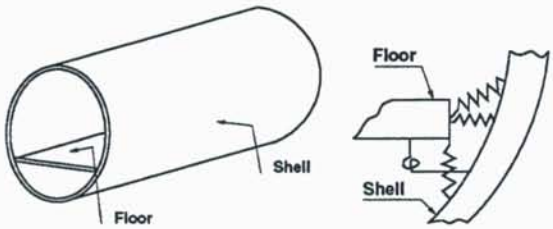

Fig. 1: Shell-floor configuration

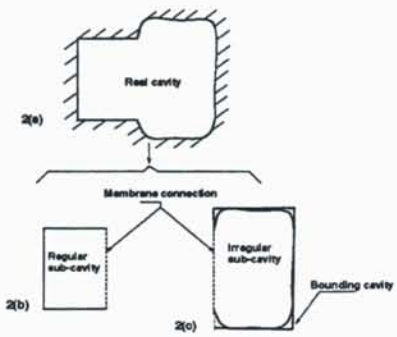

Fig. 2: Discretization procedure

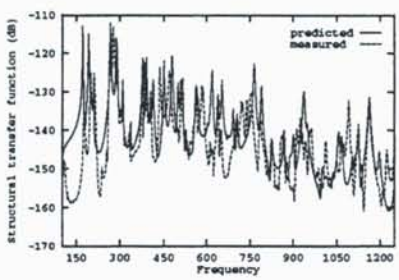

Fig. 3: Structural responses in narrow band

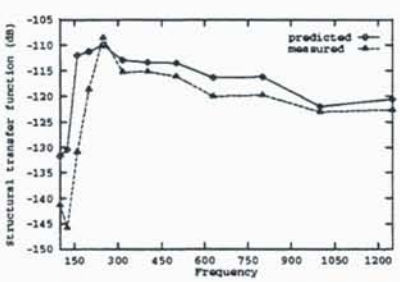

Fig. 4: Structural responses in third octave band

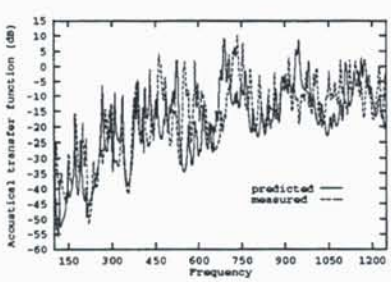

Fig. 5: Acoustical responses in narrow band

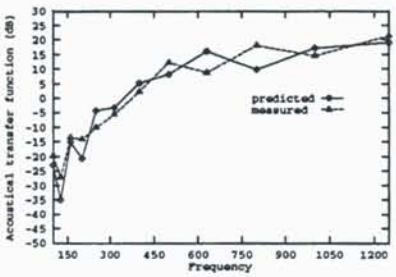

Fig. 6: Acoustical responses in third octave band

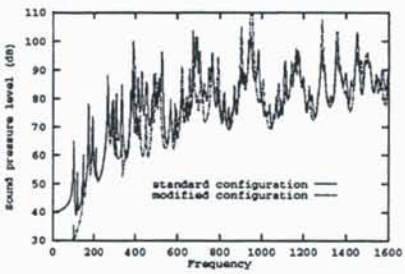

Fig. 7: Structural effects of the floor

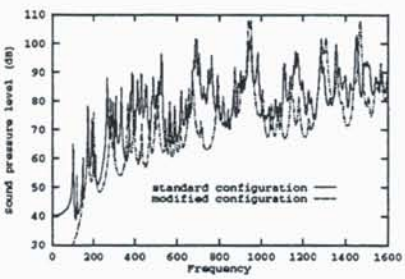

Fig. 8: Acoustic effects of the floor

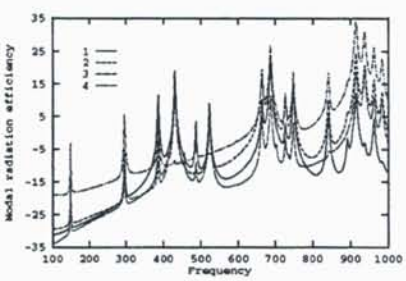

Fig. 9: Modal radiation efficiency

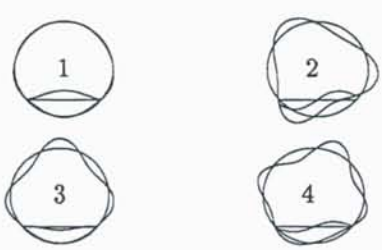

Fig. 10: Mode shapes of the selected structural modes

Limit Cycle Oscillations Of Delta Wing Models In Low Subsonic Flow

Deman Tang, James K. Henry and Earl H. Dowell
Duke University, Durham

A nonlinear, aeroelastic analysis of a low aspect, delta wing modeled as a plate of constant thickness demonstrates that limit cycle oscillations (LCO) of the order of the plate thickness are possible. The structural nonlinearity arises from double bending in both the chordwise and spanwise directions. The present results using a vortex lattice aerodynamic model for a low Mach number flow complement earlier studies for rectangular wing platforms that showed similar qualitative results. The theoretical results for the flutter boundary (beyond which LCO occurs) have been validated by comparison to the experimental data reported by other investigators for low aspect ratio delta wings. Also the limit cycle oscillations found experimentally by previous investigators (but not previously quantified prior to the present work) are consistent with the theoretical results reported here. Reduced order aerodynamic and structural models are used to substantially decrease computational cost with no loss in accuracy. Without the use of reduced order models, calculations of the LCO would be impractical. A wind tunnel model is tested to provide a quantitative experimental correlation with the theoretical results for the LCO response itself.

Linear and nonlinear aeroelastic responses of panels or plates with fixed supports on all four sides have been studied for many years from subsonic to supersonic flow, see Ref. [1] and [2]. More recently plates with free edges have been studied and these results (Ref.[3]-[4]) have provided good physical understanding of the flutter and limit cycle oscillation characteristics for such plates in a high Mach number supersonic flow. In particular, it has been demonstrated that even with only a single edge of a plate restrained, bending tension or geometrical nonlinearities can produce limit cycle oscillation amplitudes of the order of the plate thickness. For low subsonic flow speeds Ref. [5] used a three-dimensional time doman vortex lattice aerodynamic model and reduced order aerodynamic technique [6], [7] to investigate the flutter and limit cycle oscillation characteristics of a cantilevered low aspect ratio, rectangular wing-panel structure. Again limit cycle oscillations were found.

Following the work of Ref. [5], in the present paper we also use the vortex lattice aerodynamic model to investigate the flutter and limit cycle oscillation characteristics of a low aspect ratio delta wing structure at low subsonic flow speeds. The theoretical results are consistent with the experimental results of Doggett and Solstmann [8] who previously studied the flutter of low aspect ratio delta wings.

In order to validate the theoretically predicted limit cycle oscillation characteristics of the delta wing, an experimental investigation has been carried out in the Duke wind tunnel using an Ometron VPI 4000 Scanning Laser Vibrometer system [11] to measure deflections (velocities) of the delta wing. The VPI sensor is a non-contacting transducer that uses optical interferometry and electronic frequency measurements to determine the frequency shift of a beam of light reflected from a moving surface.

Theoretical and experimental results show good agreement. The present results suggest a new approach to retaining structural integrity of flexible wings in a post-flutter environment.

REFERENCES

1) Dowell, E.H., "Aeroelasticity of Plates and Shells", Kluwer Publishing, 1975.

2) Ricketts, R.H., Noll, T.E., Whitlow Jr., W., and Huttsell, L.J., "An Overview Of Aeroelasticity Studies For The National Aero-Space Plane", Proceedings of the AIAA/ASME/ASCE/AHS/ASC 34th Structures, Structural Dynamics and Materials Conference, April, 1993, pp. 152-162.

3) Hopkins, M.A. and Dowell, E.H., "Limited Amplitude Panel Flutter With A Temperature Differential", Proceedings of the AIAA/ASME/ASCE/AHS/ASC 35th Structures, Structural Dynamics and Materials Conference, April, 1994.

4) Weiliang, Y. and Dowell, E.H., "Limit Cycle Oscillation Of A Fluttering Cantilever Plate", AIAA Journal, Vol. 29, No. 11, 1991, pp. 1929-1936.

5) Tang, D.M., Dowell, E.H., and Hall, K.C., "Limit Cycle Oscillations Of A Cantilevered Wing In Low Subsonic Flow", submitted for publication to the AIAA Journal.

6) Hall, K.C. "Eigenanalysis Of Unsteady Flows About Airfoils, Cascades and Wings", AIAA Journal, Vol. 32, No. 12, 1994, pp. 2426-2432.

7) Dowell, E.H., "Eigenmode Analysis In Unsteady Aerodynamics: Reduced Order Models", AIAA Journal, Vol 34, No. 8, 1996, pp. 1578-1588.

8) Doggett, R.V. and Solstmann, D.L., "Some Low-Speed Flutter Characteristics Of Simple Low-Aspect-Ratio Delta Wing Models", NASA TM 101547, January, 1989.

9) Florea, R. and Hall, K.C., "Reduced Order Modeling Of Unsteady Flows About Airfoils", Presented at the Symposium On Aeroelasticity And Fluid/Structure Interaction ASME Winter Annual Meeting, Chicago, November, 1994.

10) Wilson, E.L., "Structural Analysis Programs 90, Version 5.10, Reference Manual", Computers and Structures, Inc., Berkeley, CA 1983.

11) Ometron, "VPI 4000 Scanning Laser Vibrometer Operator's Manual", 1997.

Dynamic Stiffness Matrix for High Order Beam Theory Vibration Analysis

Moshe Eisenberger
Faculty of Civil Engineering
Technion - Israel Intitute of Technology
Technion City 32000
Israel

May 16, 1999

Abstract

The analysis of beams has been performed over the years mostly using the Bernoulli-Euler beam theory. This theory is based on the assumption that plane sections of the cross section remain plane and perpendicular to the beam axis. A more refined beam theory is the Timoshenko beam theory which relaxes the restriction on the angle of shearing deformations that exist in the simpler theory. In recent years, due to the increase in the use of composite materials the shear deformation theory has been limited in the accuracy of computation for many situations, and although some remedies were devised, locking in the numerical analysis has become a main issue and higher order theories have emerged.

In these theories, the restriction on the warping of the cross section is relaxed, and allow variation in the longitudinal direction of the beam which is cubic. This results, for homogenous materials in the following set of equations:

$$u(x,t) = u_0(x,t) + z\left[\phi(x,t) - \frac{4}{3}\left(\frac{z}{h}\right)^2\left(\phi(x,t) + \frac{\partial w(x,t)}{\partial x}\right)\right] \tag{1}$$

$$w(x,t) = w_0(x,t) \tag{2}$$

where $u_0(x,t)$ and $w_0(x,t)$ are the axial and lateral displacements of the beam centerline, $\phi(x,t)$ represents the rotation of a normal to the axis of the beam, and h is the depth of the beam.

Using this displacement field we arrive at the equilibrium equations for a beam segment as

$$\frac{8GA}{15}\left(\frac{\partial\,\phi}{\partial x}+\frac{\partial^2 w}{\partial x^2}\right)-\frac{EI}{21}\frac{\partial^4 w}{\partial x^4}+\frac{16EI}{105}\frac{\partial^3\,\phi}{\partial x^3}=\rho A\frac{\partial^2 w}{\partial t^2}-\frac{\rho I}{21}\frac{\partial^4 w}{\partial x^2\partial t^2}-\frac{16\rho I}{105}\frac{\partial^3\,\phi}{\partial x\partial t^2} \tag{3}$$

$$-\frac{68EI}{105}\frac{\partial^2\,\phi}{\partial x^2}+\frac{16EI}{105}\frac{\partial^3 w}{\partial x^3}+\frac{8GA}{15}\left(\phi+\frac{\partial\,w}{\partial x}\right)=-\frac{68\rho I}{105}\frac{\partial^2\,\phi}{\partial t^2}+\frac{16\rho I}{105}\frac{\partial^3 w}{\partial x\partial t^2} \tag{4}$$

For the derivation of the stiffness matrix the right hand side of the above equations is taken as zero, i.e. static case. If one uses the exact solution of the differential equations as the shape functions, the resulting stiffness matrix is exact. The solution of these coupled differential equations is given in terms of six constants as

$$w(x)=C_1+C_2\,x+C_3\,x^2+C_4\,x^3+C_5\,[cosh(\alpha x)+sinh(\alpha x)]+C_6\,[cosh(\alpha x)-sinh(\alpha x)] \tag{5}$$

$$\begin{aligned}\phi(x) \;=\; & -\frac{9\,C_4\,EI+GA\,C_2}{GA}-2\,C_3\,x-3\,C_4\,x^2+\frac{1}{4}\,C_5\,\alpha\,[cosh(\alpha x)+sinh(\alpha x)]\\ & -\frac{1}{4}\,C_6\,\alpha\,[cosh(\alpha x)-sinh(\alpha x)]\end{aligned} \tag{6}$$

with

$$\alpha=\sqrt{70}\sqrt{\frac{GA}{EI}} \tag{7}$$

Applying the appropriate boundary conditions we can derive the dynamic shape functions for this beam model, and then the exact terms in the dynamic stiffness matrix, which are frequency dependent. Once all the stifness terms are known, the natural frequencies are found as the values of the frequency that cause the matrix to become singular.

The results of this analysis are compared with the results from the Bernoulli-Euler and Timoshenko beam theories and special attention will be devoted to the shear modes of vibration, also known as the second frequency spectra for Timoshenko beams.

A STUDY OF MULTI-SPAN BRIDGE DECK FREE VIBRATION BY THE METHOD OF SUPERPOSITION

by

D. J. Gorman
Dept. of Mechanical Engineering
University of Ottawa, Canada

and

Luigi Garibaldi
Dipartimento di Meccanica
Politecnico di Torino, Italy

1.Introduction

An ongoing study of the dynamic behaviour of multi-span bridges is being conducted by the second author and his colleagues at the Dipartmento di Meccanica of the Politecnico di Torino in Italy. Ultimate goals are to predict bridge response to travelling loads, etc., but as a first step it is required to obtain highly accurate solutions for the bridge deck natural frequencies and mode shapes. Accuracy is particularly important, not only because these mode shapes are utilised in the modal analysis of bridge behaviour, but it is found that some frequencies are very close to each other. Furthermore, since experimental measurements are taken along the edges of the bridge deck, and several modes may be excited, accurate mode shapes and natural frequencies must be known in order to correctly interpret these experimental measurements.

At the suggestion of the second author an analysis of multi-span continuous isotropic plate free vibration has been initiated utilising the superposition method. In fact, two quite different approaches are described. Excellent agreement between results obtained by the two approaches has been obtained.

2.The Multi-Span Approach

For illustrative purposes we have chosen to analyse the triple span bridge deck as shown schematically in figure 1. The letter "F" in the figure indicates free edges. Other external edges are given simple support with essentially simple line support being provided at the span interfaces over which the main plate passes continuously.

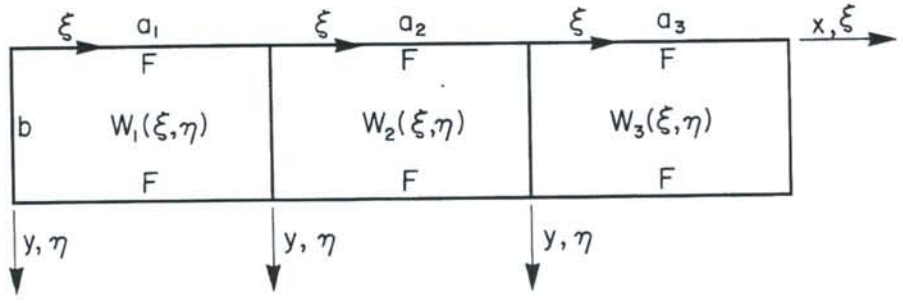

Fig 1. Triple Span Bridge Deck.

In order to conduct a free vibration analysis of the system by the superposition method a set of building blocks (forced vibration solutions) are assigned to each span. Assigned to the first span are the building blocks of figure 2.

The first building block has simple support along its opposite non-driven edges. The other non-driven edge is given slip-shear support, i.e, vertical edge reaction and slope are zero along this edge. Vertical edge reaction is also zero along the driven edge. This edge is driven by a distributed harmonic edge rotation.

A levy type solution for the first building block is expressed as,

$$W(\xi,\eta) = \sum_{m=1,2}^{\infty} Y_m(\eta)\sin(m\pi\xi) \qquad (1)$$

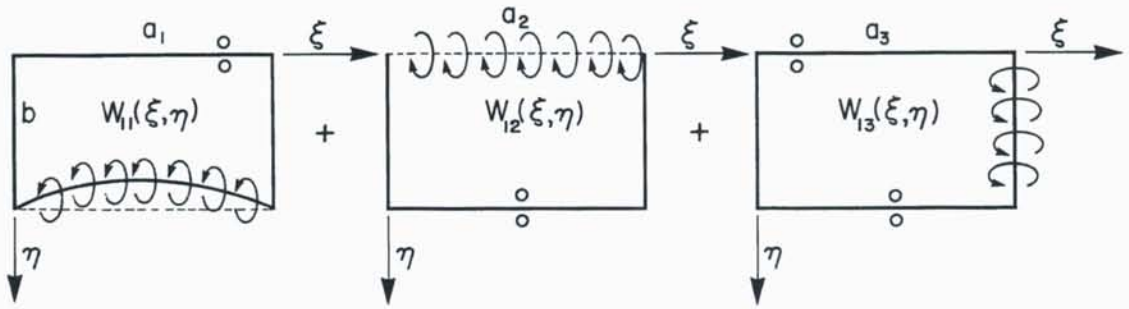

Fig 2. First Span Building Blocks.

Substituting into the governing differential equation, and separating the variables, we obtain a fourth order ordinary homogeneous differential equation governing the functions $Y_m(\eta)$.

The series on the right below represents the spatial distribution of the imposed edge rotation.

$$\frac{\partial W(\xi,\eta)}{\partial \eta}\Big|_{\eta=1} = \sum_{m=1,2}^{\infty} E_m \sin(m\pi\xi) \qquad (2)$$

An exact solution is available for response of the first building block. The response of the second building block is easily extracted from that of the first.

The third building block has slip-shear conditions imposed along its two opposite non-driven edges, the other non-driven edge being given simple support. Lateral displacement is forbidden along the driven edge which is subjected to a harmonic moment represented by a cosine series. A solution for

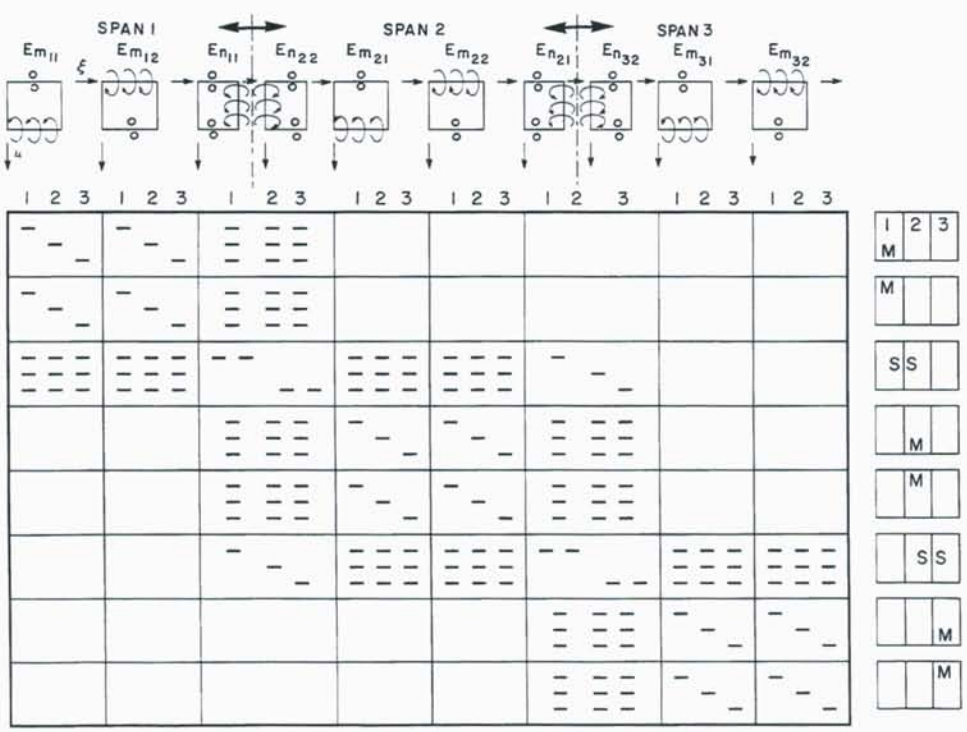

Fig 3. Schematic Representation of Eigenvalue Matrix.

response of this building block is obtained in manner identical to that described for the first. These are the only types of building blocks utilised in the entire analysis.

3.Development of Eigenvalue Matrix

A schematic representation of the eigenvalue matrix is presented in figure 3. The three groups of building blocks employed for the three spans are shown along the top of the figure. We note that four building blocks are assigned to the central span. Even though ten building blocks are shown the two adjacent building blocks at each inter-span location are not independent. This is because of moment continuity. Utilizing Fourier expansions we constrain the driving coefficients so as to satisfy boundary and continuity conditions.

4.Analysis By Means of Single Rectangular Plate Resting on line Supports

An alternate approach to the above problem is to consider the overall plate system of figure 1. as a single plate with the two long edges free, the other two being given simple support. We then analyse plate behaviour subject to the condition that two distributed harmonic line forces act in the region of interior bridge support. We require, of course, that there should be zero net lateral displacement along the lines of these distributed forces.

The entire analysis of the three span bridge is conducted with the two building blocks shown in figure 4, coupled with the first two of the previous analysis, whose aspect ratio, b/a, will now be different.

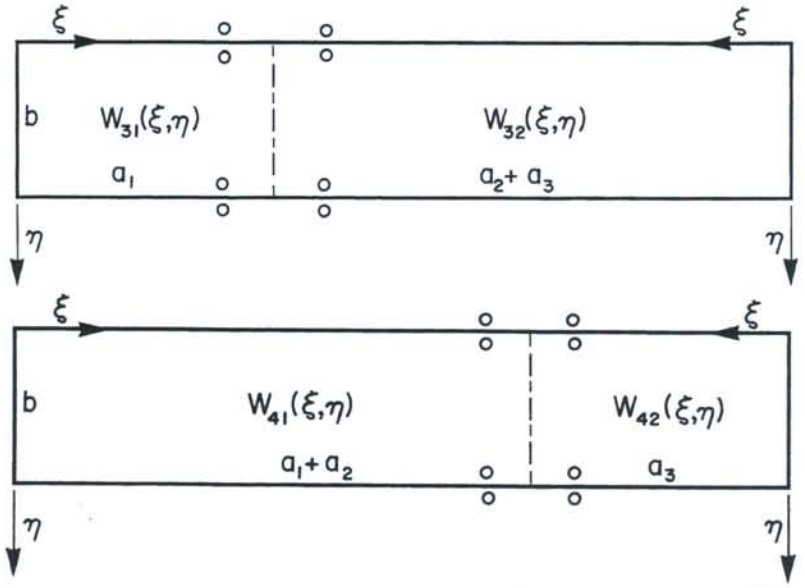

Fig 4. Building Blocks for Alternate Approach.

5. Discussion and Results

It is fortunate that exact eigenvalues for this problem are available from the theory of simply supported plates, when all three spans of the continuous plate have equal aspect ratios. Both solutions and procedures discussed above have been verified through comparison with those known results. Virtually exact agreement between the two analytical procedures has been obtained. Relative advantages of both procedures are discussed.

Mathematical Model for Vortex Excited Oscillations in Bundled Conductor of Transmission Lines

Peter Hagedorn
Dept. of Applied Mechanics
Darmstadt University of Technology
Darmstadt, Germany
hagedorn@mechanik.tu-darmstadt.de

Abstract
Wind excited oscillations of the conductors constitute the most important of the different mechanical vibration phenomena in high voltage overhead transmission lines. The most common of these wind excited vibrations are those generated by *vortex shedding*. Other types of wind excited vibrations include the low frequency *galloping*, an *aeroelastic instability* sometimes observed in winter, when ice deposits on the conductors, changing the cross section to a noncircular form.

Besides the wind excited oscillations there are also other interesting mechanical phenomena in the conductors of overhead transmission lines, which only occur under special circumstances but can nevertheless have dramatic consequences. This includes *short circuit phenomena*, which are due to the electromagnetic forces between the individual conductors. Under normal conditions these forces are extremely weak and therefore negligible. Whenever the currents in the conductors reach very large values, as e.g. during a short circuit, possibly due to lightening, these forces may become extremely large. Even if they last for only say 20 milliseconds, they may cause very large oscillations leading to impacts between the individual conductors, sometimes causing permanent damage.

This paper is devoted exclusively to vortex excited oscillations. The physical phenomenon can be explained as follows. If a rigid cylinder is immersed in a planar steady laminar flow for a wide range of Reynolds numbers, vortices will form alternately at the upper and lower edge of the cylinder. Von Kárman studied the stability of this *vortex street*. He found that it is stable only for a frequency of about 0.2*v/D, where v is the unperturbed fluid velocity upstream to the cylinder and D its diameter. The vortices separating alternately from the upper and lower edge produce a force on the cylinder which is periodic in time with a direction orthogonal to the fluid's unperturbed velocity. In first approximation this force can be assumed as harmonic.

For an elastically suspended cylinder these forces will generate *vibrations in a direction orthogonal to the flow*. In this case however, the vortex generation is complicated by the motion of the cylinder, and a *lock-in phenomenon* is observed, i.e. the frequency of the vortex generation tends to lock into the eigenfrequency of the cylinder. Similar vibrations are observed in a taut string subjected to a steady transverse flow, although in reality the flow is then no longer planar. In wind tunnel experiments the aerodynamic forces acting on an oscillating cylinder have been measured, and in the case of the vortex induced oscillations of a string, the power imparted by the fluid to the string has been determined as a function of the vibration amplitudes (*wind power*).

Such vortex excited oscillations do of course occur in the conductors of overhead transmission lines. Although they are not highly visible due to their low amplitude (less than a conductor diameter), they are however extremely common and may lead to conductor fatigue. Mathematical models are therefore necessary for the computation of these vibrations for the evaluation of the risk of damage to the line as well as for studying the effectiveness of damping measures.

For single conductor lines the so called *energy balance method* gives good results. The problem becomes more involved for *bundled conductors*, which are commonly used in high power transmission, and this problem is addressed in the present paper. The conductors are modeled as *taut strings* by the linear wave equation, possibly with some provision for an additional small bending stiffness. The damping devices as well as the *spacers* are in a first approximation treated as linear systems and are modeled by mechanical *impedance matrices* which have to be obtained from laboratory experiments or by other means, for example using a multi-body approach. Next, the free vibration problem of a bundled conductor is formulated. If the continuous system is discretized in the standard way, this leads to a rather large and *poorly conditioned matrix eigenvalue problem*. The problem becomes somewhat more manageable if the known solutions of the wave equation are used. This does however lead to a matrix eigenvalue problem in which the *matrix elements are transcendental functions of the eigenvalues*. The spectrum of this eigenvalue problem is very dense. No completely satisfactory technique for the numerical solution of this eigenvalue problem is presently known by the author.

Once the complex eigenvectors and eigenvalues are found, it is assumed that the weak aerodynamic forces, associated to the vortex street, excite conductor vibrations in resonance and that the shape of these forced vibrations corresponds to the eigenfunctions. In each mode, only one algebraic parameter representative of the amplitudes has to be calculated and this is done using *energy balance*.

This relatively coarse mathematical model seems reasonable from an engineering point of view, since any more detailed model of the aerodynamic forces requires information on wind velocity spectra, their correlation in space and time, etc. Such more elaborate models have been tried for single conductor lines, but they have not really led to new insights. The simple energy balance approach, on the other hand, gives results which agree well with field experiments, in the sense of a *worst case hypothesis*, for single conductor lines. For bundled conductors hopefully the mathematical model here presented will also provide a practical engineering tool. The numerical techniques used in the solution of the eigenvalue problem will have to be further developed to this end.

A different interesting and important problem is that of the *optimal placement of dampers* along the line. Usually, in a given frequency range as many modes as possible should be sufficiently well damped using a number of dampers as small as possible. This problem will also be addressed in the paper.

FREE VIBRATION ANALYSIS OF LAMINATED SHALLOW CYLINDRICAL SHELLS OF RECTANGULAR PLANFORM

Kenji HOSOKAWA and Toshiyuki SAKATA
Department of Mechanical Engineering
Chubu University
1200 Matsumotocho, Kasugai, Aichi 487-8501 Japan

1. Introduction

Since a laminated shallow shell is an important structural member, many studies on the free vibrations of a laminated shallow shell have been reported in the literature. On the other hand, the authors proposed a numerical approach for analyzing the free vibrations of a laminated FRP (fiber reinforced plastic) composite plate [1-3]. In the present paper, this approach is modified for application to a symmetrically laminated shallow cylindrical shell of rectangular planform. To justify the numerical results, the vibration tests of the clamped symmetrically laminated shallow cylindrical shell of square planform are carried out. And the calculated natural frequencies and mode shapes are compared with the experimental ones.

2. Numerical Approach

2.1 Frequency Equation

On the basis of Donnell's shell theory, by neglecting the body force, rotatory effect, and inplane inertia effect, the free vibration of a symmetrically laminated shallow cylindrical shell of rectangular planform is governed by

$$\left.\begin{aligned} &L_1(U,V,W)=0 \\ &L_2(U,V,W)=0 \\ &L_3(U,V,W)-\omega^2\rho hW=0 \end{aligned}\right\} \tag{1}$$

where h is the thickness, $U(\zeta,\lambda)$ and $V(\zeta,\lambda)$ are displacements, $W(\zeta,\lambda)$ is the transverse deflection, ω is the radian frequency, ρ is the density, and $L_1(\ ),L_2(\ )$, and $L_3(\ )$ are the differential operators for the static bending problem of the shallow cylindrical shell.

By dividing the shallow cylindrical shell as shown in Fig.1 and using the function $G_3(\zeta,\lambda,\zeta_n,\lambda_n)$ for the static bending problem, the frequency equation is expressed as

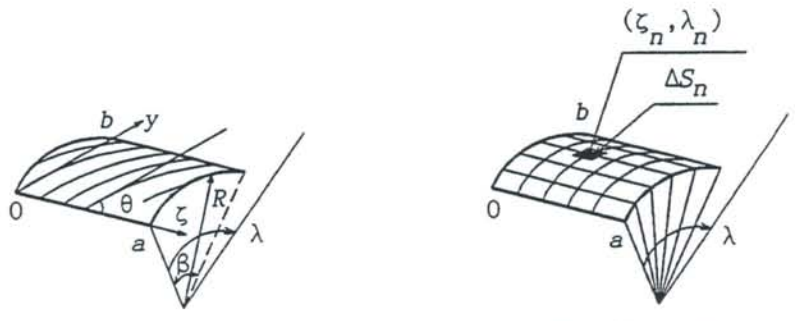

(a) Neutral plane (b) Dividing pattern

Fig.1 Laminated shallow cylindrical shell of rectangular planform

$$\det\left|\delta_{m,n} - \omega^2 \rho h G_3(\zeta_m, \lambda_m, \zeta_n, \lambda_n)\Delta S_n\right| = 0 \qquad (2)$$
$$m,n = 1,2,3,\ldots,N$$

where $\delta_{m,n}$ is Kronecker's δ, ΔS_n is the area of the nth small region of the shallow cylindrical shell shown in Fig. 1. The functions $G_1(\zeta,\lambda,\zeta_n,\lambda_n)$, $G_2(\zeta,\lambda,\zeta_n,\lambda_n)$, and $G_3(\zeta,\lambda,\zeta_n,\lambda_n)$ for the static bending problem satisfy the boundary condition of the shallow cylindrical shell and the differential equation represented by

$$\left.\begin{aligned} L_1(G_1,G_2,G_3) &= 0 \\ L_2(G_1,G_2,G_3) &= 0 \\ L_3(G_1,G_2,G_3) &= \delta(\zeta-\zeta_n)\bullet\delta(\lambda-\lambda_n) \end{aligned}\right\} \qquad (3)$$

where $\delta(\ )$ is Dirac's delta function.

2.2 Estimation of Functions G_1, G_2, and G_3

The functions are assumed in a power series form as the following equations, respectively,

$$G_1(\zeta,\lambda,\xi,\eta) = \sum_{i=1}^{I} A_i(\xi,\eta)\,\psi_1(\zeta,\lambda)\zeta^k\lambda^l \qquad (4)$$

$$G_2(\zeta,\lambda,\xi,\eta) = \sum_{i=1}^{I} B_i(\xi,\eta)\,\psi_2(\zeta,\lambda)\zeta^k\lambda^l \qquad (5)$$

$$G_3(\zeta,\lambda,\xi,\eta) = \sum_{i=1}^{I} C_i(\xi,\eta)\,\psi_3(\zeta,\lambda)\zeta^k\lambda^l \qquad (6)$$

where $A_i(\xi,\eta)$, $B_i(\xi,\eta)$, and $C_i(\xi,\eta)$ are constants determined by the position (ξ,η) where unit load acts, k and l are non-negative integers determined according to the positive integer i. The functions $\psi_1(\zeta,\lambda)$, $\psi_2(\zeta,\lambda)$, and $\psi_3(\zeta,\lambda)$ are determined such that the functions G_1, G_2, and G_3 satisfy the boundary conditions of the shallow cylindrical shell, respectively. In case of the clamped shallow cylindrical shell shown in Fig. 1, the functions $\psi_1(\zeta,\lambda)$, $\psi_2(\zeta,\lambda)$, and $\psi_3(\zeta,\lambda)$ may be expressed as

$$\psi_1(\zeta,\lambda) = \psi_2(\zeta,\lambda) = \zeta(\zeta-a)\lambda(\lambda-\beta) \qquad (7)$$

$$\psi_3(\zeta,\lambda) = \zeta^2(\zeta-a)^2\lambda^2(\lambda-\beta)^2 \qquad (8)$$

By applying Galerkin's method to equation (3), one gets $A_i(\xi,\eta)$, $B_i(\xi,\eta)$, and $C_i(\xi,\eta)$. By substituting $A_i(\xi,\eta)$, $B_i(\xi,\eta)$, and $C_i(\xi,\eta)$ into the equations (4), (5), and (6), respectively, one can obtain the functions G_1, G_2, and G_3.

3. Comparison of Numerical and Experimental Results

To justify the numerical results, experimental studies are carried out for a eight layered ($[0°_2/90°_2/90°_2/0°_2]$) shallow cylindrical shell of square planform (a=b=0.2[m], R=0.4[m]). The shallow cylindrical shell with shell thickness $h = 1.60\times10^{-3}$ [m] is used. Each layer material is a carbon fiber reinforced plastic (CFRP). The measured material properties of the lamina are : $E_1 = 95.4$ [GPa], $E_2 = 6.35$ [GPa], $G_{12} = 5.22$ [GPa], $\nu_{12} = 0.32$, $\rho = 1495$ [kg/m^3]. As shown in Fig. 2, the shallow cylindrical shell is clamped to a rigid clamping fixture. Natural frequencies and mode shapes of the shallow

cylindrical shell are obtained by using the experimental modal analysis technique. Figure 3 shows the natural frequencies and mode shapes obtained numerically and experimentally. As the vibration pick-up, a strain gage is affixed at the location where nodal lines disappear. From this figure, one can see that the difference between experimental and numerical natural frequencies is about 9% at the most. In Fig. 3, the narrow line represents the nodal line obtained by the experimental modal analysis technique and the heavy line shows those calculated by the numerical approach. From this figure, one can see the good agreement between numerical and experimental nodal patterns.

4. Conclusions

The numerical approach for analyzing the free vibrations of a symmetrically laminated shallow cylindrical shell of rectangular planform was proposed. This approach was applied to the clamped symmetrically laminated shallow cylindrical shell of square planform. Furthermore, by the vibration tests of the clamped symmetrically laminated shallow cylindrical shell of square planform, natural frequencies and mode shapes were obtained. From the comparison of numerical and experimental results, one can see the good agreements between these results. Accordingly, it follows that one can accurately estimate natural frequencies and mode shapes by using the numerical approach proposed by the authors.

References

1. K. HOSOKAWA, T. YADA and T. SAKATA 1993 *JSME International Journal* Series C 36, 296-300. Free vibrations of symmetrically laminated composite plates.
2. K. HOSOKAWA, Y. TERADA and T. SAKATA 1996 *Journal of Sound and Vibration* 189, 525-533. Free vibrations of clamped symmetrically laminated skew plates.
3. K. HOSOKAWA, Y. YAMADA and T. SAKATA 1998 *Journal of Applied Mechanics* 65, 341-345. Free-vibration analysis of clamped antisymmetrically laminated elliptical plates.

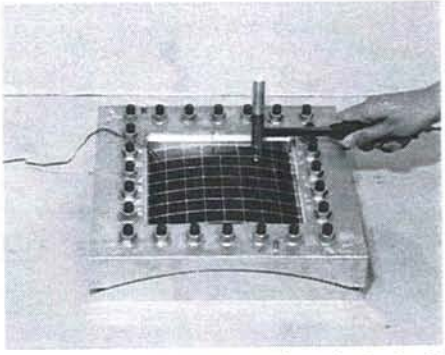

Fig. 2 Vibration test of clamped shallow cylindrical shell of square planform

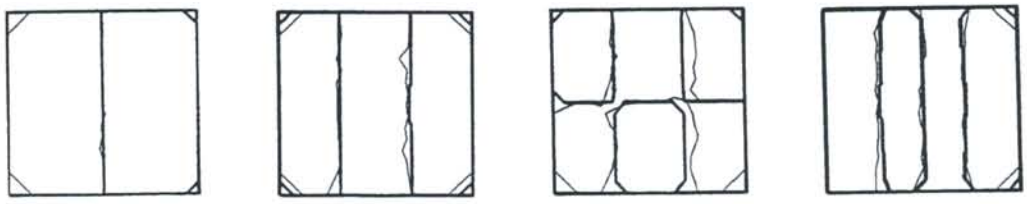

	1st mode	2nd mode	3rd mode	4th mode
Experiment	699.9[Hz]	846.6[Hz]	1296[Hz]	1315[Hz]
Analysis	762.6[Hz]	844.4[Hz]	1332[Hz]	1362[Hz]

Fig. 3 Natural frequencies and nodal patterns of clamped eight layered shallow cylindrical shell of square planform

On the Vibration of Composite Cylinders

James R. Hutchinson
Civil and Environmental Engineering Department
University of California, Davis CA 95616

Introduction

The cylinders considered in this paper are composed of concentric layers of different isotropic materials. The three dimensional elasticity solution is for infinitely long cylinders, which can be interpreted as finite length cylinders with very specific end boundary conditions. The cylinders can be either fixed or free at the inner and outer radii. The inner material can be solid (i.e.. no hole). Comparisons are made to previous research, and plots of a specific example are presented.

Background

The infinitely long solid cylinder was first investigated by Pochhammer in 1876 and independently by Chree in 1889. The work of Armenàkas Gazis and Herrmann (1) gives extensive numerical results for infinitely long hollow cylinders which are free on the inner and outer radii, as well as results for solid cylinders. In the 1960's several authors considered cylinders with fixed outer radii among these is my work (2). In 1969 Armenàkas (3) considered the vibrations of an infinitely long composite cylindrical rod. His composite was a solid core with one surrounding sleeve which was free on its outer radius.

Solution

Tables of solution forms were published in a number of my previous papers e.g. (4). These solution forms represent solutions of the three dimensional equations of isotropic linear elasticity. A slightly modified version of these previous tables is shown in Table 1.

Table 1. Solution of elasticity equations. J_n denotes the n^{th} order Bessel function of the first kind. Identical solutions exist for the Bessel functions of the second kind (substitute Y for J). G is the shear modulus, ρ is the density and ν is Poisson's ratio. Primes denote differentiation with respect to the argument. $k = \rho\omega^2\nu/(1-\nu)/G$ and the wave numbers α, β, δ and the frequency ω are related by $\alpha^2 + \beta^2 = \rho\omega^2/G$ and $\alpha^2 + \delta^2 = \rho\omega^2(1-2\nu)/2/(1-\nu)/G$. The wave number n equals 0, 1, 2, ... The three basic forms have a common multiplier in the last column.

	Form 1	Form 2	Form 3	Multiplier
u_r	$\delta J_n'(\delta r)$	$-\beta J_n'(\beta r)$	$-nJ_n(\beta r)/r$	$\sin(\alpha z)\cos(n\theta)$
u_z	$\alpha J_n(\delta r)$	$\beta^2 J_n(\beta r)/\alpha$	0	$\cos(\alpha z)\cos(n\theta)$
u_θ	$-nJ_n(\delta r)/r$	$nJ_n(\beta r)/r$	$\beta J_n'(\beta r)$	$\sin(\alpha z)\sin(n\theta)$
σ_r	$2G\delta^2 J_n''(\delta r)$ $-k\lambda G J_n(\delta r)$	$-2G\beta^2 J_n''(\beta r)$	$-2Gn\beta J_n'(\beta r)/r$ $+2nJ_n(\beta r)/r^2$	$\sin(\alpha z)\cos(n\theta)$
τ_{rz}	$2G\alpha\delta J_n'(\delta r)$	$G(\beta^2-\alpha^2)\beta J_n'(\beta r)/\alpha$	$-Gn\alpha J_n(\beta r)/r$	$\cos(\alpha z)\cos(n\theta)$
$\tau_{r\theta}$	$-2Gn\delta J_n'(\delta r)r$ $+2GnJ_n(\delta r)/r^2$	$2Gn\beta J_n'(\beta r)/r-$ $2GnJ_n(\beta r)/r^2$	$G\beta^2 J_n''(\beta r)-G\beta J_n'(\beta r)/r$ $+Gn^2 J_n(\beta r)/r^2$	$\sin(\alpha z)\sin(n\theta)$
σ_θ	$2G\delta J_n'(\delta r)/r$ $-G(k+2n^2/r^2)J_n(\delta r)$	$-2G\beta J_n'(\beta r)/r$ $+2Gn^2 J_n(\beta r)/r^2$	$2Gn\beta J_n'(\beta r)/r$ $-2GnJ_n(\beta r)/r^2$	$\sin(\alpha z)\cos(n\theta)$
σ_z	$-G(k+2\alpha^2)J_n(\delta r)$	$-2G\beta^2 J_n(\beta r)$	0	$\sin(\alpha z)\cos(n\theta)$
$\tau_{\theta z}$	$-2Gn\alpha J_n(\delta r)/r$	$-Gn(\beta^2-\alpha^2)J_n(\beta r)/r/\alpha$	$G\alpha\beta J_n'(\beta r)$	$\cos(\alpha z)\sin(n\theta)$

From Table 1 α can be determined from the relation that $\alpha L = \pi$ where L is the wave length. For a given L, radius r, physical properties and value of n the tabulated values are a function of the frequency alone. The solution for a wavelength of L can also be interpreted as the solution of a cylinder of length L and end boundary conditions of either u_r, u_θ, and σ_z equal zero or u_z, τ_{rz} and $\tau_{r\theta}$ equal zero.

For multiple layers, the layers and interface face radii are numbered from the outside in. The outer radius is r_1 and the outer layer is material 1. For example the radius r_3 is the interface radius between material 2 and material 3.

A 3x3 displacement matrix $\mathbf{D}_J$ is formed using the first three rows and columns of the functions listed in Table 1 (without the multiplier). Two more subscripts are attached to this matrix, the first denoting the material number and the second denoting the radius number. Thus $\mathbf{D}_{J34}$ would refer to the first three rows of Table 1 for the third material at radius r_4. A similar matrix $\mathbf{D}_Y$ is formed where Y replaces J in Table 1. A stress matrix $\mathbf{S}_J$ is formed using the next three rows of Table 1. These are the stress components which appear on the interface of the materials. The stress matrix $\mathbf{S}_Y$ is formed in the same way but with Y replacing J. To satisfy boundary and interface conditions it is simply a matter of combining these matrices. As an example the characteristic matrix for solution of a three layered shell which is free at the inner and outer radius is,

$$\begin{bmatrix} \mathbf{S}_{J11} & \mathbf{S}_{Y11} & & & & \\ \mathbf{S}_{J12} & \mathbf{S}_{Y12} & -\mathbf{S}_{J22} & -\mathbf{S}_{Y22} & & \\ \mathbf{D}_{J12} & \mathbf{D}_{Y12} & -\mathbf{D}_{J22} & -\mathbf{D}_{Y22} & & \\ & & \mathbf{S}_{J23} & \mathbf{S}_{Y23} & -\mathbf{S}_{J33} & -\mathbf{S}_{Y33} \\ & & \mathbf{D}_{J23} & \mathbf{D}_{Y23} & -\mathbf{D}_{J33} & -\mathbf{D}_{Y33} \\ & & & & \mathbf{S}_{J34} & \mathbf{S}_{Y34} \end{bmatrix} \{\mathbf{C}\} = \{\mathbf{0}\} \qquad (1)$$

The matrices in the first row make the stress on the outer boundary equal zero. The matrices in the second row are for the matching of the stress at the interface of the outer layer and its adjacent layer. The matrices in the third row are for matching of the displacements at the interface of the outer row and its adjacent layer. Subsequent rows of matrices are for interface matching. The matrices in the last row make the stress at the inner radius equal zero. To solve the problem of a fixed outer boundary the matrices in the first row $\mathbf{S}_{J11}$ $\mathbf{S}_{Y11}$ are replaced with $\mathbf{D}_{J11}$ and $\mathbf{D}_{Y11}$. Similarly, if the inner radius were fixed the matrices in the last row $\mathbf{S}_{J34}$ $\mathbf{S}_{Y34}$ would be replaced with $\mathbf{D}_{J34}$ and $\mathbf{D}_{Y34}$. To solve a solid cylinder (one layer) only the matrix $\mathbf{S}_{J11}$ in the upper left corner is used. To solve a single layered hollow cylinder the two by two set of matrices in the upper left is used. To solve a two layered cylinder with a solid core the three by three is used. To solve a two layered hollow cylinder the four by four set is used. To solve a three layered solid core system the five by five is used and so on. It can be seen that the assembly process for any number of layers follows a simple pattern and the imposition of free or fixed conditions at the inner or outer boundaries is also easily accomplished.

The above description is for n greater than zero. For n equal zero it is necessary to split the matrices into the axisymmetric case and the torsion case. For the axisymmetric case the matrices **D** and **S** become 2x2 matrices which are the upper left 2x2 terms in the 3x3's previously defined from Table 1. For the torsion case the **D** and **S** become the single lower right term in the 3x3's previously defined. Thus $\mathbf{D}_J$ is $\beta J_n'(\beta r)$. The assembly for these smaller matrices follows the same procedure as for the 3x3's as shown in Equation 1.

Numerical results

Extensive comparisons were made with reference (1) the answers were in complete agreement to the 5 place accuracy given in that reference. Complete agreement was found for the fixed outer boundary solutions in reference (2). There was also complete agreement with the two layer composite solutions given in reference (3), although, in that paper only plots were given.

Plots

The plots shown below compare a 5 layered cylinder with a one layered cylinder. In both cases the cylinder has an inner radius of half the outer radius. The 5 layered cylinder has interface radii at 0.9, 0.8, 0.7, and 0.6 of the outer radius. The Poisson's ratio for all layers is 0.3. The shear modulus and the density of layers 1, 3 and 5 are the same. Layers 2 and 4 have a shear modulus and density of half that of layers 1,3 and 5. The dimensionless frequency parameter in the plots is the frequency times the outer radius divided by the shear wave velocity ($\sqrt{G/\rho}$). Note, for this example the shear wave

velocity is the same for each layer. These frequency parameter vs. diameter to wavelength plots show the eight lowest frequencies. The solid lines are the 5 layered cylinder and the dashed lines are the single layered cylinder. Some of the frequencies for the five layer solution coincide or nearly coincide with the frequencies for the one layered system. This is true of the first (lowest) frequency and the sixth frequency in Figure 1 and the second frequencies in Figures 3 and 4.

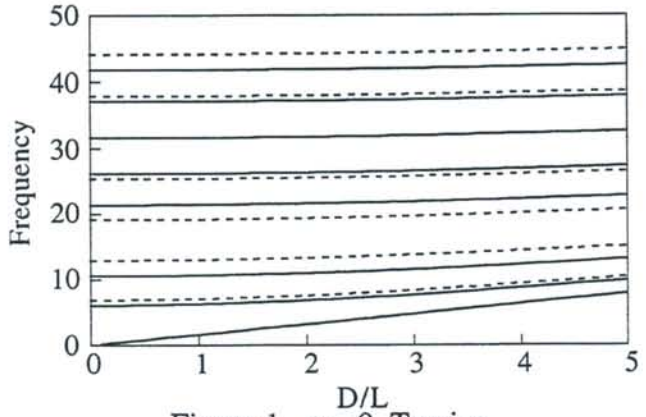

Figure 1. n = 0 Torsion

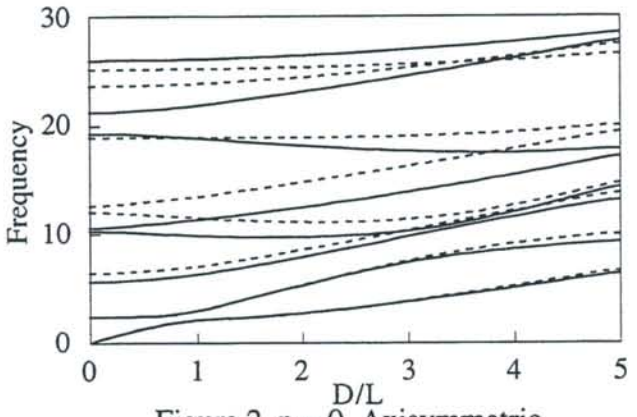

Figure 2. n = 0 Axisymmetric

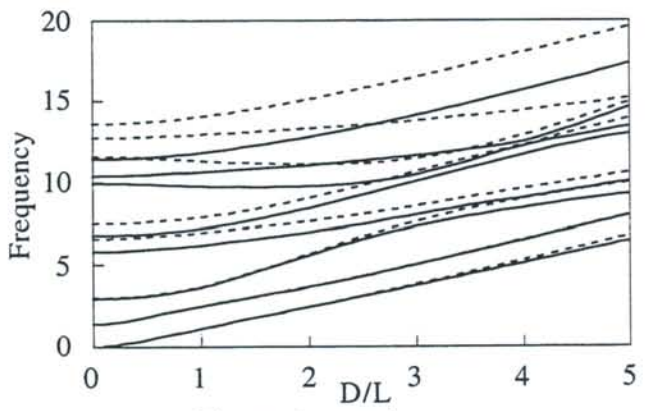

Figure 3. n = 1

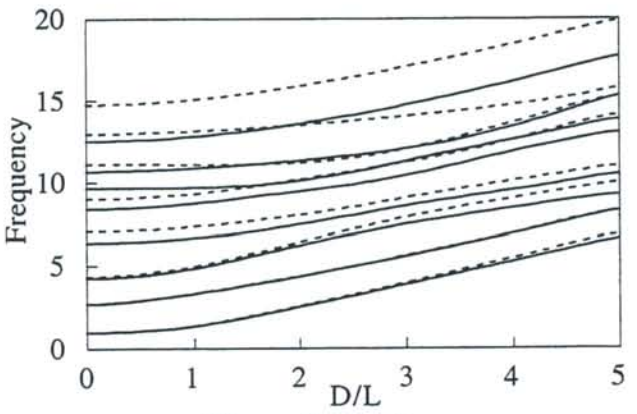

Figure 4. n = 2

Conclusions

It can be seen that in this example the lower frequencies for the five layered system differ little from the one layered system; whereas, for the higher frequencies there is marked difference. In this brief paper it was not possible to consider all of the many parameters which might be of importance. The method of solution; however, is straight forward and applicable to any number of layers. The FORTRAN program used in this paper is available to serious researchers by email at jrhutchinson@ucdavis.edu.

References

1. Armenàkas, A.E., Gazis, D.C. and Herrmann, G., *Free Vibrations of Circular Cylindrical Shells*, Pergamon Press, 1969.

2. Hutchinson J.R., "Axisymmetric Vibrations of a Solid Elastic Cylinder Encased in a Rigid Container", *Journal of the Acoustical Society of America*, Vol.42, 1967, pp. 398-402.

3. Armenàkas, A.E, "Propagation of Harmonic Waves in Composite Circular-Cylindrical Rods", *Journal of the Acoustical Society of America*, Vol. 47, 1969, pp. 822-837.

4. Hutchinson, J.R. and El-Azhari, S.A. "Vibrations of Free Hollow Circular Cylinders", *Journal of Applied Mechanics*, Vol. 53, September 1986, pp. 641-646.

NONLINEAR VIBRATION ANALYSIS OF CROSS-PLY LAMINATED SHALLOW SHELLS

Yukinori KOBAYASHI, Gen YAMADA and Masahiro SATOH
Division of Mechanical Science, Hokkaido University, Sapporo, 060-8628 ,Japan

INTRODUCTION

This paper presents a nonlinear vibration analysis of cross-ply laminated shallow shells. Governing equations of the system are derived by the Hamilton's principle considering geometrical nonlinearity. Applying Galerkin's procedure to the equations, we can obtain ordinal differential equations with a quadratic nonlinear term as well as cubic one. The obtained equations are solved by the method of multiple scales. When we analyze the second primary resonance, we must use the first mode function as well as the second one. Applying the method to simply supported shells subjected to lateral harmonic force, nonlinear steady state response of shells is obtained numerically.

ANALYSIS

Figure 1 shows a shallow shell which has a rectangular boundary and principal curvature radii R_x and R_y. The thickness of the shell is h and lengths of edges are a and b. The displacement components are u, v and w in the x, y and z directions, respectively. The principal directions of elasticity are denoted as 1- and 2-axes and the 3-axis is coincident to the z-axis. The angle between 1- and x- axes is θ. Assuming the uniformely distributed lateral force $q_0 \cos\Omega' t$ and $1+z/R_i \fallingdotseq 1$ ($i=x, y$), the equations of motion of the shell are derived as

$$\begin{aligned}
&\frac{\partial N_x}{\partial x}+\frac{\partial N_{xy}}{\partial y}+\frac{1}{R_x}\left(\frac{\partial M_x}{\partial x}+\frac{\partial M_{xy}}{\partial y}\right)=0, \qquad \frac{\partial N_{xy}}{\partial x}+\frac{\partial N_y}{\partial y}+\frac{1}{R_y}\left(\frac{\partial M_{xy}}{\partial x}+\frac{\partial M_y}{\partial y}\right)=0,\\
&\frac{\partial}{\partial x}\left(N_x\frac{\partial w}{\partial x}+N_{xy}\frac{\partial w}{\partial y}\right)+\frac{\partial}{\partial y}\left(N_{xy}\frac{\partial w}{\partial x}+N_y\frac{\partial w}{\partial y}\right)+\frac{\partial^2 M_x}{\partial x^2}+2\frac{\partial^2 M_{xy}}{\partial x\,\partial y}+\frac{\partial^2 M_y}{\partial y^2}-\frac{N_x}{R_x}-\frac{N_y}{R_y}\\
&+q_0\cos\Omega' t=\rho h\frac{\partial^2 w}{\partial t^2}+c\frac{\partial w}{\partial t},
\end{aligned} \tag{1}$$

where c is a viscous damping coefficient, ρ is the mass density of the shell, N_x , N_y , N_{xy} are inplane force resultants and M_x , M_y , M_{xy} are moment resultants, respectively. In-plane and rotational inertia terms are neglected in the above equations. Following nondimensional parameters are introduced to simplify the analysis:

$$\left.\begin{aligned}
&\xi=\frac{x}{a},\quad \eta=\frac{y}{b},\quad U=\frac{u}{h},\quad V=\frac{v}{h},\quad W=\frac{w}{h},\quad \alpha=\frac{a}{b},\quad H=\frac{h}{a},\quad r_x=\frac{R_x}{a},\quad r_y=\frac{R_y}{a},\\
&\tau=\frac{1}{a^2}\sqrt{\frac{D_0}{\rho h}}t,\quad \Omega=\Omega' a^2\sqrt{\frac{\rho h}{D_0}},\quad D_0=\frac{E_2 h^3}{12(1-\nu_{12}\nu_{21})},\quad q^*=\frac{a^3}{D_0 H}q_0,\quad C=\frac{a^3}{D_0 H}c,
\end{aligned}\right\} \tag{2}$$

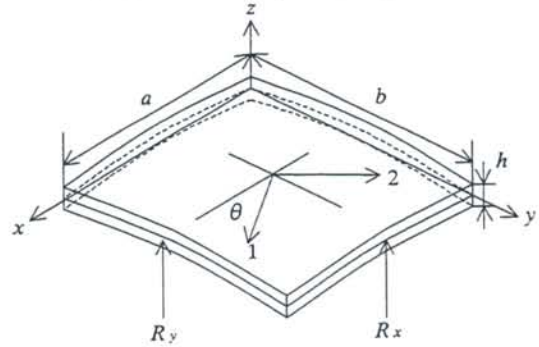

Fig.1 Coordinate System of a Shallow Shell

where τ is nondimensional time, and E_2 is the Young's modulus in the direction of 2-axis and ν_{12} and ν_{21} are Poisson's ratios.

We assume that the shell is simply supported along edges. Applying Galerkin's procedure and eliminating variables except transverse displacement, the governing equations are reduced as follows:

$$\frac{d^2W_i}{d\tau^2}+C\frac{dW_i}{d\tau}+\omega_i^2W_i+\sum_{j,k=1}r_{ijk}W_jW_k+\sum_{l,p,q}s_{ilpq}W_lW_pW_q=F_i\cos\Omega\tau, \tag{3}$$

where

$$\{W_i\}=\{W_{11},W_{12},\cdots,W_{1N},\cdots,W_{MN}\},\quad F_i=4q^*\int_0^1\int_0^1\sum_{m=1}^{M}\sum_{n=1}^{N}\sin(m\pi\xi)\sin(n\pi\eta)d\eta d\xi.$$

Coefficients ω_i, r_i, s_i and F_i express linear natural frequency, coefficients of second and third order nonlinear terms and amplitude of external load, respectively. When the external load is so weak as to induce the amplitude of responses smaller than the thickness of the shell, equation (3) is rewritten as

$$\frac{d^2X_n}{d\tau^2}+2\varepsilon^2\mu\frac{dX_n}{d\tau}+\omega_n^2X_n+\varepsilon\sum_{j,k=1}r_{njk}X_jX_k+\varepsilon^2\sum_{l,p,q=1}s_{nlpq}X_lX_pX_q=2\varepsilon^2f_n\cos\Omega\tau, \tag{4}$$

where

$$W_n=\varepsilon X_n,\quad C=2\varepsilon^2\mu,\quad F_n=2\varepsilon^2f_n$$

and ε is a non-dimensional small parameter.

We apply the method of multiple scales to solve the equation (4) and use the detuning parameter σ

$$\Omega=\omega_n+\varepsilon\sigma \tag{5}$$

and the time scale

$$T_n=\varepsilon^n\tau \qquad (n=0,1,2,\cdots). \tag{6}$$

Considering the first and second modes of vibration and following the procedure of the method of multiple scales, the steady state responses of the shell are obtained as

Primary resonance of the first mode：

$$\left.\begin{aligned}W_1&=a_1\cos(\Omega\tau-\hat{\gamma}_1)+\varepsilon\frac{R_{111}}{6\omega_1^2}a_1^2\left[\cos(2\Omega\tau-2\hat{\gamma}_1)-3\right],\\W_2&=0,\end{aligned}\right\} \tag{7}$$

Primary resonance of the second mode：

$$\left.\begin{aligned}W_1&=-\varepsilon\frac{R_{122}}{2}a_2^2\left[\frac{1}{\omega_1^2-4\omega_2^2}\cos(2\Omega\tau-2\hat{\gamma}_2)+\frac{1}{\omega_1^2}\right],\\W_2&=a_2\cos(\Omega\tau-\hat{\gamma}_2),\end{aligned}\right\} \tag{8}$$

where

$$\hat{\gamma}_n=\sigma T_2-\gamma_n,\quad R_{njk}=r_{njk}+r_{nkj}.$$

Coefficients a_1 and a_2 express the amplitudes of response which are dependent on the strength of the external load f_n and γ_n is the phase. While the response W_1 is independent of coefficients R_{2jk} for the primary resonance of the first mode and W_2 =0 in eq. (7), the response W_1 is induced by the effect of the coefficient R_{122} in eq. (8) when we analyze the primary resonance of the second mode, even if we do not assume any internal resonance.

RESULTS AND DISCUSSION

Three layered cross-ply laminated shells (0°/90°/0°) made of graphite/epoxy are treated in the following numerical examples. Each lamina is assumed made of graphite/epoxy whose material properties are

$$\frac{E_1}{E_2}=15.4,\quad \frac{G_{12}}{E_2}=0.79,\quad \frac{G_{23}}{E_2}=0.5,\quad \nu_{12}=0.3,$$

and the thickness of the shell is H=0.01.

Figure 2(a) and (b) show the resonances W_1 for f_1=23 and W_2 for f_2=30, respectively, around the first and second natural frequencies and the comparison between results obtained by the single-mode analysis and two-mode analysis. Abscissa denotes the detuning parameter from each natural frequency. The response of the first mode W_1 is determined from eq. (7). Result for the first mode shows the soft spring behavior and there is no differece between the results by the single- and two-mode analyses. In Fig.2(b), dotted line denotes the result obtained by the single mode analysis neglecting R_{122} in eq. (8) and solid line denotes the result of two-mode analysis considering the effect of R_{122}. While the result of single-mode analysis shows hard spring behavior in Fig.2(b), that of two-mode analysis shows soft spring behavior. This is similar to the results for a beam resting on a nonlinear elastic foundation using the direct method by Nayfeh and Lacarbonara[1].

Figure 3 shows the responses for various ratios of r_x/r_y by the two-mode analysis when f_2=30. The amplitude of the first mode W_1 is very small, it is however induced by R_{122} in eq. (8). As seen from the figure, responses of the first and second modes for the spherical shell (r_x/r_y=1) show the soft spring behavior. With a decreasse in the ratio r_x/r_y, the response curves change from soft spring behavior to hard one.

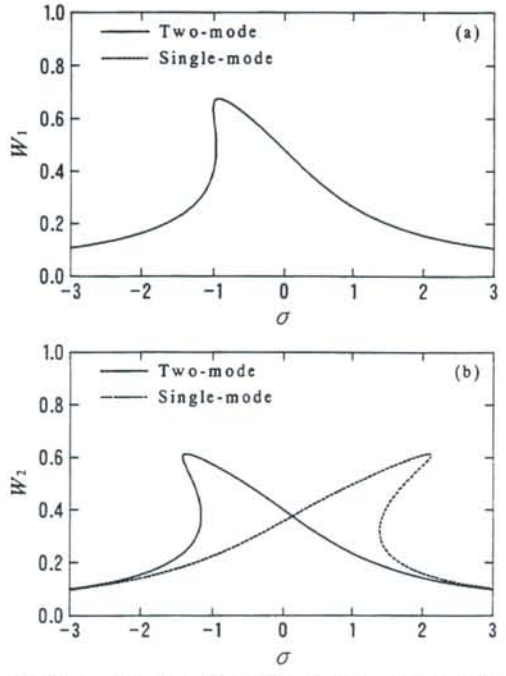

Fig.2 Frequency-response curves for the primary resonances (a) first mode (b) second mode
(0°/90°/0°, α=1, r_x=r_y=10, μ=0.50, (a) f_1=23, (b) f_2=30)

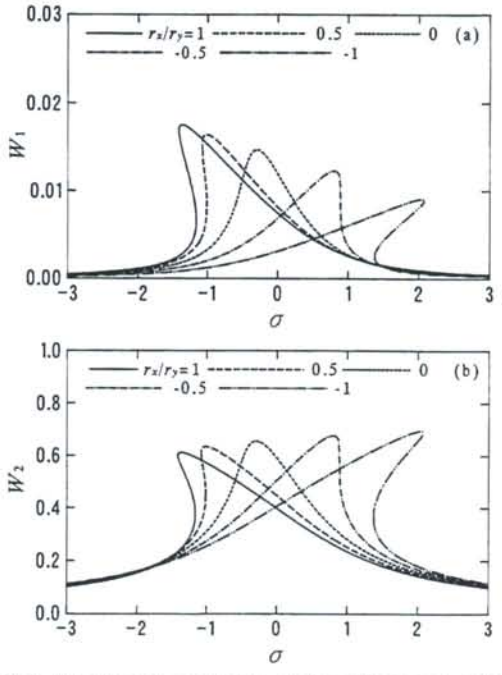

Fig.3 Frequency-response curves of second primary resonance for various curvature ratios
(0°/90°/0°, α=1, r_x=10, μ=0.50, f_2=30)

REFERENCE

(1) Nayfeh, A.H. and Lacarbonara, W., On the Discretization of Ditributed-Parameter Systems with Quadratic and Cubic Nonlinearities, *Nonlinear Dynamics*, **13**(1997), 203-220.

Modal Interaction of a Randomly Excited Hinged-Clamped Beam

W. K. LEE
Department of Mechanical Engineering, Yeungnam University,
Gyongsan 712-749, Korea

D. S. CHO
Reactor Mechanical Engineering Department,
Korea Power Engineering Company, Inc., Taejon 305-353, Korea

A straight beam with fixed ends experiences mid-plane stretching when deflected. The influence of this stretching on the dynamic response increases with the amplitude of the response. This situation can be described with nonlinear strain-displacement equations and a linear stress-strain law which give us the nonlinear beam equation. Nonlinear dynamic responses of a straight beam with fixed ends have been studied by many authors. Under harmonic excitation, Nayfeh and his colleagues[1,2], and Lee and his colleagues[3-5] considered two or three mode interaction to study the steady state responses of a hinged-clamped beam. Lee and Soh[3] showed that there exists no significant difference between two and three mode interactions' influences on the responses.

On the other hand, Ibrahim and his colleagues[6,7] have studied the stochastic bifurcation of the unexcited mode of a clamped-clamped beam under wide band random excitation when initial static axial load is applied to the beam. When the axial static does not exceed the Euler buckling load[6], the Gaussian closure failed to predict bifurcation of unexcited second mode. But both non-Gaussian closure and Monte Carlo simulation predicted second mode bifurcation. When the axial static exceeds the Euler buckling load[7], The Gaussian closure and Monte Carlo simulation solutions predicted the bifurcation points of the second mode at relatively higher excitation level than the non-Gaussian closure.

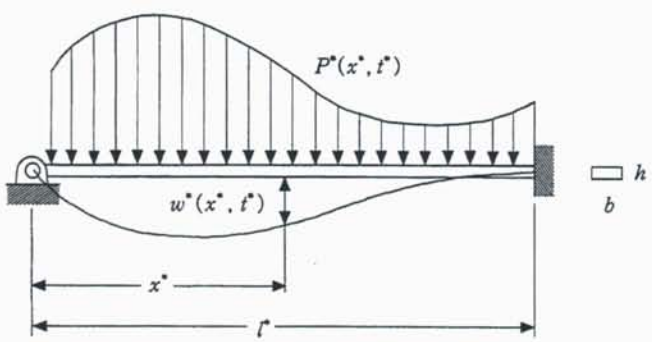

Fig. 1 A schematic diagram of a hinged-clamped beam

In this study, we investigate the modal interaction of a hinged-clamped beam with a random excitation as shown in Fig. 1.

Using Galerkin's method, the governing equation of motion of the hinged-clamped beam[3] in terms of dimensionless variable is reduced to a system of coupled nonlinear ordinary differential equations as follows:

$$\frac{d^2u_n}{dt^2}+\omega_n^2u_n=\varepsilon[\ -2c_n\frac{du_n}{dt}+s_{n0}u_1^3+s_{n1}u_1^2u_2+s_{n2}u_1u_2^2+s_{n3}u_2^3+s_{n4}u_1^2u_3+s_{n5}u_1u_2u_3$$
$$+s_{n6}u_2^2u_3+s_{n7}u_1u_3^2+s_{n8}u_2u_3^2+s_{n9}u_3^3+F_n(t)],\quad n=1,2,3. \tag{1}$$

where $\varepsilon=r^2/(l^*/2)^2=(2h/l^*)^2/12$, $l=l^*/(l^*/2)^2=2$ = nondimentialized length of beam, c_n = damping coefficients, s_{ij} = nonlinear coefficients, ω_n = natural frequencies ($\omega_1=3.855, \omega_2=12.491, \omega_3=26.062$), $F_n(t)=\int_0^l P(x,t)\varphi_n(x)dx$ = random excitation, $P(x,t)=(l^*/2)^7/(r^6EA)P^*(x^*,t^*)$, $t^*=\rho(l^*/2)^4/(Er^2)^{1/2}t$, $\varphi_n(x)$ = eigenfunctions, h = thickness of beam, l^* = length of beam, E = Young's modulus, r = radius of gyration, ρ = density of beam.

To investigate influences of the energy transfer from the externally excited modes (u_1, u_3) to the unexcited mode (u_2) through nonlinear coupling, we select the node of the second natural mode as external excitation point. In this case, the excitation corresponding to each mode is as follows:

$$F_1(t)=f_1W(t),\quad F_2(t)=f_2W(t),\quad F_3(t)=f_3W(t)$$
$$W(t)=P(0.885,t),\quad f_1=\varphi_1(x_W)=1.063,\quad f_2=\varphi_2(x_W)=0,\quad f_3=\varphi_3(x_W)=0.979. \tag{2}$$

Random excitation $W(t)$ is assumed to be zero mean white noise having the autocorrelation function

$$R_{WW}(\Delta t)=E[W(t)W(t+\Delta t)]=2D\,\delta(\Delta t) \tag{3}$$

where $2D$ represents the spectral density when we express the frequency by $f(=\omega/2\pi)$, and $\delta(\Delta t)$ is the Dirac delta function.

Equation (1) can be transformed into the Fokker-Planck equation for the joint probability density function $p(\mathbf{x},t)$ as follows:

$$\frac{\partial}{\partial t}p(\mathbf{x},t)=-\sum_{j=1}^{6}\frac{\partial}{\partial x_j}[a_j(\mathbf{x},t)p(\mathbf{x},t)]+\frac{1}{2}\sum_{j=1}^{6}\sum_{k=1}^{6}\frac{\partial^2}{\partial x_j\partial x_k}[b_{jk}(\mathbf{x},t)p(\mathbf{x},t)] \tag{4}$$

where $a_j(\mathbf{x},t)$ and $b_{jk}(\mathbf{x},t)$ are the drift and diffusion coefficients, respectively.

It is impossible to obtain the exact solution $p(\mathbf{x},t)$ to the Fokker-Planck equation (4). However, equations for the moments of $p(\mathbf{x},t)$ of any order n may be obtained by multplying equation (4) by $x_1^{\alpha_1}x_2^{\alpha_2}x_3^{\alpha_3}x_4^{\alpha_4}x_5^{\alpha_5}x_6^{\alpha_6}$, where $n=\alpha_1+\alpha_2+\alpha_3+\alpha_4+\alpha_5+\alpha_6$, and integrating by over the entire state space $-\infty<x_i<\infty$. Equations for the moments constitute a set of infinite coupled equations because the differential equation of order n contains moment terms of order $n+1$ and $n+2$. In order to obtain the response statistics we truncate these equations by using Gaussian and non-Gaussian closure schemes. The Gaussian closure is based on the assumption that the response process is nearly Gaussian and is carried out by setting third- and fourth-order cumulants to zero. In this case we can generate a system with 14 coupled differential equations for first- and second-order moments. For non-Gaussian processes the cumulants of order greater than the second do not vanish. However, their contribution diminishes as their order increases if the process is slightly deviate from Gaussian. Thus the non-Gaussian closure is carried out by setting fifth- and sixth-order cumulants to zero. In this case we can obtain a system with 69 coupled differential equations.

We investigate the long-term behavior of the moments by integrating numerically the ordinary differential equation obtained by Gaussian and non-Gaussian closure. Fig. 2 represents limits of mean square responses as function of the $2\varepsilon^2D$ proportional to

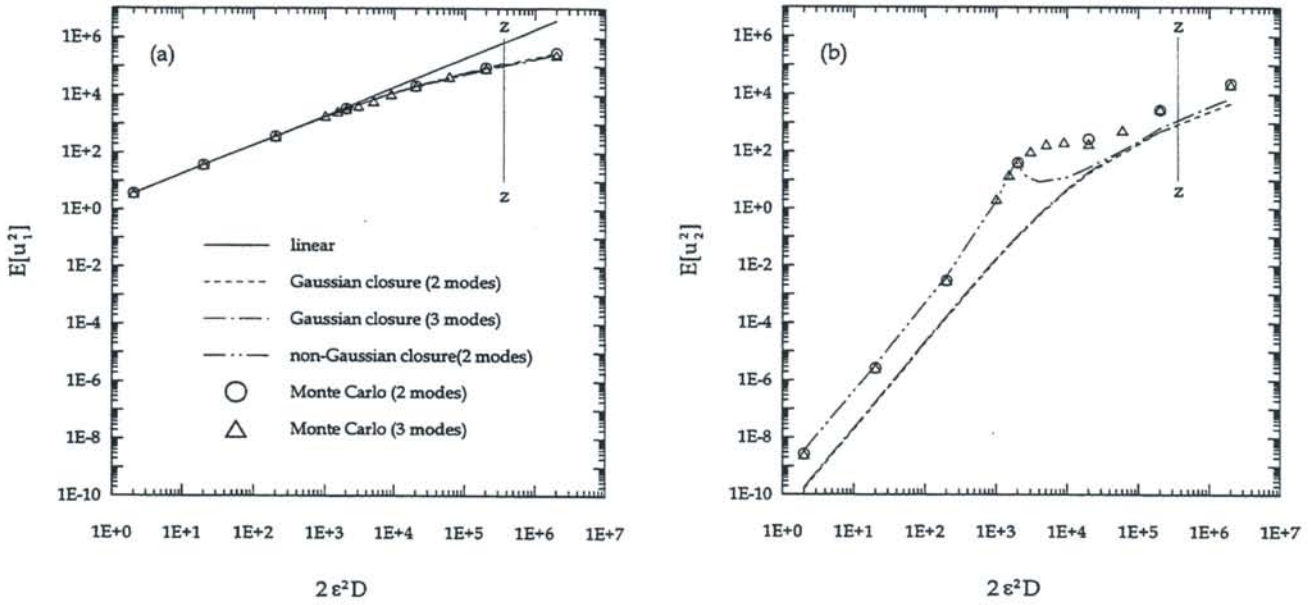

Fig. 2 Limits of mean square response plotted against $2\varepsilon^2 D$ according to Gaussian closure, non-Gaussian closure, and Monte Carlo simulation ($c_1 = c_2 = c_3 = 100, \varepsilon = 0.0001$).

mean square excitation σ_W^2, and represents the results of linearized system, two and three mode interactions by the Gaussian closure, two mode interaction by the non-Gaussian closure, and two and three mode interactions by Monte Carlo simulation. The non-Gaussian closure scheme doesn't give us any reliable results beyond the excitation level z-z. The mean square response of the second mode which is not excited directly increases as $2\varepsilon^2 D$ or σ_W^2. The first mode response predicted by Monte Carlo simulation is in good agreement with those predicted by two analytical schemes. The second mode response predicted by Monte Carlo simulation is in good agreement with that predicted by non-Gaussian closure scheme up to $2\varepsilon^2 D = 2000$. These results show that there exists no difference between two and three mode interactions.

References

[1] Nayfeh, A. H., Mook, D. T. and Sridhar, S., 1974, *Journal of Acoustical Society of America*, 55(2), 181-291, Nonlinear Analysis of the Forced Response of Structural Elements.

[2] Sridhar, S., Nayfeh, A. H. and Mook, D. T., 1975, *Journal of Acoustical Society of America*, 58(1), 113-123, Nonlinear Resonances in a Class of Multi-Degree-of-Freedom Systems.

[3] Lee, W. K. and Soh, K. Y., 1994, *Nonlinear Dynamics*, 6, 49-68, Nonlinear Analysis of the Forced Response of a Beam with Three Mode Interaction.

[4] Lee, W. K. and Ghang, M. R., 1994, *ASME Journal of Applied Mechanics*, 61, 144~151, Domains of Attraction of a Forced Beam by Interpolated Mapping.

[5] Lee, W. K. and Kim, C. H., 1997, *Nonlinear Dynamics*, 14, 37-48, Evolution of Domains of Attraction of a Forced Beam with Two-Mode Interaction.

[6] Ibrahim, R. A., Lee, B. H., and Afaneh, A. A., 1993, *ASME Journal of Vibration, Acoustics, Stress, and Reliability in Design*, 115, 193-201, Structural Modal Multifurcation With Internal Resonance-Part 2: Stochastic Approach.

[7] Lee, B. H. and Ibrahim, R. A., 1994, *Probabilistic Engineering Mechanics*, 9, 23-32, Stochastic Bifurcation in Non-linear Structural Systems near 1:1 Internal Resonance.

CURVE VEERING REVISITED

Arthur W. Leissa, Professor
Applied Mechanics Program, Ohio State University

Three decades ago, while studying the approximately 500 references that were included in his plate vibration monograph [1], the writer encountered theoretical curves for free vibration frequencies which would appear to cross, as a certain geometrical parameter (e.g., aspect ratio, or thickness ratio) was varied, but did not. Instead, they veered sharply away from each other as the apparent crossing point was approached.

The question arose in the writer's mind as to whether these veerings were realistic, or induced by approximations in the solution method or the theory. Some years later he showed [2] conclusively that the veering could be the result of an approximate solution method. The Galerkin method was used to obtain free vibration frequencies for a classical, taut, rectangular membrane as its aspect ratio (b/a) was varied. The well known exact solution yields straight line frequency curves which cross; the Galerkin method produced a sharp veering.

The writer continued to ponder this "curve veering" phenomenon subsequently. Some aspects of it were investigated several years ago by one of his graduate students [3]. In the present paper it is first demonstrated in exact solutions of some one-dimensional problems----vibrations and buckling of beams having interior springs attached. Then the two-dimensional membrane problem of [2] is revisited, with more accurate Galerkin solutions being used, resulting in more acute curve veering. But approximate solutions by the finite difference method do not produce veering. Finite difference results for plate vibration frequencies are also shown and discussed. Curves of frequency versus b/a are found to cross when exact solutions exist, but veer when they are not exact (variables separable exact solutions do not exist which satisfy the boundary conditions).

References

1. A.W. Leissa, Vibration of Plates, U.S. Govt. Printing Office, 1969 (Reprinted by The Acoustical Society of America, 1993).

2. A.W. Leissa, "On a Curve Veering Aberration" Journal of Applied Mathematics and Physics (ZAMP), Vol. 25, pp. 99-111, 1974.

3. J. Tsai, "Further Investigation of Curve Veering Phenomena", Ph.D. Dissertation, Ohio State Univ., 1993.

Stationary Random Vibration of Continuous Systems

Andrew Y. T. Leung
School of Engineering, Manchester University, M13 9PL, UK
Andrew.leung@man.ac.uk

For a continuous member under stationary random excitation which is time and spatially correlated, the number of spatial and time co-ordinates is doubled. An Euler beam is taken as an example. The Fourier transformed governing equation is a fourth order partial differential equation (PDE) in the two correlated spatial co-ordinates. Methods to solve this PDE and to integrate over the frequency to give the standard deviations are suggested.

Investigating the Limit of Turbomachinery Blade Modelling with Linear Pretwist

C. W. Lim[1] and S. Kitipornchai[2]

[1] *Department of Mechanical Engineering, The University of Hong Kong, Pokfulam Road, Hong Kong*

[2] *Department of Civil Engineering, The University of Queensland, Brisbane, Queensland 4072, Australia*

1. Introduction

Structures with an initial angle of pretwist have been widely used in many engineering applications ranging from huge civil structures to minute components of micro-electro-mechanical systems, commonly known as MEMS. Recent development in MEMS has indicated that the size of a turbine or a motor can be reduced to the size smaller than the diameter of a human hair. As such, the structural integrity and performance of the turbine or motor blades are critical. Precise modelling of turbomachinery blades is becoming more demanding.

Vibration and buckling analysis of turbomachinery blades has had a considerable history of research both in theory and experiment [1-4]. Turbomachinery blades were once modelled as beams with an initial angle of pretwist. However, actual turbomachinery blades do not always feature a large length-to-width aspect ratio thus rendering a pretwisted beam model unsatisfactory. Research in plate and shell modelling of blades were conducted after the eighties [2-8] in experiments and using the finite element method [2-4]; and also employing an energy method with admissible polynomial shape functions [5-8]. Although accurate vibration frequencies and greater numerical efficiency as compared to the finite element method have been reported, the mathematical models in these analyses are only valid for plates or shallow shells with a small angle of pretwist. Noting that a turbomachinery blade normally features a large angle of pretwist ($> 45°$), the plate and shallow shell models are certainly inadequate.

In this study, a natural orthogonal twisting coordinate system is formulated based on curvilinear coordinate transformation. As there is no geometry discretization or approximation, exact turbine midsurface is represented in this analysis. Unlike the plate and shallow shell models [5-8], this analysis is valid for an arbitrary angle of pretwist. Furthermore, the twisting curvature is nonlinear in the direction perpendicular to the twisting axis, although the angle of pretwist is uniform or the rate of change of angle of pretwist is a constant.

2. Theory and Formulation

The midsurface of a pretwisted plate with length a, radius R, projected angle θ_o, thickness h is shown in Figs. 1 and 2. A curvilinear coordinate system tangential and perpendicular to the helix and lying in the osculating plane of $(\vec{r}, \partial\vec{r}/\partial\theta)$ is adopted. Together with the binormal vector to the helix, it forms an orthogonal coordinate system.

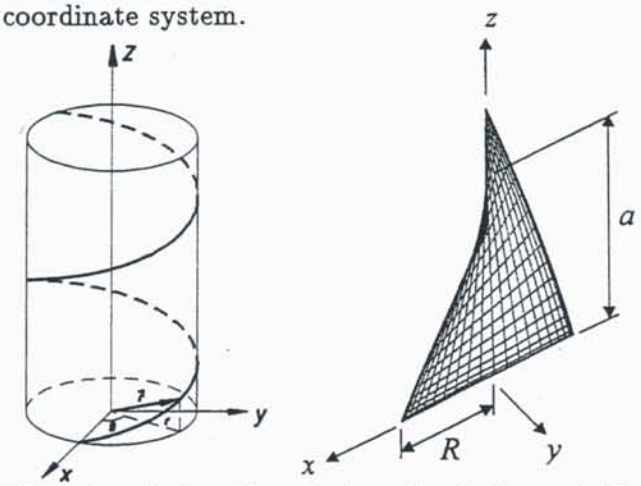

Figs. 1 and 2. Geometries of a helix and the helicoidal midsurface of a pretwisted plate with $a/2R = 1$ and $\theta_o = 45°$.

The coordinate transformation between such a helicoidal system (r,θ) and the Cartesian system $(\boldsymbol{i},\boldsymbol{j},\boldsymbol{k})$ is

$$\vec{r} = \boldsymbol{r} = r(\cos\theta\, \boldsymbol{i} + \sin\theta\, \boldsymbol{j}) + \frac{\theta}{\varphi}\, \boldsymbol{k} \qquad (1)$$

where $\varphi = \theta_o/a$ is the rate of change of projected angle θ along the z-axis.

In accordance with the theory of surfaces, a pretwisted surface as illustrated in Fig. 2 has infinite radius of curvature with respect to the coordinates of the twisting surface. However, the surface is geometrically twisted and the dimensional and dimensionless radii of twist can be derived as

$$\frac{1}{R_{r\theta}} = -\frac{\varphi}{1+\varphi^2 r^2} \quad ; \quad \frac{a}{R_{r\theta}} = -\frac{\theta_o}{1+\theta_o^2(r/a)^2} \qquad (2)$$

which is also defined as the torsion of the space curve $\boldsymbol{r}$. For $\varphi r \ll 1$ or $\varphi \ll 1/r$,

$$\frac{1}{R_{r\theta}} \approx -\varphi = -\frac{\theta_o}{a} \qquad (3)$$

The relationship of $|a/R_{r\theta}|$ with respect to r/a and θ_o is illustrated in Figs. 3 and 4. It is obvious that the twisting curvature is nonlinear and it decreases in the direction perpendicular to the axis of twist z, with the highest curvature being along the axis of twist, $r = 0$. It is interesting to note that if the angle of twist of a helix with constant r/a is increased steadily, its twisting curvature does not increase correspondingly. Rather, a maximum twisting curvature is reached at a certain θ_o and $|a/R_{r\theta}|$ decreases beyond this value. It suggests that we can not derive higher twisting curvature of a helix by increasing the angle of twist. Upon differentiating $|a/R_{r\theta}|$ with respect to θ_o and setting it to zero, the maximum twisting curvature

$$\left|\frac{a}{R_{r\theta}}\right|_{max} = \frac{\theta_o}{2} \tag{4}$$

occurs at

$$\theta_o|_{|a/R_{r\theta}|=max} = \frac{a}{r} \tag{5}$$

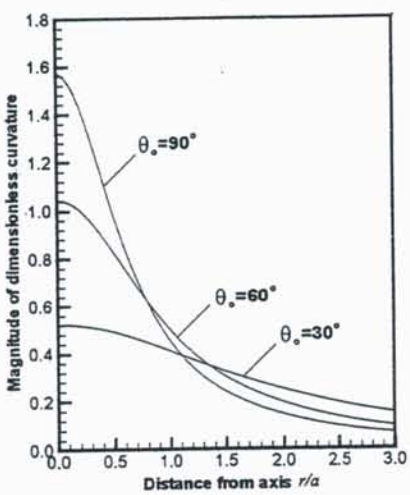

Fig. 3. Large nonlinear $|a/R_{r\theta}|$ for constant θ_o.

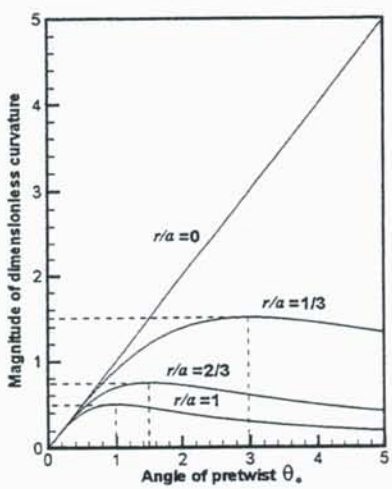

Fig. 4. Large nonlinear $|a/R_{r\theta}|$ for constant r/a.

From Fig. 3, it is obvious there exists two inherent approximations in assuming $\frac{1}{R_{r\theta}} \approx -\varphi \approx -\tan\varphi$ [5-8], the first being $\varphi \approx \tan\varphi$ and the second $\varphi r \ll 1$. An error analysis shows that an approximately 10% error will incur for $\theta_o = 30°$ according to the first assumption while for the second assumption, $\theta_o(r/a) = 0.26 \ll 1$ for $r/a = 0.5$ (aspect ratio 1) is also far less than satisfactory.

Let the orthogonal displacement components be u_r, u_θ in the osculating plane and and u_b in the binormal direction, the normal and shear strains can be expressed as

$$\epsilon_{rr} = \frac{\partial u_r}{\partial r} \quad ; \quad \epsilon_{\theta\theta} = \frac{1}{h_\theta}\frac{\partial u_\theta}{\partial \theta} + \frac{r u_r}{h_\theta^2} \tag{6a,b}$$

$$\gamma_{r\theta} = \frac{\partial u_\theta}{\partial r} - \frac{r u_\theta}{h_\theta^2} + \frac{1}{h_\theta}\frac{\partial u_r}{\partial \theta} - \frac{2u_b}{\varphi h_\theta^2} \tag{6c}$$

$$\kappa_{rr} = -\frac{3}{2\varphi h_\theta^2}\frac{\partial u_\theta}{\partial r} + \frac{3ru_\theta}{2\varphi h_\theta^4} - \frac{\partial^2 u_b}{\partial r^2} + \frac{1}{2\varphi h_\theta^3}\frac{\partial u_r}{\partial \theta} \tag{6d}$$

$$\kappa_{\theta\theta} = -\frac{3}{2\varphi h_\theta^3}\frac{\partial u_r}{\partial \theta} - \frac{1}{h_\theta^2}\frac{\partial^2 u_b}{\partial \theta^2} - \frac{r u_\theta}{2\varphi h_\theta^4} - \frac{r}{h_\theta^2}\frac{\partial u_b}{\partial r} + \frac{1}{2\varphi h_\theta^2}\frac{\partial u_\theta}{\partial r} \tag{6e}$$

$$\tau_{r\theta} = -\frac{1}{h_\theta}\frac{\partial^2 u_b}{\partial r \partial \theta} + \frac{r}{h_\theta^3}\frac{\partial u_b}{\partial \theta} - \frac{1}{\varphi h_\theta^2}\frac{\partial u_r}{\partial r} - \frac{1}{\varphi h_\theta^3}\frac{\partial u_\theta}{\partial \theta} + \frac{r u_r}{\varphi h_\theta^4} \tag{6f}$$

where $h_\theta = (1/\varphi)\sqrt{1 + r^2\varphi^2}$.

The strain and kinetic energy components are formulated in this twisting coordinate system. For linear, elastic free vibration, the maximum strain energy in a vibratory cycle is

$$U_{max} = \left(U_s\right)_{max} + \left(U_b\right)_{max} \tag{7a}$$

$$\left(U_s\right)_{max} = \frac{6D}{h^2}\int\int_A \left[\epsilon_r^2 + \epsilon_\theta^2 + 2\nu\epsilon_r\epsilon_\theta + \frac{1-\nu}{2}\gamma_{r\theta}^2\right] h_\theta \, dr \, d\theta \tag{7b}$$

$$\left(U_b\right)_{max} = \frac{D}{2}\int\int_A \left[\kappa_r^2 + \kappa_\theta^2 + 2\nu\kappa_r\kappa_\theta + 2(1-\nu)\tau^2\right] h_\theta \, dr \, d\theta \tag{7c}$$

where U_s and U_b are the stretching and bending strain energy components. The kinetic energy is

$$T_{max} = \frac{\rho h\omega^2}{2}\int\int_A \left(U_r^2 + U_\theta^2 + U_b^2\right) h_\theta \, dr \, d\theta \tag{8}$$

where A is the pretwisted midsurface area, ρ the mass density per unit volume and ω the angular frequency.

By representing displacement components as admissible polynomial functions, the energy components can be minimized in accordance with the Ritz method to obtain the following governing eigenvalue equation

$$(\boldsymbol{K} - \lambda^2 \boldsymbol{M})\,\{C\} = \{\mathbf{0}\} \qquad (9a)$$

$$\lambda = \omega R^2 \sqrt{\frac{\rho h}{D}} \qquad (9b)$$

where the eigenvalue λ represents the nondimensional frequency parameter.

3. Discussion

It has been shown that the assumption of constant twisting curvature $1/R_{x\theta} = -\tan\varphi$ for a pretwisted midsurface is subjected to two restrictions and it is only valid for a small angle of pretwisted. Analytical and computational free natural vibration solutions based on this assumption have been presented for pretwist angles as large as $\theta_o = 45°$ [5-8]. However, no analysis on the limits and validity of the application of that assumption has been investigated. Although finite element and experimental results are available for turbomachinery blades with $\theta_o < 60°$, there is a wide spectrum of results [1-4]. Results for $\theta_o > 60°$ are rare. An analysis using a natural twisting coordinate system to model the pretwisted midsurface, such as that presented here, is certainly necessary in providing benchmark solutions for comparison.

A comparison of solutions by various methods is presented in Table 1. In particular, an energy method assuming constant twisting curvature was employed in [5] and [6]. Apparently, discrepancy of results is larger for large φ as predicted. A detailed error analysis will follow.

Table 1: Comparison of $\lambda = \omega a(2R)\sqrt{(\rho h/D)}$ for a CFFF thin pretwisted plate with $\nu = 0.3$, $b/h = 20.0$ and $a/b = 1.0$.

ψ	Modes	Symmetric Modes					Antisymmetric Modes				
		Petricone and Sisto [1]	Beam Theory [5]	Leissa and Ewing [5]	Liew and Lim [6]	Present	Petricone and Sisto [1]	Beam Theory [5] Without C_1	Beam Theory [5] With C_1	Leissa and Ewing [5]	Liew and Lim [6]	Present
10°	1	3.48	3.344	3.453	3.4501	3.459	9.58	7.949	9.943	9.509	9.5018	8.604
	2	—	—	—	—	16.954	32.8	23.85	34.76	31.66	31.632	31.034
	3	21.4	20.38	21.10	21.089	21.491	—	—	—	—	—	33.563
20°	1	3.47	3.336	3.387	3.3838	3.345	12.0	11.34	13.24	12.16	12.158	9.711
	2	20.6	19.46	20.48	20.464	19.467	35.2	34.03	43.82	33.72	33.695	31.961
	3	27.6	—	27.32	27.311	25.925	—	—	—	64.65	64.543	56.232
30°	1	3.48	3.322	3.265	3.2627	2.923	15.0	15.42	17.23	16.08	16.065	12.106
	2	19.6	18.21	19.41	19.395	18.206	37.8	46.27	55.11	37.35	37.304	33.775
	3	27.9	—	27.94	27.931	26.229	—	—	—	65.21	65.114	63.385
45°	1	3.51	3.294	2.939	2.9364	3.011	19.3	21.99	23.71	24.35	24.336	17.035
	2	18.0	16.19	17.18	17.169	15.984	42.6	65.96	73.77	46.45	46.374	37.439
	3	28.6	—	30.56	30.536	26.895	—	—	—	66.96	66.888	63.153
1 rad	1	—	—	—	—	3.249	—	—	—	—	—	21.255
	2	—	—	—	—	14.640	—	—	—	—	—	40.538
	3	—	—	—	—	27.967	—	—	—	—	—	63.334

References

[1] R. D. Petricone and F. Sisto, *ASME J. of Eng. Power*, **93**(1) 103-112, 1971.

[2] A. W. Leissa, J. C. MacBain and R. E. Kielb *J. Sound Vib.*, **96**, 159-173, 1984.

[3] J. C. MacBain, R. E. Kielb and A. W. Leissa *ASME J. Eng. Gas Turbines Power*, **107**, 187-196, 1985.

[4] R. E. Kielb, A. W. Leissa and J. C. MacBain *I. J. Num. Meth. Eng.*, **21**, 1365-1380, 1985.

[5] A. W. Leissa and M. S. Ewing, *ASME J. of Eng. Power*, **105**, 383-392, 1983.

[6] K. M. Liew and C. W. Lim, *Comp. Meth. Appl. Mech. Eng.*, **114**, 233-247, 1994.

[7] C. W. Lim and K. M. Liew, *Acta Mechanica*, **111**, (3-4) 193-208, 1995.

[8] C. W. Lim, K. M. Liew and S. Kitipornchai, *AIAA J.*, **35**(2), 327-333, 1997.

AXISYMMETRIC VIBRATION ANALYSIS OF ROTATING ANNULAR PLATES BY A 3-D FINITE ELEMENT

Chorng-Fuh Liu
Department of Mechanical Engineering
National Sun Yat-Sen University
Kaohsiung, Taiwan, R. O. C.

Axisymmetric vibration of spinning annular disks is analyzed by a modified axisymmetric finite element in the present study. This element is based on the three-dimensional elasticity and is a modification of the conventional axisymmetric finite element by including the circumferential displacement. Therefore, axisymmetric circumferential vibration modes can be revealed, as well as the other vibration modes. The present study represents a first attempt, to the author's knowledge, to analyze the vibration of rotating annular plates by a 3-D approach.. The major differences between the conventional methods and the present one are that the rotation-induced nonzero stresses of the former are $\sigma_r, \sigma_z, \sigma_\theta$ and τ_{rz} instead of only the in-plane σ_r and σ_θ by the conventional approaches, and that all the inertial terms in the axial, circumferential and thickness directions are included in the kinetic energy in the present formulation while only transverse velocity is considered conventionally. In addition to the above, the present method is able to impose the displacement boundary condition exactly.

The formulation follows that in [1], except that the circumferential displacement is present now. So, $\gamma_{r\theta}$ and $\gamma_{z\theta}$ and their corresponding terms appear in the strain energy. The velocities in the three coordinate directions are $\dot{u} - \Omega v$, $(r+u)\Omega + \dot{v}$ and $\dot{w}$ where Ω is the rotational speed of the plate. The rotation-induced stresses are derived from Hamilton's principle and the finite element method by solving the obtained matrix equation with the time-dependent terms dropped. Integration of the products of the induced stresses and the nonlinear strains produces the geometric matrix [G] and we then end up with the system equation as follows,

$$[M]\{\ddot{U}\} + [C]\{\dot{U}\} + ([K] + [G])\{F\}$$

Since [C] can be neglected[2], the system equation, after dropping the forcing term {F}, becomes

$$([K] + [G])\{U\} = \omega^2 [M]\{U\}$$

where ω is the natural frequency of axisymmetric vibration of the rotating annular plate. A closer examination of the above equation will show that the motion in the radial and the thickness directions are uncoupled from those in the circumferential direction and can be solved separately.

Table 1 shows the first nondimensional frequencies of transverse vibration of annular plates

with various combinations of ratios of inner-to-outer radius, radius-to-thickness ratios, boundary conditions and rotational speeds. h, a, and b are the plate thickness, outer radius and inner radius, respectively, and $\overline{\Omega}$ is the nondimensional, rotational speed of the plate. The boundary conditions used are shown in Fig. 1.

From the results shown, we may find that the most remarkable differences between the present method and a conventional one[3],which used a plate-theory-based approach with Mindlin's transverse shear deformation and rotary inertia terms considered, are: 1. The trends of $\overline{\omega}_1$ with the changing of a/h when $\overline{\Omega}$ becomes larger are different for C-F boundary condition. 2. The difference in nondimensional frequencies obtained by the two methods is getting larger for large $\overline{\Omega}$, small a/h and small b/a. 3. Results with SS3-F are quite different from those with the conventional simply supported boundary condition. It is also noteworthy that some circumferentially vibrating modes(in-plane torsional modes) are revealed and even appear as the lowest modes in some cases. Fig. 2 shows one of them.

More complete results will be shown in [4].

1. Liu,C.F. and Chen, G.T.(1995). A simple finite element analysis of axisymmetric vibration of annular and circular plates. *Int. J. Mech. Sci.* **8**, 861-871.
2. Leissa, A.W.(1984). Coriolis effects on the vibrations of rotating beams and plates. *Proc. 12th Southeast Conf. Theoret. Appl. Mech.*, 508-513.
3. Sinha, S.K.(1987). Determination of natural frequencies of a thick spinning disk using a numerical Rayleigh-Ritz's trial function. *J. Acoust. Soc. Am.*, **81**, 357-369.
4. Liu, C.F., Lee, J.F. and Lee, Y.T.(1999). Axisymmetric vibration analysis of rotating annular plates by a 3-D finite element. *Int. J. Solids Struc.*(in revision).

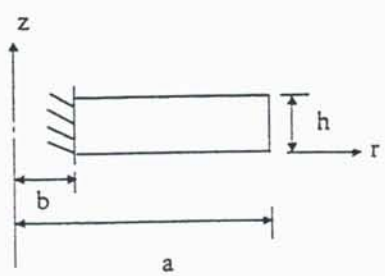

C-F

Fig. 1 : Boundary Conditions

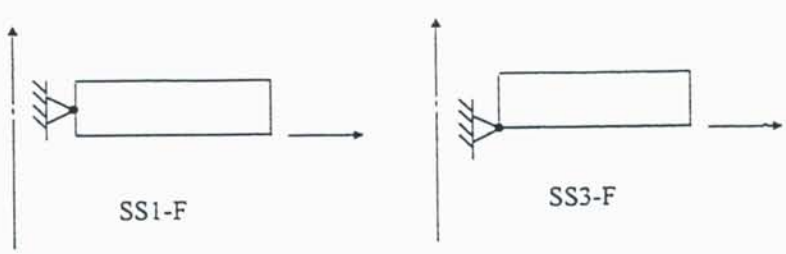

$\overline{\Omega}$	a/h / B.C.	b/a=0.1 5	10	20	50	b/a=0.25 5	10	20	50	b/a=0.5 5	10	20	50	
	C-F	3.950*	4.167	4.225	4.241	5.455	5.747	5.825	5.842	11.61	12.65	12.97	13.03	present
						5.56	5.76		5.83	11.97	12.71		13.02	Sinha 1987
0	SS1-F	3.208*	3.392	3.436	3.448	3.232	3.329	3.352	3.359	3.985	4.088	4.113	4.120	Present
						3.33	3.35		3.37	4.09	4.15		4.16	Sinha 1987
	SS3-F	3.505*	3.788*	3.899	3.969	4.135*	4.431	4.616	4.712	6.211	6.720	7.045	7.167	Present
	C-F	5.906*	6.163*	6.241	6.262	7.865	8.140	8.221	8.238	14.22	15.16	15.46	15.52	Present
						7.87	8.11		8.21	14.47	15.17		15.51	Sinha 1987
2	SS1-F	4.963*	5.231*	5.323	5.381	5.833	6.048	6.179	6.246	8.301	8.655	8.856	8.932	Present
						6.32	6.29		6.30	9.13	9.02		8.99	Sinha 1987
	SS3-F	5.031*	5.593*	5.737	5.818	6.088*	6.447	6.608	6.692	8.304	8.801	9.076	9.181	Present
	C-F	9.611*	9.738*	9.830	9.858	12.71*	12.78	12.84	12.85	20.25	20.93	21.20	21.26	Present
						12.33	12.65		12.81	20.21	20.83		21.23	Sinha 1987
4	SS1-F	8.277*	8.476*	8.624	8.765	10.59*	10.69	10.92	11.05	15.56	15.87	16.22	16.37	Present
						11.24	11.16		11.14	16.81	16.55		16.47	Sinha 1987
	SS3-F	7.434*	8.664*	8.921*	9.023	9.656*	10.18	10.32	10.39	12.95	13.22	13.41	13.49	Present

(To be continued)

$\overline{\Omega}$	a/h / B.C.	b/a=0.1 5	10	20	50	b/a=0.25 5	10	20	50	b/a=0.5 5	10	20	50	
	C-F		17.87*	17.56*	17.52		23.65*	23.22	23.14		35.77	35.74	35.74	present
						22.46	22.79		23.07	34.79	35.10		35.70	Sinha 1987
8	SS1-F		16.03*	15.90*	16.15		21.32*	21.19	21.32		31.68	31.76	31.93	present
						21.70	21.53		21.49	32.91	32.29		32.11	Sinha 1987
	SS3-F		15.11*	15.59*	15.67		18.69*	18.49	18.43		24.40	23.84	23.75	present
	C-F		27.67*	25.66*	25.30		36.41*	34.17	33.70		52.69	51.48	51.24	present
						33.01	33.27		33.64	50.61	50.45		51.19	Sinha 1987
12	SS1-F		25.32*	23.70*	23.79		34.03*	31.99	31.81		49.41	47.78	47.69	present
						32.33	32.08		32.00	49.21	48.21		47.91	Sinha 1987
	SS3-F		22.35*	22.44*	22.33		29.00*	27.09	26.64		39.79	35.16	34.51	present
	C-F		40.96*	34.28*	33.16*		52.59*	45.71*	44.39		71.85*	67.84	67.03	present
						43.70	43.89		44.34	66.82	66.16		66.98	Sinha 1987
16	SS1-F		38.16	32.08*	31.59*		50.98*	43.42*	42.44			64.32	63.57	present
						42.99	42.67		42.57	65.57	64.17		63.76	Sinha 1987
	SS3-F		31.15	29.64*	29.03*		43.43	36.32*	34.96			47.46	45.48	present

Table1 : Nondimensionalized frequencies of the first axisymmetric transverse vibration mode, $\overline{\omega}_1$'s, of rotating annular plates.

Fig.2: An axisymmetric circumferential vibrating mode (in-plane torsional mode), $\overline{\omega} = 6.568$, for C-F boundary condition, b/a=0.1, a/h=10 and $\overline{\Omega} = 4$ (u=w=0.0)

Time-Domain Simulations of Nonlinear, Unsteady, Aeroelastic Behavior

by

S. Preidikman*, B. Hall, and D. Mook
Department of Engineering Science and Mechanics
Virginia Polytechnic Institute and State University
Blacksburg, Virginia USA 24061

A method for simulating unsteady, nonlinear, subsonic aeroelastic behavior of an aircraft wing is described. The flowing air and deforming structure are treated as the elements of a single dynamic system, and all of the governing equations are integrated numerically, simultaneously, and interactively in the time domain. Our version of the general nonlinear, unsteady, vortex-lattice method, which is capable of simulating arbitrary subsonic maneuvers of the wing and accounts for the history of the motion, is used to predict the aerodynamic forces. A linear finite-element model of the wing, which can be derived from MSC/NASTRAN, is used to predict the deformations of the wing. A control system is also modeled in some cases. The models are coupled in such a way that the structural and aerodynamic grids can be chosen arbitrarily. The deformation of the wing is expressed as an expansion in terms of the linear free-vibration modes obtained from the finite-element model, and the time-dependent coefficients in the expansion serve as the generalized coordinates for the entire dynamic system. A predictor-corrector method is adapted to solve the equations governing the generalized coordinates. The arrangement is modular and allows independent modifications to the aerodynamic, structural, and control subsystems. The simulations are not restricted to periodic motions or simple geometries. To illustrate the technique, two examples are considered: the first uses a wing similar to those found on modern business jets and the second uses a wing similar to those found on High-Altitude, Long-Endurance (HALE) aircraft. The results clearly show that, when the speed is low, the responses to initial disturbances decay, but that the responses become more organized as the speed increases. Finally, at the onset of flutter, all of the modes, after an initial transient period, respond at the same frequency. It appears that the flutter-causing instability is a supercritical Hopf bifurcation. At and above the critical speed, the amplitudes of the responses appear to grow linearly with time initially, but then the responses become limit cycles. The amplitudes of the limit cycles grow as the speed increases, and eventually it appears that the limit cycles experience a secondary supercritical Hopf bifurcation and become unstable; their amplitudes and phases modulate. In some cases, the simulation includes a controller that responds to changes in the loads and bending moments on the wing via a distributed actuator (e.g., piezoelectric elements) that applies a distributed torque along the span of the wing to reduce the angle of attack. In the simulations, flutter is readily suppressed, but peak gust loads are only marginally reduced.

* Currently, Profesor de Ingeniería Mecánica, La Universidad Nacional de Río Cuarto, Río Cuarto, Provincia de Córdoba, Argentina

Some Problems in Applying the Plate and Shell Theories to Vibration Optimization of Laminated Components

Yoshihiro Narita
Department of Mechanical Engineering
Hokkaido Institute of Technology
7-15 Maeda, Teine-ku, Sapporo 006-8585, Japan
e-mail: narita@hit.ac.jp, fax: +81-11-681-3622

Laminated composite materials are known as "tailored material", because designers can consider optimization of structural behaviors by properly choosing the fiber orientation angle and layer thickness as design variables. Generally speaking, structural optimization consists of two parts, i.e., structural analysis and optimization method. When one attempts to optimize vibration behaviors of laminated plates and shells, typically maximizing the fundamental frequencies, one of various plate and shell theories is inevitably used in the structural analysis part.

In the plate and shell theories, there are discrepancies that stem from different approximations in evaluating effects of transverse shear, cross-elasticity term, strain-displacement relation and so on. As expected, natural frequencies are obtained somewhat differently depending on the theories and this difference may affect numerically the optimal solutions. Although a number of previous publications are found dealing with effects of different plate and shell theories on calculated frequencies, little attention has been given to the effect of using various theories on the optimal solution.

Some topics relating the above problem are considered in this presentation. A symmetric laminate with angle-ply $[(\theta/-\theta)_{L/4}]_S$ (θ: fiber orientation angle, L: number of plies, S: symmetric) is taken as a numerical example, and an optimal fiber angle θ_{opt} is searched to give the maximized fundamental frequency. A typical configuration is shown in Figure 1 in the case of shallow shell.

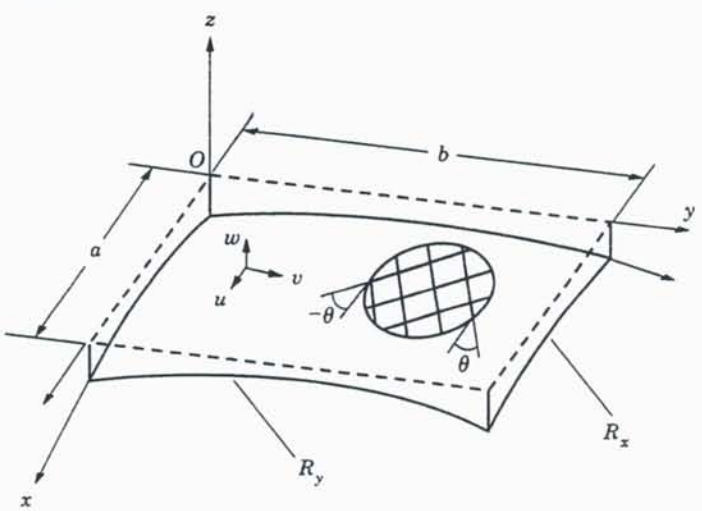

Figure 1. Laminated shallow shell and co-ordinate system.

The followings will be discussed.

(1) *Effect of the cross-elasticity terms in the optimization of laminated plates and shallow shells*

In the moment-curvature relation $\{M\}=[D]\{\kappa\}$, there are terms D_{16} and D_{26} (sometimes called, cross-elasticity stiffness) in $[D]$ which couple normal moments with twisting curvature, and the values of D_{16} and D_{26} are nonzero for angle-ply laminates. When one solves the differential equations governing vibration of laminated plates and shells, it is often desirable to neglect terms with the stiffness. To clarify the validity of this reduction, frequency equations are derived by using the Ritz approach for laminated plates and shallow shells. Two sets of natural frequencies are calculated with/without the D_{16} and D_{26} terms, and effects of the cross-elasticity terms are evaluated quantitatively.

(2) *Effect of the thickness shear in the optimization of laminated shallow shells*

The classical theory (CT) is widely accepted in the vibration analysis of laminated plates and shells, but the transverse shear deformation sometimes should be taken into account for laminated FRP composites. The first order shear deformation theory (FSDT) is relatively simple, and it can consider the thickness shear by assuming that normals to the middle surface still remain straight during bending and their rotation angles are independent. Here four types of vibration solutions are derived by using CT and FSDT, and in addition the inplane inertia effect is included or neglected in each theory. Discrepancies among the optimal fiber angles caused by using the four different solutions are clarified for an angle-ply laminated shallow shell.

(3) *Effect of different approximation in the shell theories in optimizing laminated cylindrical shells*

Unlike in the plate theories, there are different kinds of deep shell theories, such as Flügge theory, Love theory and Donnell theory, with respect to approximation in the strain-displacement relation. Calculated natural frequencies somewhat vary depending on the theories, and such effect of using different theories in optimization is not known. Analytical solutions are derived here by using the above-mentioned theories and the optimal solutions are calculated for a angle-ply laminated cylindrical shell simply supported at both ends. Then optimal fiber angles and frequencies are compared each other to study the effect of using the different shell theories in the vibration optimization.

Verification of Chaotic Oscillations of a Post-buckled Beam with a Concentrated Mass

Ken-ichi Nagai
Department of Mechanical Engineering,
Gunma University, 1-5-1 Tenjincho, Kiryu, Gunma, 376-8515, JAPAN
Takao Yamaguchi
SUBARU Research Center Co, Ltd., Ota, Gunma, 373-0026, JAPAN
Hakubo Hattori and Hisashi Suzuki
Gunma University, Kiryu, Gunma, 376-8515, JAPAN

1. Introduction

This paper presents detailed analytical results for chaotic oscillations of a post-buckled beam carrying a concentrated mass to compare with the experimental results[5]. Governing equation of the beam with both ends clamped includes the effects of an initial constraint and an initial imperfection.

Introducing the mode shape function multiplied with truncated power series and trigonometric function to the Galerkin procedure, ordinary differential equation with a multiple-degree of freedom system is reduced. Steady state response is calculated by the harmonic balance method. Detailed numerical results of the chaotic response are obtained by the Runge-Kutta-Gill method. The analytical results agreed fairly well to the experimental results.

2. Governing Equation of Motion

As shown in Figure 1, the post-buckled beam is excited laterally by a periodic acceleration. $w(\xi,\tau)$, $w_0(\xi)$ and $u(\xi,\tau)$ denote the non-dimensional total deflection, initial deflection and axial displacement, respectively. The non-dimensional governing equation is given by

$$[1+\beta\delta(\xi-\xi_0)]w_{,\tau\tau}+(w-w_0)_{,\xi\xi\xi\xi}-[-u_c+\frac{1}{2}\int_0^1 (w_{,\xi}^2-w_{0,\xi}^2)d\xi]w_{,\xi\xi}$$
$$-p_s-q_s\delta(\xi-\xi_0)-[p_d+q_d\delta(\xi-\xi_0)]\cos\omega\tau=0 \qquad (1)$$

where, $\delta(\xi-\xi_0)$ is the Kronecker's delta function. β is mass ratio of the concentrated mass to the whole mass of the beam. u_c is the non-dimensional displacement of axial compression. p_s and p_d are the non-dimensional intensities of distributed loads. q_s and q_d are the non-dimensional concentrated loads. ω and τ are the non-dimensional exciting frequency and time, respectively.

3. Procedure of Analytical Solution

To satisfy the clamped edges of the beam, we introduced the mode shape function as;

$$[w, w_0]=\sum_j [b_j(\tau), a_j]\zeta_j(\xi),\ (j=1,2,3,...)$$
$$\zeta_j(\xi)=f(\xi)e_j(\xi),\ f(\xi)=\xi^2-2\xi^3+\xi^4,\ e_j(\xi)=\cos(j-1)\pi\xi \qquad (2)$$

Using foregoing function, the Galerkin method reduces the governing equation (1) to a coupled nonlinear differential equation[6]. Omitting the dynamical terms in the equation, the static deflection can be obtained. Using the linear natural frequency $\tilde{\omega}_i$ and the corresponding natural modes of vibration $\tilde{\zeta}_i$, a set of coupled ordinary equations with a linear normal coordinate $\tilde{b}_i$ can be transformed to;

$$\tilde{b}_{i,\tau\tau}+2\varepsilon_i\tilde{\omega}_i\tilde{b}_{i,\tau}+\tilde{\omega}_i^2\tilde{b}_i+\sum_j\sum_k\tilde{D}_{ijk}\tilde{b}_j\tilde{b}_k+\sum_j\sum_k\sum_l\tilde{E}_{ijkl}\tilde{b}_j\tilde{b}_k\tilde{b}_l-p_d\tilde{G}_i\cos\omega\tau=0 \quad (i,j,k,l=1,2,3,...) \qquad (3)$$

where, linear damping term is introduced. The chaotic responses of the beam are confirmed by the Fourier spectrum analysis, the Poincaré projection onto phase plane and the maximum Lyapunov exponent. Moreover, interactions of the mode of vibration generated in the chaos are discussed for the location of the concentrated mass on the beam.

4. Experimental Procedure

A test beam is cut from a duralumin sheet of thickness $h = 0.506$ mm to breathe $b = 30.0$ mm and length $L = 180$ mm. To increase an effect of damping to the beam, vinyl tapes are pasted to the both surfaces of the beam. To get the post-buckled form of the beam, the initial displacement is controlled by the thermal elongation of the beam to the base frame. Initial deflection of the beam is found to be less than 3 percent of the fundamental mode of static deformation. The beam was excited periodically by an electro-magnetic vibrator. Measuring the relative deflection of the beam to the base frame by two laser displacement sensors, the chaotic responses of the beam are recorded[5].

5. Results and Discussions

To find the regions of chaotic oscillations are excited, frequency response curves are examined. Figure 2 shows both experimental and analytical results. In the figure, the regions of the chaotic vibration are assigned by the symbol $C_{m,n}$. Subscripts m and n denotes the generated mode of vibration and the type of resonance, respectively. For example, $C_{1,1/2}$ means the chaos bifurcated from the subharmonic resonance of 1/2 order cooperated mainly with the fundamental mode of vibration. $(m,n:)$ denotes the steady-state resonance response. In Figures 3, the Poincaré maps of the chaos are recorded. The analytical results show the figure in each phase delay θ degree measured from the maximum amplitude of the exciting force. Both results coincide very well. Changing the position of the concentrated mass on the beam, the Lyapunov exponents λ_r (r=1,2,3) are calculated in the equation (3). Positive Lyapunov exponent indicates the chaos. The variations of the Lyapunov exponents in the frequency domain are shown in Figure4. As the concentrated mass traverses from the end to the midspan of the beam, the positive maximum Lyapunov exponent also degreases. Changing the excitation amplitude p_d, instability regions of chaotic responses are obtained as shown in Figure 5. On the higher frequency of the instability boundary, the chaotic response and the steady state response are mixed in the narrow region. It exists so-called 'the window of the chaos'.

6. Conclusion

The analytical results are examined to the experimental results for the chaotic oscillations of the post-buckledbeam with the concentrated mass. The main results can be summarized as follows:

(1) The chaos bifurcates from each resonance response of subharmonic resonance both of 1/2 and 1/3 orders, super harmonic resonance of 2nd order and ultra subharmononic resonance of 5/4 order.
(2) Chaotic attractor and the Lyapunov exponents of the system are well simulated by adopting more than three fundamental modes of vibration.
(3) The wide instability region of the chaos generated in the frequency range is corresponding to the response of subharmonic resonance of both 1/2 and 1/3 orders.
(4) The concentrated mass on the beam decreases both the modes of vibration and the Maximum Lyapunov exponent contributed to the chaos.

References

(1) Nagai, K., "Nonlinear vibrations of a shallow arch under periodic lateral force (Theory)", *Trans. Jpn. Soc. Mech. Eng.*, (in Japanese), **51**(471), 1985, 2820-2827.
(2) Nagai, K., "Nonlinear vibrations of a shallow arch under periodic lateral force (2nd Report, Experiment)", *Trans. Jpn. Soc. Mech. Eng.*, (in Japanese), **52**(484), 1986, 3047-3054.
(3) Nagai, K. ,"Experimental study of chaotic vibration of a clamped beam subjected to periodic lateral forces" , *Trans. Jpn. Soc. Mech. Eng.*, (in Japanese), **56**(525), 1990, 1171-1177.
(4) Nagai, K., Yamaguchi, T., Tanifuji, K. and You, H. , "Experiment on chaotic vibrations of a cantilevered beam deformed by a stretched cable", *Trans. Jpn. Soc. Mech. Eng.*, (in Japanese), **60**(569), 1994, 3-9.
(5) Nagai, K. and Yamaguchi, T., "Chaotic vibrations of a post-buckled beam carrying a concentrated mass (1st Report, Experiment)",*Trans. Jpn. Soc. Mech. Eng.*, (in Japanese), **60**(579), 1994, 3733-3740.
(6) Yamaguchi, T. and Nagai, K., "Chaotic vibrations of a post-buckled beam carrying a concentrated mass (2nd Report, Theoretical Analysis)", *Trans. Jpn. Soc. Mech. Eng.*, (in Japanese), **60**(579), 1994, 3741-3748.
(7) Yamaguchi, T. and Nagai, K.,"Chaotic Vibrations of a Cylindrical Shell-Panel with an In-Plane Elastic-Support at Boundary", Nonlinear Dynamics, **13**-3,1997, 259-277.
(8) Nagai, K., Kasuga, K., Kamada, M., Yamaguchi, T. and Tanifuji, K., Experiment on Chaotic Oscillations of a Post-Buckled Reinforced Beam Constrained by an Axial Spring, JSME International J.,**41**-3,1998, 563-569.

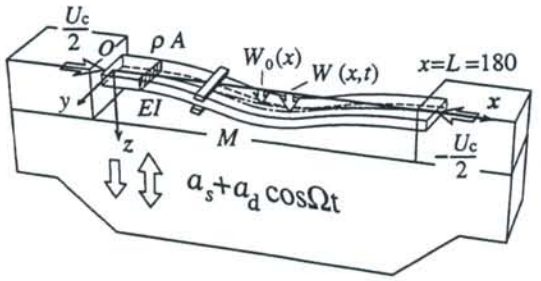

Figure 1 Post-buckled beam with concentrated mass

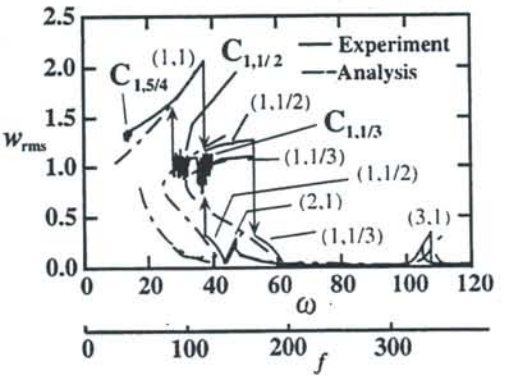

Figure 2 Frequency response curve $u_c = 50, p_d = 500, \xi_0 = 0.4$

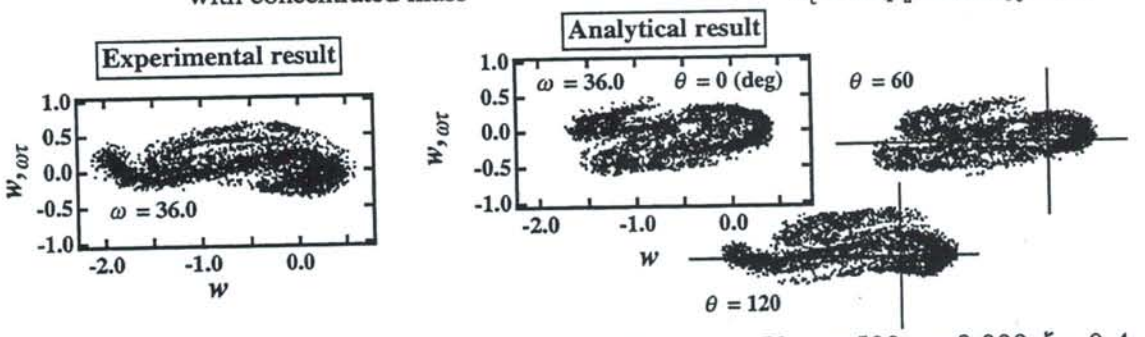

Figure 3 Poincare map of chaotic response $C_{1,1/3}$, $u_c = 50, p_d = 500, \varepsilon_i = 0.009, \xi_0 = 0.4$

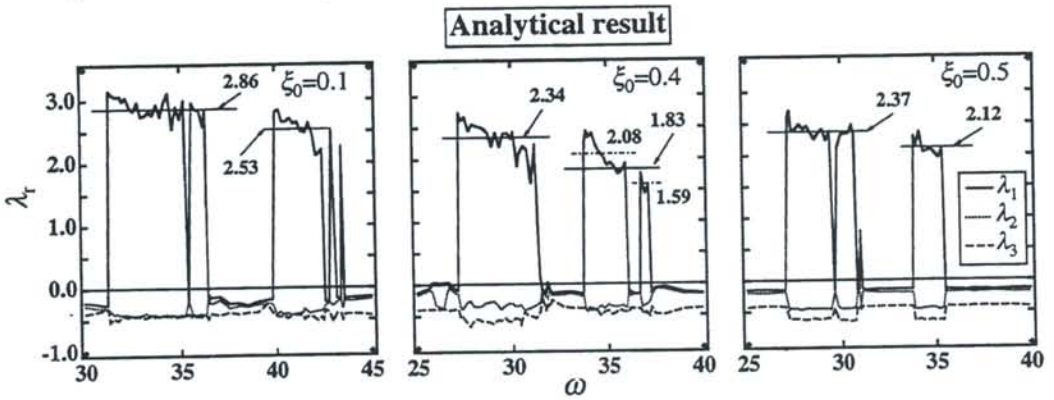

Figure 4 Lyapunov exponent in the different position of the concentrated mass $u_c = 50, p_d = 500, \varepsilon_i = 0.009, \Delta\omega = 0.2$

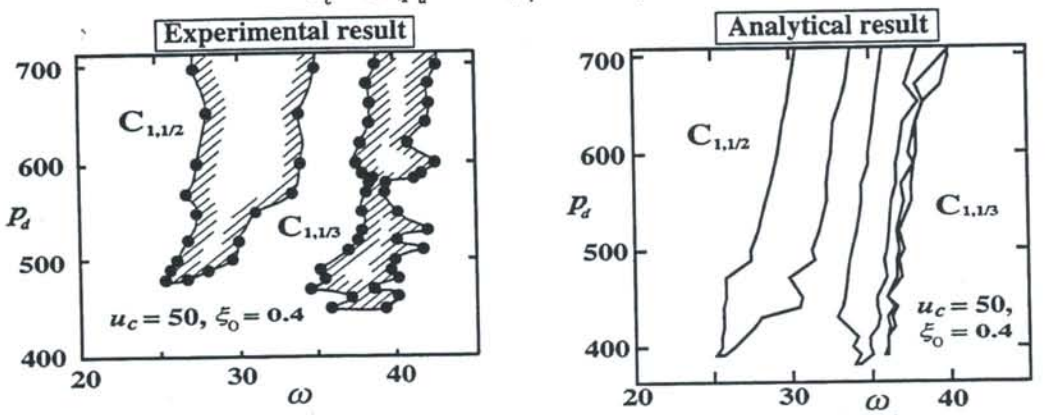

Figure 5 Instability regions of chaos, $u_c = 50, \varepsilon_i = 0.009$

Stability of "Stiff" Gravity Pendulums and of Centrifugal Pendulums.

S. Naguleswaran
Department of Mechanical Engineering, University of Canterbury, Christchurch, New Zealand.

Summary

Consider an uniform beam OB pinned or clamped at the end O and with a rigid pendulum bob attached to the end B. The beam is of flexural rigidity EI, mass per unit length m and length L. The bob is of mass M_e and of moment of inertia J about the centre of mass G which is at a distance e from B. e is considered positive if OG > OB and negative if OG < OB. The vibration and stability of this unit in a uniform gravity field (gravity pendulum) and in a centrifugal field (centrifugal pendulum) are discussed in this paper.

Euler-Bernoulli theory of bending and d'Alembert's principle are used to derive the differential equation of motion. If O is chosen as the origin and if $T(x)$ is the tension at abscissa x, then for the gravity pendulum, i.e. the unit in vertical 'hanging' position under gravity,

$$T(x) = (M_e + mL)g - mgx,$$

and for the centrifugal pendulum, i.e. if the unit is attached radially in outward configuration to a hub of radius R_o and rotating at a speed p,

$$T(x) = M_e p^2(R_o + L + e) + mp^2(R_o + L/2)L - mp^2(R_o + x/2)x.$$

For free vibration of the unit at frequency ω (for centrifugal pendulum vibrations normal to the plane of rotation i.e. out-of-plane vibrations) the amplitude of vibration $y(x)$, bending moment $M(x)$ and shearing force $Q(x)$, then one has

$$M(x) = EId^2y(x)/dx^2, \qquad Q(x) = -dM(x)/dx + T(x)dy(x)/dx, \quad dQ(x)/dx + m\omega^2 y(x) = 0.$$

The boundary conditions at O are:

$$\text{if clamped: } y(0) = 0 = dy(0)/dx, \qquad \text{or if pinned: } y(0) = 0 = EId^2y(0)/dx^2$$

and the boundary conditions at the end B are:

$$Q(L) - M_e\omega^2[y(L) + edy(L)/dx] = 0, \qquad e[Q(L) - T(L)dy(L)/dx] - M(L) + J\omega^2 dy(L)/dx = 0.$$

Introduction of the dimensionless variables $X = x/L$, $Y(X) = y(x)/L$, operators $D^n = d^n/dX^n$ and $M(X) = m(x)L/EI$, $Q(X) = Q(x)L^2/EI$, $\beta(X) = T(x)L^2/EI$, $\Omega^2 = m\omega^2L^4/EI$ will result in

$$M(X) = D^2Y(X), \qquad Q(X) = -D^3Y(X) + \beta(X)D(X),$$

$$D^4Y(X) - D[\beta(X)DY(X)] - \Omega^2Y(X) = 0.$$

The dimensionless mode shape differential equation is subject to the boundary conditions,

if clamped at O: $Y(0) = 0$ & $DY(0) = 0$, or if pinned: $Y(0) = 0$ & $D^2Y(0) = 0$ and

$$D^3Y(1) + [\delta\Omega^2\varepsilon - \beta(1)]DY(1) + \delta\Omega^2Y(1) = 0 \quad \text{and} \quad \varepsilon Y^3(1) + D^2Y(1) - \Delta\Omega^2DY(1) = 0,$$

in which $\varepsilon = e/L$, $\delta = M_e/mL$, $\Delta = J/mL^3$.

For the gravity pendulum

$$\beta(X) = (\delta + 1)\gamma - \gamma X, \qquad \text{in which } \gamma = mgL^3/EI,$$

and for the centrifugal pendulum

$$\beta(X) = \delta\eta^2(1+\rho+\varepsilon) + \eta^2(\rho+1/2) - \eta^2(\rho+X/2)X, \qquad \text{in which } \rho = R_o/L,\ \eta^2 = mp^2L^4/EI.$$

The mode shape differential equation to be solved is

$$D^4Y(X) - b_oD^2Y(X) - b_1D[XDY(X)] - b_2D[X^2Y(X)] - \Omega^2Y(X) = 0.$$

For the gravity pendulum

$$b_o = (1+\delta)\gamma, \quad b_1 = -\gamma, \text{ and } b_2 = 0$$

while for the for the centrifugal pendulum

$$b_o = \delta\eta^2(1+\rho+\varepsilon) + \eta^2(\rho+1/2), \quad b_1 = -\eta^2\rho \quad \text{and} \quad b_2 = -\eta^2/2.$$

Details of the solution of the differential equation by the method of Frobenius will be submitted in the main paper presentation where it will be shown that the solution is $Y(X) = \Sigma C_cY(X,c)$, where C_c, $(c = 0, 1, 2, 3)$ are the four constants of integration and the coefficients of the polynomials $Y(X,c) = \Sigma a_{n+1}(c)X^{c+n}$ $(n = 0, 1, 2 \ldots\ldots\infty)$ are chosen with $a_1(c) = 1$ and the recursive relationship (conditional to a coefficient being zero if the subscript is zero or negative) is

$$(c+n)(c+n-1)(c+n-2)(c+n-3)a_{n+1}(c) = b_o(c+n-2)(c+n-3)a_{n-1}(c) + b_1(c+n-3)^2a_{n-2}(c)$$
$$+ [b_2(c+n-4)(c+n-3) + \Omega^2]a_{n-3}(c).$$

The derivatives of the four functions are 'similar' polynomials obtained by differentiation of individual terms. The polynomials and derivatives converged.

The frequency equation is of the form, $a_{11}a_{22} - a_{12}a_{21} = 0$, in which if O is clamped,

$a_{11} = D^3Y(1,2) + [\delta\Omega^2\varepsilon - \beta(1)]DY(1,2) + \delta\Omega^2Y(1,2)$, $a_{22} = \varepsilon D^3Y(1,2) + D^2Y(1,2) - \Delta\Omega^2DY(1,2)$,

$a_{12} = D^3Y(1,3) + [\delta\Omega^2\varepsilon - \beta(1)]DY(1,3) + \delta\Omega^2Y(1,3)$, $a_{21} = \varepsilon D^3Y(1,3) + D^2Y(1,3) - \Delta\Omega^2DY(1,3)$,

or if O is pinned,

$a_{11} = D^3Y(1,1) + [\delta\Omega^2\varepsilon - \beta(1)]DY(1,1) + \delta\Omega^2Y(1,1)$, $a_{22} = \varepsilon D^3Y(1,1) + D^2Y(1,1) - \Delta\Omega^2DY(1,1)$,

$a_{12} = D^3Y(1,3) + [\delta\Omega^2\varepsilon - \beta(1)]DY(1,3) + \delta\Omega^2Y(1,3)$, $a_{21} = \varepsilon D^3Y(1,3) + D^2Y(1,3) - \Delta\Omega^2DY(1,3)$.

The roots of the frequency equation were determined by detecting sign changes in $(a_{11}a_{22} - a_{12}a_{21})$ followed by an iterative procedure. Details will be included in the main paper presentation.

The parameters (common to both pendulums) which influence the frequencies are the mass parameter δ, moment of inertia parameter Δ and centre of mass offset parameter ε. The additional parameter for the gravity pendulum is the gravity parameter γ and for the centrifugal pendulum the additional parameters are the root offset parameter ρ and the rotational speed parameter η.

For the two pendulums, the first three values of $\Omega^{1/2}$ tabulated for $\varepsilon = -0.1, 0$ & 0.1 and for various combinations of the system parameters will be shown in the main paper presentation.

For the gravity pendulum it was found that for negative values of ε, increase in γ results in decrease in Ω_1, and for a critical value of γ, $\Omega_1 = 0$, i.e. the system is on the threshhold of instability although the distribution of tension in the beam is wholly tensile. The critical γ_c is

independent of Δ but depends on δ and ε. Tables of γ_c for combinations of δ and ε will be presented in the main paper. Also presented will be Tables of ε_c for combinations of δ and γ and of δ_c for combinations of γ and ε.

The frequency equations of the centrifugal pendulum exhibited trends 'similar' to those of the gravity pendulum. Here, in place of γ, there are η and ρ and so there is an additional phenomenon, *viz* a 'tuned' frequency when a natural frequency coincided with the rotational speed, i.e. $\Omega_l = \eta$. This is similar to whirling of shafts. The 'tuned' rotational speeds η_t depend on δ, Δ, ρ and ε. 'Tuned' frequencies will not occur if $\Delta = 0$. Tables of the first η_t will be included in the main paper presentation.

For the centrifugal pendulum it was found that for negative values of ε, increase in η results in decrease in Ω_l and for a critical value of η, $\Omega_l = 0$, i.e. the system is on the threshhold of instability although the distribution of tension in the beam is wholly tensile. The critical η_c is independent of Δ but depends on δ, ρ and ε A Table of η_c for combinations of δ, η and ε, a Table of ε_c for combinations of δ, ρ and η and a Table of δ_c for combinations of η, ρ and ε will be discussed in the main paper presentation.

Vibrations of the centrifugal pendulum in the plane of rotation (in-plane vibrations) will be 'similar' to that of out-of-plane vibrations.

For both pendulums, Δ had a greater influence on the frequencies compared to δ. An apparent crossover of the first and second mode frequencies will be discussed.

For the case when the pendulums are clamped at O, it was found that for some combinations of the system parameters, the second mode was nodeless.

The inherent limitation on the precision in the VAX computer admitted calculations to only certain ranges of the system parameters. Most of the results for presentation were obtained with double precision. Some needed computation in quadruple precision (e.g the range $500 < \gamma < 1000$) and for some even this was insufficient (e.g $\eta > 15$ and $\rho > 2$)

It was possible to calculate only the first value of a parameter for the condition of onset of instability (i.e when a natural frequency is zero) and the first value of 'tuned' rotational speed although second and higher values exist.

Reviews and comments on several references are made in the main paper. Some of the references are listed below.

Selected References

1. B. SCHAFER 1985 *Ingenieur-Archiv* **55**, 66-80. The vibrations of a gravity loaded clamped-free beam.
2. S. NAGULESWARAN 1996 *Journal of Sound and Vibration* **191**, 1-14. The vibration of a 'stiff' gravity pendulum with a particle bob.
3. C. H. J. FOX and J. S. BURDESS 1979 *Journal of Sound and Vibration* **65**, 151-158. The natural frequencies of a thin rotating cantilever with offset root.
4. A. D. WRIGHT, C. E. SMITH R, W. THRESHER and J. L. C. WANG 1982 *Journal of Applied Mechanics* **49**, 197-202. Vibration modes of centrifugally stiffened beams.
5. S. NAGULESWARAN 1994 *Journal of Sound and Vibration* **175**, 613-624. Lateral vibration of a centrifugally tensioned Euler-Bernoulli beam.

On the Discretization of Spatially Continuous Systems with Quadratic and Cubic Nonlinearities

Ali H. NAYFEH
Department of Engineering Science and Mechanics, MC 0219
Virginia Polytechnic Institute and State University
Blacksburg, Virginia 24061

Methods for the study of weakly nonlinear continuous (distributed-parameter) systems are discussed. Approximate solution procedures treating reduced-order models of systems with quadratic and cubic nonlinearities obtained with the Galerkin procedure are contrasted with direct application of the method of multiple scales to the governing partial-differential equations and boundary conditions. By means of several examples, it is shown that low-order reduced models of nonlinear continuous systems can lead to erroneous results.

Lacarbonara, Nayfeh, and Kreider carried out an experiment to validate the suitability of reduction methods for studying nonlinear vibrations of distributed-parameter system. They analyzed nonlinear planar vibrations of a clamped-clamped buckled beam about its first post-buckling configuration. They investigated the case of primary resonance of the nth mode of the beam, when no internal resonances involving this mode are active. They obtained approximate solutions by applying the method of multiple scales to a single-mode model discretized via the Galerkin procedure and by directly attacking the governing integro-partial-differential equation and boundary conditions with the method of multiple scales. Frequency-response curves for the case of primary resonance of the first mode were generated using both approaches for several buckling levels and were contrasted with experimentally obtained frequency-response curves for two test beams. For high buckling levels above the first crossover point of the beam, the computed frequency-response curves are qualitatively as well as quantitatively different. The experimentally obtained frequency-response curves for the directly excited first mode are in agreement with those obtained with the direct approach and in disagreement with those obtained with the single-mode discretization approach.

A method for producing reduced-order models that overcome the shortcomings of the Galerkin procedure is discussed. Treatment of these models yields results in agreement with those obtained experimentally and those obtained by directly attacking the continuous system. Convergence of the reduced-order models as the order increases is also discussed.

Key words: Buckled beam, experiment, Galerkin method, direct approach, method of multiple scales.

On the Displacement Functions in Vibration Analysis of FRP Laminated Composite Thick Plates

Yoshiki OHTA
Department of Mechanical Engineering
Hokkaido Institute of Technology, Sapporo, JAPAN

Introduction

Recently Fiber Reinforced Plastics (FRP) are being increasingly used in the structural applications due to the technical merits of high strength-weight ratio and stiffness-weight ratio of the FRP materials. It is known that anisotropic property in FRP materials considerably affects the dynamic characteristics of structural elements such as plates and shells, and thus a large number of theoretical and experimental studies have been conducted on the dynamic problems of FRP composite laminates. In most of the theoretical analyses, the FRP laminated plate is macroscopically modeled as a thin plate of general anisotropy, and is analyzed by using Classical Plate Theory (CPT)[1] or First-order Shear Deformation Theory (FSDT)[2-4]. Reddy[5] also has proposed Higher-order Shear Deformation Theory (HSDT).

The purpose of this paper is to examine the assumptions of displacement functions employed in vibration analysis of FRP laminated thick plates. For this purpose, the strain and kinetic energies of a cross−ply laminated plate are evaluated analytically, and the displacement functions of the rectangular plate, which is simply-supported at all edges, are expanded into the polynomial forms of arbitrary order with respect to thickness coordinate. A frequency equation is derived by using the energy approach of minimizing a Lagrangian. In numerical calculations, natural frequencies, stress distributions along the thickness and modal damping ratios are obtained for various plates with different stacking sequence and thickness ratios by using sets of different displacement functions. Then not only the validity of the assumption of displacements but also the applicability of the plate theories applied to the FRP laminated plate are discussed by comparing the numerical results.

Analysis

We consider a N− layer laminated rectangular plate ($a \times b \times H$), which is simply-supported at all edges. In the present analysis, the Cartesian coordinate system (x, y, z) is taken at the middle surface of the laminated plate. The maximum displacements (vibration amplitudes) of the plate in the x, y and z directions are denoted by u, v and w, respectively.

Maximum strain and kinetic energies of the plate are expressed as follows :

$$U_{\max} = \frac{1}{2}\int_V \left(\sigma_x \varepsilon_x + \sigma_y \varepsilon_y + \sigma_z \varepsilon_z + \tau_{yz}\gamma_{yz} + \tau_{zx}\gamma_{zx} + \tau_{xy}\gamma_{xy}\right) dV$$
$$T_{\max} = \frac{1}{2}\int_V \rho_m \omega^2 \left(u^2 + v^2 + w^2\right) dV \qquad (1)$$

where ρ_m is a mean mass density of FRP material and ω means a circular frequency.

For the generality of the present analysis, the following nondimensional quantities are introduced :

$$\xi = \frac{x}{a},\quad \varsigma = \frac{y}{b},\quad \eta = \frac{z}{H/2},\quad h = \frac{H}{a},\quad l = \frac{b}{a}$$
$$\bar{u} = \frac{u}{H},\quad \bar{v} = \frac{v}{H},\quad \bar{w} = \frac{w}{H},\quad \lambda^2 = \frac{\rho_m H a^4 \omega^2}{D_0} \tag{2}$$

where D_0 means a reference bending stiffness.

For cross-ply laminated plates simply-supported at all edges, displacements can be assumed as follows :

$$\bar{u} = \cos m\pi\xi \sin n\pi\varsigma \sum_{i=1}^{I} U_i \eta^{i-1}$$
$$\bar{v} = \sin m\pi\xi \cos n\pi\varsigma \sum_{i=1}^{I} V_i \eta^{i-1} \tag{3}$$
$$\bar{w} = \sin m\pi\xi \sin n\pi\varsigma \sum_{j=1}^{J} W_j \eta^{j-1}$$

where m and n are half wave numbers in x and y direction, respectively, and U_i, V_i and W_j are unknown coefficients.

By substituting Eqs.(2) and (3) into Eq.(1), and minimizing the Lagrangian ($L = T_{max} - U_{max}$) with respect to the unknown coefficients U_i, V_i and W_j for a stationary value,

$$\frac{\partial L}{\partial U_i} = \frac{\partial L}{\partial V_i} = \frac{\partial L}{\partial W_j} = 0 \qquad (i = 1,2,\cdots,I\,;\, j = 1,2,\cdots,J) \tag{4}$$

a following frequency equation is derived :

$$\left| [K] - \lambda^2 [M] \right| = 0 \tag{5}$$

The determinant of the coefficient matrix of Eq.(5) is set equal to zero, which yields frequency parameters, and substituting each eigenvalue back into Eq.(5) gives the corresponding unknown coefficients (vibration mode) in the usual manner. Modal damping ratios are also obtained form the complex frequency parameters by introducing complex elastic constants with loss factors.

Numerical Results

Numerical studies are carried out for cross-ply laminated square plates (l=1) with different stacking sequence and thickness ratios. In numerical calculations, frequency parameters, stress distributions and modal damping ratios of the plates are obtained by using the displacements with different I and J terms in the displacement functions [Eq.(3)]. This means that each result is calculated from the displacement functions that have polynomial forms of (I-1)-th and (J-1)-th order for in-plane and transverse displacements, respectively. A graphite/epoxy, which is highly orthotropic fiber reinforced plastics material, is chosen and the material properties used in calculations are E_1/E_2=20, G_{12}/E_2=0.65,

$G_{23}/E_2=0.5$, $\nu_{12}=0.25$, $\nu_{23}=0.25$.

Table 1 and 2 show the convergence of frequency parameters for 2-layered [0°/90°] and 3-layered [0°/90°/0°] square plates, respectively, when the number (I and J) of terms employed in displacement functions are increased, respectively. It is found for each plate from the results that frequency parameters are converged increasing the number of terms, and also that the displacement functions with the terms more than $I=4$ and $J=3$ give the converged frequencies. However, higher order functions for in-plane displacements is needed for the 2-layered, non-symmetrically laminated plates than for the 3-layered plates.

Table 1 Frequency parameters of 2-layer laminated plate [0° /90°] ($m=n=1$, $l=1$, $h=0.1$)

	$I=2$	$I=3$	$I=4$	$I=5$	$I=6$	$I=7$
$J=2$	31.39	31.31	31.19	31.14	31.12	31.12
$J=3$	31.00	30.92	30.82	30.77	30.75	30.75
$J=4$	31.00	30.92	30.82	30.77	30.75	30.75
$J=5$	31.00	30.92	30.82	30.77	30.75	30.75
$J=6$	31.00	30.92	30.82	30.77	30.75	30.75

Table 2 Frequency parameters of 3-layer laminated plate [0° /90° /0°] ($m=n=1$, $l=1$, $h=0.1$)

	$I=2$	$I=3$	$I=4$	$I=5$	$I=6$	$I=7$
$J=2$	43.34	43.34	42.30	42.30	42.28	42.28
$J=3$	43.05	43.05	42.06	42.06	42.04	42.04
$J=4$	43.05	43.05	42.06	42.06	42.04	42.04
$J=5$	43.05	43.05	42.06	42.06	42.04	42.04
$J=6$	43.05	43.05	42.06	42.06	42.04	42.04

Reference

(1) Vinson, J.R. and Sierakowski, R.L., 1986, "The Behavior of Structures Composed of Composite Materials," Martinus Nijhoff Publishers, Dordrecht.

(2) Dong, S.B. and Tso F.K.W., 1972, ASME J. Appl. Mech., Vol. 39, No. 4, pp. 1091–1097.

(3) Whitney, J.M. and Pagano, N.J., 1970, ASME J. Appl. Mech., Vol. 37, No. 4, pp. 1031–1036.

(4) Yang, P.C., Norris, C.H. and Stavsky, Y., 1966, Int. J. Solids Struc., Vol. 2, pp. 665–684.

(5) Reddy, J.N., 1984, ASME J. Appl. Mech., Vol. 51, No. 4, pp. 745-752.

VIBRATORY PHENOMENA IN ROTATING DISK-SPINDLE SYSTEMS

Robert G. Parker
Department of Mechanical Engineering
Ohio State University
206 W. 18th Ave.
Columbus, OH 43210-1107
parker.242@osu.edu

High-speed machinery applications such as turbomachinery, disk drives, rotor dynamics, cutting tools, and geared transmissions have motivated substantial research on the dynamics of spinning systems. Research on the dynamics of these and similar applications has generated two major bodies of literature on spinning systems: spinning shafts and spinning disks. Developments in these two areas have occurred largely independently of each other despite the common features deriving from the rotational effects. Virtually all of the spinning shaft vibration analyses assume that attachments to the spinning shaft are rigid. A similar majority of the spinning disk research neglects the dynamics of the supporting structure such as the spindle. This work addresses the spinning system problem wherein an elastic disk is mounted on an elastic spindle via a rigid clamp (Fig. 1). The continuing trends toward higher operating speeds and lighter, more flexible devices necessitate such a model for high-precision machinery. The need for expanded modeling is most apparent in applications with naturally coupled mechanics. For example, disk vibration is a major concern in disk drives, yet the bearings are a primary source of excitation. Alternatively, the dominant excitation in geared transmissions is generated at the tooth mesh, yet the major dynamic concern is acoustic radiation from the gearbox housing of the vibration transmitted via the spindle. Bearing excitation drives disk response in one case, and disk (tooth mesh) excitation drives spindle dynamics in the other.

Figure 1 depicts the disk-spindle system wherein the disk is a uniform Kirchhoff plate augmented by membrane stress contributions, the spindle is a uniform Euler-Bernoulli beam, and the coupling clamp is a 3-dimensional rigid body. The system rotates with steady speed about the fixed axis passing through the spindle end supports. The following effects are incorporated in the model: 1) disk and clamp center of mass offsets from the rotation axis, 2) non-diagonal clamp and disk inertia tensors, 3) differing spindle bending stiffnesses in the two bending planes, and 4) general disk and spindle boundary conditions. The dimensionless variables are:

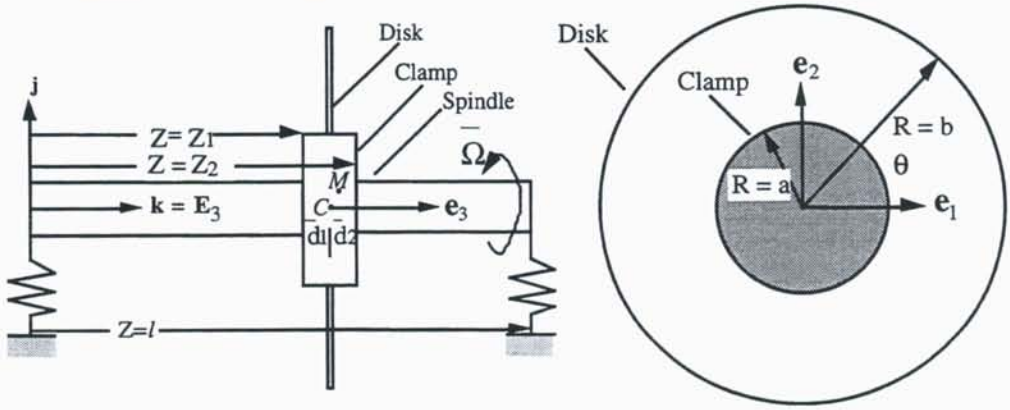

disk deflection - $w(r, \theta, t)$, spindle deflections - $u(z, t), v(z, t)$, deflections of clamp point C - $u^c(t), v^c(t)$, and clamp rotations - $\phi(t), \psi(t)$. The coupled equations of motion consist of three partial differential equations for the disk and spindle deflections and four ordinary differential equations for the clamp deflections and rotations.

The inherent gyroscopic continuum structure is clarified with a novel formulation of the governing equations in terms of extended operators acting on an extended variable. In particular, the extended operator formulation yields a symmetric and positive-definite inertia operator, symmetric elastic bending stiffness operator, symmetric rotational stiffness operator, and skew-symmetric gyroscopic operator. This structure, which is not evident from the component equations, is the keystone of the extended operator formulation. Cast in this form, known results for gyroscopic system response and stability apply to disk-spindle systems. Additionally, Galerkin, perturbation, and other approximate methods that require classical operator and inner product structure can be efficiently applied. This is a powerful result because these techniques, though well-known, are not readily applicable to the component equations.

The implications of this formulation and its utility for spinning disk-spindle vibration mode coupling, discretization methods, modal analysis, and response are examined. Specific results include:

1. Disk-spindle coupling of the zero speed vibration modes occurs only for the one nodal diameter modes for axisymmetric systems. Disk asymmetries (e.g., nonuniform boundary conditions, thickness variation, discrete asymmetries such as slots, etc.), as opposed to spindle and clamp asymmetries, are the only asymmetries that lead to expanded coupling in other than the one nodal diameter modes. This coupling is predicted in terms of simple formulae in terms of the Fourier distribution of the disk asymmetry.
2. Approximate spinning disk-spindle free vibration and response solutions are achievable by classical Galerkin discretization of the extended operator formulation. The zero speed and critical speed extended eigenfunctions are solvable in closed-form and provide the necessary set of complete comparison functions. Symmetry of the extended operators is preserved in the discretized matrix operators.
3. The vibration modes can be characterized as predominantly disk or spindle by a strain energy ratio. Interaction of the associated disk and spindle natural frequencies with changing speed follows a pattern rich with natural frequency veering. Strong disk-spindle coupling of the vibration modes occurs in the veering regions.
4. Forced response analyses demonstrate that disk-spindle coupling allows excitation applied to one component to drive vibration of the other, particularly in the presence of curve veering. Proper design choices can limit this coupling. This is an important concern in practical applications.
5. An exact solution for the eigensolutions of a disk-spindle system is calculated. While cumbersome, it is valuable as confirmation of the Galerkin discretization results as evident from excellent natural frequency comparisons.

References

Parker, R. G. (1998). "Analytical Vibration of Spinning, Elastic Disk-Spindle Systems." Journal of Applied Mechanics, in press.

Parker, R. G., and Mote, C. D., Jr. (1996). "Vibration and Coupling Phenomena in Asymmetric Disk-Spindle Systems." Journal of Applied Mechanics, 63, 953-961.

Parker, R. G., and Sathe, P. J. (1998). "Exact Solutions for the Free and Forced Vibration of a Rotating Disk-Spindle System." Journal of Sound and Vibration, in press.

Sathe, P. J., and Parker, R. G. (1998). "Free Vibration and Stability of a Spinning Disk-Spindle System." Journal of Vibration and Acoustics, submitted.

CONTINUUM REPRESENTATIONS FOR THE VIBRATION OF VEHICLE TRACKS

N. C. Perkins
C. Scholar

Mechanical Engineering and Applied Mechanics
University of Michigan
Ann Arbor, MI 48109-2125
USA

Heavy vehicles driven by tracks include construction vehicles, mining equipment, agricultural vehicles, military tanks and others. Regardless of their use, all tracked vehicles are subject to very substantial vibration levels; partly from the rough terrain that they frequently traverse and partly from the construction and motion of their track systems. This vibration limits the service life of many components and adversely affects vehicle performance. For instance, the vibration environment found inside military vehicles can be so severe as to seriously degrade the performance of on-board instrumentation, electronics and personnel. In addition, the associated acoustic emissions can themselves compromise the missions of these vehicles. This presentation will focus on a model used to examine the vibration response of the tracks that drive these vehicles. In doing so, we discuss the merits of viewing the track as an equivalent continuum.

Prior models of vehicle tracks have considered them to be large dimensional, multi-body systems composed of individual rigid links (pitches). This approach invariably leads to models of tracked vehicles possessing hundreds of degrees of freedom resulting in considerable computational effort to deduce even relatively simple responses. The novel approach discussed here is to model the track as an equivalent elastic continuum which is then coupled to the (rigid body) elements forming the remainder of the vehicle suspension system. To this end, a continuum model will be presented which describes the dynamic deformation of a track element within the vertical plane. This element model accounts for 1) the stretching of the track and resulting dynamic track tension, 2) the transverse vibration of the track spans, and 3) the static track sag. The element model is then extended in forming a model for the entire track system including typical suspension elements. The natural frequencies and mode shapes associated with this system model are then employed to evaluate the forced response of the track system using classical modal analysis methods. Figure 1 presents an example of this calculation and illustrates the first four vibration modes of a military vehicle. The forced responses considered derive from dominant sources of excitation for tracked vehicles including rough terrain and drive train excitation.

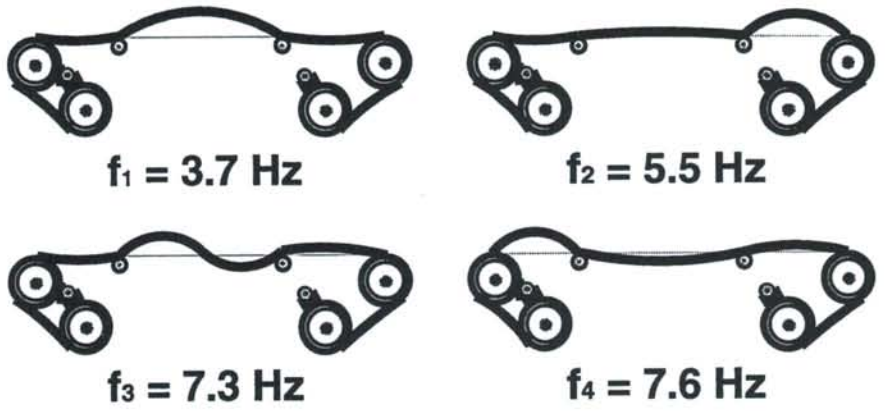

Figure 1: Track system modes.

The modeling of a vehicle track as a continuum is unique and requires justification. As a means towards this end, we shall review experimental results on the vibration response of track segments and critically compare these with predictions from the continuum model. Figure 2 illustrates experimentally measured frequency response functions for a sample track from which the natural frequencies are quite apparent. Once the accuracy and limits of the continuum model have been established, we shall then review how it is employed in the simulation of entire tracked vehicles traversing rough terrain.

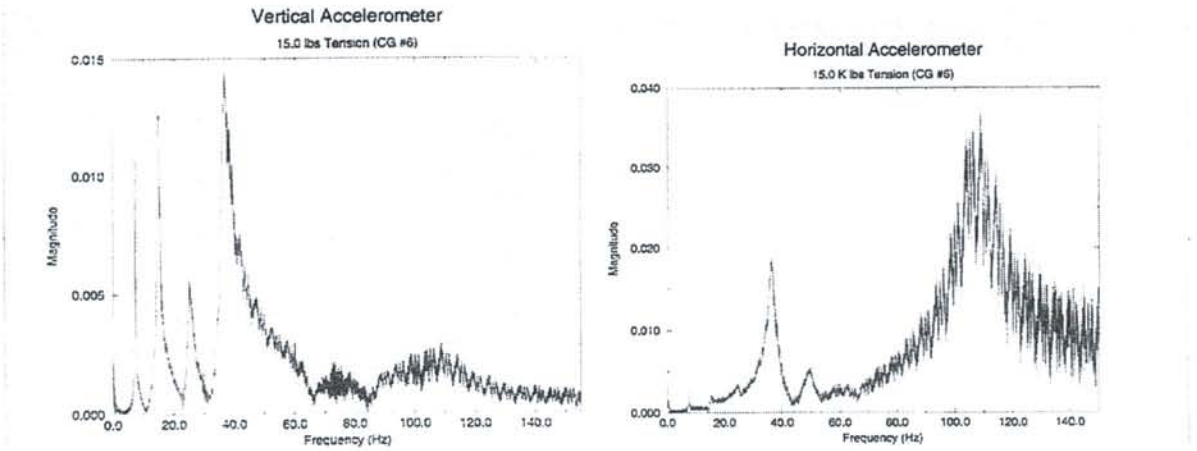

(a) (b)

Figure 2: Experimental frequency responses; (a) Vertical accelerometer; (b) Horizontal accelerometer.

SOME OBSERVATIONS ON SHELL VIBRATIONS

Mohamad S. Qatu
Technology Center, DANA Corporation, Fluid System Products
1900 Opdyke Court, Auburn Hills, MI 48326
Tel: (248) 377-0700, Fax: 377-1930, E-mail: mqatu@fsg.echlin.com

Thin-walled structural components make-up the vast majority of a typical automotive, aerospace, marine as well as other structures. Many of these thin-walled components have flat surfaces, or plates, and others have curved surfaces, or shells. Vibrations of plates and shells received considerable attention over the last few decades. Shell structures introduce considerable additional complexity in their analyses when compared with plate structures. Most of these complexities are due to vast number of shapes and curvatures shells may have (spherical, cylindrical, ...) and the fact that in-plane (or membrane) forces are coupled with out-of-plane forces (shear) as well as bending moments. This increases the order of the differential equations from 4 (for plates) to 8 for the simplest shell structures. Lamination material construction and thicker shells add to the complexity of the shell theory and the equations used. Thin shallow shells, often referred to as curved plates, are probably the simplest shell structures.

In a typical research or publication, the theory, the approach to the solution procedure, the numerical results and conclusions are often displayed. Rarely researchers try to look at the results and understand why a certain shell behaves in a certain way. Such information and explanation is usually of major interest to the engineer who is designing a particular component. In other words, and to be specific, if a particular natural frequency is occurring in a certain range where excitation is very probable, the challenge is to find the changes the engineer can make to the design of the component to get that natural frequency outside the range of excitation. If the engineer has a good insight to the shell behavior and that natural frequency and its mode shape, a solution can be proposed to solve the problem fast. Having said that, it should be mentioned that the engineer also works with other constraints like packaging, aerodynamics, cost and even 'style'. Some of the limitations restrict the curvature, thickness, and even the boundary conditions that can be worked with for a particular design.

Effect of Shell Curvature and Boundary Conditions

The table below shows the fundamental natural frequencies that correspond to symmetric modes obtained by the Ritz method for a cylindrical shallow shell (Qatu and Leissa, 1992). A unity aspect ratio of the shell and a Poisson's ratio of 0.3 are used to obtain all results. Two thickness ratios are used, the first is 500 representing a very thin shell and the second is 20 describing a thicker shell. Eight boundary conditions are studies (more can be obtained from the above paper), ranging from completely clamped edge C1to a simply supported edge with free inplane motion (S4) The above manuscript shows results for shells with other geometries.

It will be difficult to explain the changes in the frequencies without referring to the fundamental symmetric mode and the energy associated with it. This is mainly a bending mode. Notice the difference in this frequency made by releasing the inplane constraints (from C1 to C4) for thin shells. This observation can not be explained properly without reference to the bending and membrane energies in the system. Obviously, more membrane energy can be stored in the system where the inplane motion is restrained. Furthermore,

restraining the motion in the axial direction perpendicular to the boundary is of much more importance than restraining the other inplane motion to obtain higher frequency. The results obtained for higher curvature reinforces the same observation, as shells with higher curvature posses higher membrane energy. Going to thicker shells, the differences are noticed to be smaller when some inplane restrains are removed.

Fundamental Natural frequency parameters Ω for circular cylindrical shallow shells $\nu = 0.3$, $a/b = 1$

B/Ry								b/h = 500
	C1	C2	C3	C4	S1	S2	S3	S4
0.2	22.4	7.88	22.2	6.17	22.0	26.0	21.4	26.0
0.5	27.0	10.2	27.0	7.7	26.8	26.1	26.6	26.1
								b/h = 20
0.2	3.81	3.59	3.80	3.53	1.63	15.8	1.41	15.6
0.5	5.16	4.01	5.15	3.77	3.94	19.4	3.47	18.4

Curvature effects on isotropic barrel shells:

A recent publication presents the theory and vibration results for barrel shells (Qatu, 1999). Barrel shells are cylindrical shells with addition curvature along the axial direction. The table below presents the natural frequencies for closed isotropic barrel shells with Poisson's ratio of 0.3 and thickness ratio of $R_\beta/h=100$. The curvature ratio (a/R_α) along the longitudinal axis varies from -0.5 to 0.5.

The first observation made is that a slight curvature in the barrel shell with $a/R_\alpha = 0.1$ resulted in a considerable change in the natural frequencies (Qatu, 1999). For longer closed shells with $a/mR_\beta = 8$, changing a/R_α from zero (i.e. perfect cylindrical shells) to 0.1, resulted in increasing the natural frequency parameter by 27%. This change in a/R_α has less effect for shorter shells. For shells with $a/mR_\beta = 0.5$, this change increased the frequencies by only 3%.

The second observation made is that introducing a negative curvature $a/R_\alpha = -0.1$, decreased the fundamental natural frequency parameter, in general. This decrease is observed to reach a minimum, at $a/R_\alpha = -0.3$ for closed shells with $a/mR_\beta = 8$. This minimum is also observed in some of the higher frequencies. For example, the second minimum natural frequency is achieved at $a/R_\alpha = -0.1$, for $a/mR_\beta = 8$. For the third and higher frequencies, introducing a negative curvature did yield higher frequencies.

Another observation is made here when the frequencies of open and closed shells are compared. Note that the results presented for closed shells are also valid for open shells with $b/R_\beta = \pi$. The fundamental frequency parameters occur at a lower n value for open shells. Interestingly enough, the frequency parameters are found to increase as b/R_β decreases for shorter shells ($a/mR_\beta = 0.5, 1$) and the opposite is found for longer shells in some cases.

Natural frequency parameters for isotropic closed barrel shells ν=0.3, Rβ /h=100.

a/Rα	a/mRβ	n=0	1	2	3	4	5	6	7	8	9	10
	8	0.24354	0.05443	**0.02226**	0.04838	0.06759	0.09036	0.11959	0.15579	0.19884	0.24855	0.30475
	4	0.48709	0.24021	0.07083	**0.02521**	0.05098	0.08153	0.11509	0.15365	0.19803	0.24851	0.30517
-0.5	2	0.97417	0.58152	0.30733	0.15937	0.09221	**0.08473**	0.11186	0.15154	0.19787	0.24993	0.30774
	1	0.99731	0.88031	0.66603	0.47741	0.34088	0.25389	0.21123	**0.20741**	0.23230	0.27512	0.32925
	0.5	1.00638	0.97920	0.90659	0.80876	0.70588	0.61242	0.53722	0.48530	0.45896	**0.45791**	0.47944
	8	0.24354	0.09165	0.03410	**0.02830**	0.04542	0.07191	0.10500	0.14428	0.18964	0.24107	0.29856
	4	0.48709	0.26929	0.11851	0.06542	**0.05819**	0.07670	0.10755	0.14612	0.19123	0.24255	0.30000
0.0	2	0.97313	0.60045	0.34326	0.20527	0.13891	**0.11776**	0.12832	0.15833	0.19990	0.24967	0.30639
	1	0.99546	0.88628	0.68468	0.50689	0.37812	0.29493	0.25062	**0.23969**	0.25557	0.29081	0.33957
	0.5	1.00594	0.98045	0.91230	0.82039	0.72364	0.63562	0.56451	0.51474	0.48829	**0.48507**	0.50310
	8	0.24354	0.12873	0.08679	**0.07764**	0.08222	0.09793	0.12363	0.15802	0.20011	0.24928	0.30515
	4	0.48709	0.29836	0.16634	0.11838	**0.10469**	0.11071	0.13125	0.16296	0.20362	0.25200	0.30742
0.5	2	0.96190	0.61900	0.37926	0.25145	0.18863	**0.16356**	0.16449	0.18464	0.21883	0.26357	0.31687
	1	0.99320	0.89186	0.70314	0.53634	0.41551	0.33676	0.29273	**0.27782**	0.28711	0.31554	0.35861
	0.5	1.00539	0.98159	0.91791	0.83193	0.74135	0.65887	0.59202	0.54476	0.51881	**0.51419**	0.52946

References

Leissa, A. W., (1973). *Vibration of Shells*, NASA SP-288, U.S. Government Printing Office, Washington, D.C. Reprinted by the Acoustical Society of America, 1993.

Qatu, M.S. and Leissa, A.W. (1992), Effect of Edge Constraints Upon Shallow Shell Frequencies, *Thin Walled Structures*, **14**, 347-379,

Qatu, M.S. (1999), Theory and Vibration Analysis of Laminated Barrel Thin Shells, to appear, J. Vibration and Control.

FINITE DYNAMICS OF ELASTIC SUSPENDED CABLES: ANALYTICAL APPROACHES, EXPERIMENTAL TECHNIQUES, AND NONLINEAR PHENOMENA

Giuseppe Rega
Dipartimento di Ingegneria Strutturale e Geotecnica,
Università di Roma "La Sapienza", Italy

Finite oscillations of elastic suspended cables have received strong attention in the recent literature due to their notable interest in applied mechanics and engineering. The suspended cable can indeed be considered as a meaningful archetypal model for the analysis of the nonlinear behaviour of the important class of elastic structural systems with initial curvature. Due to the simultaneous occurrence of even and odd nonlinearities, it allows one, on one side, to examine and compare the merits of different approaches adopted for describing the system asymptotic dynamics. On the other side, it allows one to illustrate the richness of nonlinear dynamic phenomena, which ranges from the varied regular and nonregular responses exhibited already by the relevant s.d.o.f. model, to the whole complexity of multimodal interactions, bifurcations, and chaos of various possible m.d.o.f. models.

Apart from topics concerned with system mechanical and mathematical modelization which would require further investigations and refinements, meaningful research achievements have recently been obtained as to the performances of different techniques in the investigation of the system response and to the variable aspects of its dynamic and bifurcational behaviour. Consistent with the intent of the conference, and within the aforementioned general framework, the present work is aimed at reporting on some interesting and partially unexpected topics in the field, as they have been detected by the writer in a perspective of long-term research activity with collaborators.

Three main topics will be considered. (i) The performances of different analytical approaches which can be used to construct asymptotic models able to highlight the actual nonlinear response of cables to an harmonic excitation, and some relevant problems connected with the identification of reduced-order models and with higher-order approximations of the responses. (ii) The problems arising in the experimental analysis of the finite dynamics of such flexible systems, and the techniques and tools from applied nonlinear dynamics that have to be employed to get a reliable in-depth description of the system complex behaviour. (iii) Some main related bifurcational aspects, and the ensuing steady attractors of the dynamics, as they are detected by using suitable response invariant measures derived from dynamical systems theory.

(i) The finite forced vibrations of elastic suspended cables around their initial configurations are governed by a set of general integro-partial differential equations. A common practice to obtain approximate solutions of the relevant unimodal or multimodal dynamics through an asymptotic technique is to construct Galerkin discretized models by retaining in the expansion the only eigenmode excited by the resonance or just the eigenmodes involved in the (possibly simultaneous) internal resonances. A more recent procedure consists in applying the asymptotic technique (such as the method of multiple time scale) directly to the original partial differential equations: one main associated feature is its capability to account for the contribution of the system infinite eigenmodes in its spatial dynamics, without any *apriori* assumptions. A critical comparison between the two procedures is made by analyzing the conditions for their non-equivalence and by showing in particular: (a) The occurrence of breakdown of one-dimensional (symmetric) models above some

thresholds of cable sag-to-span ratio, due to the underestimation of the softening effects associated with quadratic nonlinearities, which become more important in the system actual dynamics owing to the contribution of higher symmetric eigenmodes. (b) The occurrence of qualitatively and quantitatively different bifurcations characterizing some classes of 3D responses of multimodal models developed in conditions of multiple internal resonances.

Two specific but meaningful topics are also addressed within the above mentioned framework. The first one is concerned with the detection of minimum reduced-order models that can reproduce, at least qualitatively, the correct system dynamics arising in given resonance conditions. The second addresses the problem of reconstitution of the modulation equations arising at different nonlinear orders of the perturbation solution when the higher-order approximation of the response needed to account for both the 2:1 and 1:1 internal resonances occurring in cable dynamics at crossover points is accomplished.

(ii) Side by side with the analytical investigation, experimental analyses of the finite forced response of suspended cables show very rich and varied regular and nonregular dynamics. Such tools as phase portraits, Poincaré maps and power spectra of measures from given points in the system allow one to obtain informations on the nature of attractors in regular regime. However, understanding system complex dynamics requires characterization of attractors in terms of dimensionality, strangeness and possible chaoticity, description of bifurcation paths in parameter space - with main attention devoted to transition from regular to nonregular response, and finally identification of space configuration variables mostly contributing to the latter. The analysis of the asymptotic motion in nonregular condition is performed on attractors reconstructed by means of the delay-embedding technique, and the dimension of the reconstructed phase space is evaluated using the singular value decomposition and the saturation of some attractor invariant. Determining system dimensionality, and deciding about the minimum number and the features of the configuration variables needed to reliably describe an observed motion, is one main question in nonlinear dynamics of continuous systems, whose infinite-dimensionality may actually be activated under nonregular response conditions. The topic of system dimensionality is tackled, on one hand, on the reconstructed attractor by connecting its dimension with the dimension of the linear phase space; on the other hand, it ensues from the analysis of the spatial structure of the nonregular flow and of the relevant dominating experimental eigenfunctions (proper orthogonal modes), which are obtained via correlation measures of the response at different points and a linear decomposition technique.

(iii) The transition from regular to nonregular dynamics in various external resonance zones under in-phase or out-of-phase support motion is characterised by means of bifurcation paths and involved configuration variables. The former are traced back to canonical scenarios of dynamical systems, which are here seen to be sometimes simultaneous and competing with each other: (a) the quasiperiodic scenario and (b) a scenario in which is involved the global bifurcation of an homoclinic invariant set of the symmetric flow. In the primary resonance region under in-phase support motion, the quasiperiodic scenario is characterized by the successive involvement of two harmonics of incommensurable frequency in the formerly unimodal system dynamics, giving rise to a two-frequency and then a three-frequency quasiperiodic motion (motion on 2-Torus and 3-Torus, respectively). The spatial coherence analysis allows one to identify the modes responsible for the various incommensurabilities. The ensuing rich and varied behaviour of the system is due to the variety of response

regimes going along with the three-dimensional torus breakdown. In the overall transition region the model exhibits: (i) two-frequency quasiperiodic motions on two-dimensional manifolds; (ii) two-frequency phase-locked quasiperiodic motions on three-dimensional manifolds; (iii) stable three-frequency quasiperiodic motions; (iv) chaotic motions ensuing from evolution of unstable three-frequency quasiperiodic motions; (v) phase-locked periodic solutions on three-dimensional manifolds. Various types of bifurcation are documented, with involvement in the response of further configuration variables. Almost the whole response power can however be decomposed on a well-identified three-modal basis, thus showing how the dynamics of the continuous system - which is governed by relatively few modes in the regular response regions - remains substantially low-dimensional in nonregular regions, too. Robustness of the observed scenarios with respect to variations of the system mechanical parameters is checked by considering both a slightly slacker cable and a cable at first crossover condition. In the latter case, the existence of a nearly perfect 2:2:1:2 internal resonance involving in-plane and out-of-plane symmetric and antisymmetric modes makes periodic coupled responses more robust, while preventing quasiperiodicity and chaos from occurrence.

The second recognised scenario involves the bifurcation of an homoclinic invariant set in a symmetric flow, and manifests itself at one edge of the stability zones of antisymmetric ballooning regular motions. This scenario is of general interest because it concerns all frequency zones in which such regular classes of motion are present under out-of-phase support motion, for the slacker as well as the crossover cable. Due to the nature of the phenomenon, the experimental analysis regards not only the attractor global properties but also the presence and the features of invariant sets of the flow structure. When the cable model follows the aforementioned scenario, the attractors exhibited in chaotic zones show the lowest observed dimensionality: indeed, the transition from regular to nonregular behaviour happens without increasing the number of involved modes over the two already present in neighbouring regular zones.

Recognizing meaningful proper orthogonal modes allows one to associate with each class of complex response a class of reduced (and minimal) analytical models able to describe its nonlinear dynamics. A link can thus be established with the approximate techniques for obtaining asymptotic solutions to the theoretical cable model discussed at point (i). Indeed, either more reliable reduced discretized models are obtainable in the framework of a Galerkin procedure by using the identified proper orthogonal modes, or a connection can be established between these experimental eigenfunctions and the nonlinear normal modes identified as a natural, and very useful, byproduct of the direct attack of the partial differential equations of motion through the asymptotic procedure.

Measurement of the bonding quality of piezoelectric elements by impedance measurements of electrically excited beam vibration

Wolfgang Seemann
University of Kaiserslautern
Kaiserslautern
Germany

In smart and adaptive structures very often piezoceramic elements are used as sensors or actuators. If these elements are used as actuators in active damping applications or for the excitation of ultrasonic motors, an optimized bonding is necessary for a good efficiency of the overall structure.

In experiments it is observed, that the quality of the bonding depends on several factors. The coupling between the ceramic and the elastic structures can be very good or very bad. Those parameters having the highest influence are the thickness, the stiffness and permittivity of the bonding layer. Also damping effects may be important to interpret the results.

The lecture shows theoretically that investigations concerning an optimized bonding can be done by measuring the electric impedance of a piezoceramic element which is bonded to an elastic beam. In the piezoceramic material electric and mechanical fields are coupled so that a time-harmonic voltage applied to the piezoceramic element will result in forced harmonic vibration of the beam. If only one element is bonded to one surface of the beam both longitudinal and bending vibration are excited due to the asymmetric configuration.

However, the amplitudes of the beam vibration depend on the coupling between the piezoceramic element and the beam. For a good coupling the mechanical resonances can be clearly seen in the curve of the electric impedance of the element.

For theoretical investigations a piezoceramic element is considered which is bonded to an elastic beam by a bonding layer of finite thickness. The equations of motion for the beam are derived under the assumptions that the cross-section of the beam remains planar and that the longitudinal strain in the piezoceramic does not depend on the thickness coordinate. Hamilton's principle leads to the coupled partial differential equations for the longitudinal and transverse displacement of the beam and the piezoceramic. The electric excitation of the piezoceramic influences only the boundary conditions.

For time harmonic vibration the remaining ordinary differential equations can be solved and and the solution can be fitted to the boundary and transition conditions. If the motion and therefore the strain in the piezoceramic element is known the electric charge or the electric current can be determind. For given amplitudes of the applied voltage and the corresponding current the electric impedance can be calculated.

Results for the impedance as well as for the vibration amplitudes are shown both for damped and undamped beams for various thicknesses of the bonding layer. These results show good agreement with measurements.

Vibration of shell structures and Fourier Series

Dr C B Sharma
Department of Mathematics, UMIST
PO Box 88, Manchester, M60 1QD, UK

The object of the present work is to develop an analytical approach to study the free vibration characteristics of shells and related structures. Various well known direct approximate procedures have their own limitations like non-uniform choice of modal functions to study the influence of arbitrary support conditions on various shell vibration characteristics and in the case of numerical methods: requirements of efficiency as well as accuracy. Hence more exact and accurate analytical approaches are required in which case a number of references can be cited e.g. [1], [2] which analyze vibration characteristics of isotropic and materially monoclinic cylindrical shells respectively. Both these papers use an exact but iterative technique given in [1] where an axial modal dependence in exponential form is utilized. In reference [3] double Fourier series method is used to find simple solutions of various boundary value problems of isotropic rectangular plates. A general exposition of the method for the analysis of the free vibration of linear structure with arbitrary end conditions is given in [4]. Here an analytical method for the free vibrations of any linear structure with arbitrary support conditions is given based upon the formalism of Lagrange equations in conjunction with Lagrange multipliers. Examples to analyze various linear structures are also provided. The author claims that "in view of the power and simplicity of the method it is remarkable that so little literature precedes the present paper".

A modified Rayleigh-Ritz method along with Lagrange multipliers is developed in [5] to analyze free vibrations of isotropic thin cylindrical shells. A Fourier series component mode method coupled with Lagrange multipliers is utilized in [6] to study the free vibrations of a multi-segment cylindrical shell with a common mean radius.

In the present work this analysis is modified and extended to include the study of the free vibration characteristics of single and multi-layered orthotropic circular cylindrical shells and shell panels. The influence of boundary conditions, various degrees of orthotropy and shell geometrical parameters etc on natural frequencies, mode shapes and modal forces and moments are studied and accounted for in detail. An exact but iterative procedure is employed here too like the one given in [1] and [2]. Equations of motion are solved directly with the use of half-range Fourier series as the axial dependence of modal forms. Since it is necessary to differentiate Fourier series the Stokes' transformation is used to legitimise this procedure based on the end values of the functions involved. For example, while using a sine series to represent a function, the end values of functions are rendered zero. With Stokes' transformation [7], however, the end values of such functions are released by being specified separately and these values are then included in the successive differentiation of Fourier series. To illustrate the usefulness and efficiency of the analytical procedure involved some illustrative examples are to be provided which will include a comprehensive study of the free vibration characteristics of cylindrical shells, their dependence on the end conditions as well as shell geometrical and material parameters.

References

1. **Forsberg, K.**, *Influence of boundary conditions on the modal characteristics of thin cylindrical shells*, AIAA J. **2** (12), 2150-2157 (1964).

2. **Vanderpool, M.E.** and **Bert, C.W.**, *Vibration of materially monoclinic, thick-wall circular cylindrical shell,* AIAA J. **10** (5), 634-641 (1981).

3. **Green, A.E.**, *Double Fourier series and boundary value problems,* Proc. Cambridge Phil. Soc., **40** (3), 222-228 (1944).

4. **Dowell, E.H.**, *Free vibrations of a linear structure with arbitrary support conditions,* Journal of Applied Mechanics, **38** , 595-600 (1971).

5. **Chung, H.**, *A general method of solution for vibrations of cylindrical shells,* PhD Thesis, Tufts University, Medford, Massachusetts, USA (1974).

6. **Chang, S-D**, and **Greif, R.**, *Vibrations of segmented cylindrical shells by a Fourier series component mode method,* J. Sound and Vib. **67** (3), 315-328 (1979).

7. **Bromwich, T.J.**, *An Introduction to the Theory of Infinite Series,* 2nd edition, Macmillan, London (1955).

NUMERICAL PROCEDURE FOR THE NONLINEAR FREE VIBRATION ANALYSIS OF SHALLOW SHELL DEFINED BY A QUADRILATERAL DOMAIN

A. V. Singh and K. Lan
The Department of Mechanical and Materials Engineering
The University of Western Ontario
London, Ontario, Canada, N6A 5B9

Introduction. In linear vibration theory, the overall stiffness properties is independent of the displaced shape of the plate or shell structure. Consequently, the theoretical frequencies of such structures are also independent of the amplitude of vibration. This is not the case when the analysis is based on the geometrically nonlinear equations from the theory of elasticity. The stiffness, which basically controls the values of the natural frequencies of the vibrating plate or shell, depends upon the displaced configuration. The amplitude of the order of the plate (or shell) thickness has been seen to alter significantly the stiffness properties. The result, therefore, is that frequencies predicted from the linear free vibration theory are no longer valid. Considerable amount of work has appeared in the literature on the free nonlinear vibration of plates. Satyamoorthy (1983 and1987) published two review papers and wrote a book in 1997 on this subject. Review of literature reveals that the nonlinear free vibration of doubly curved shallow shells defined in Cartesian coordinates has not received the same degree of attention as the plates.

This paper presents a brief treatment of the nonlinear free vibration of shallow shells defined in the x-y plane by four straight edges. The geometrically nonlinear strain-displacement relations are linearized in a manner similar to the one by Rao et. al (1976). The first order shear deformation shell theory including the rotary inertia is used in the formulation. The quadrilateral boundary is mapped using the natural coordinates ξ and η into a square (Weaver and Johnston, 1984). The Ritz method, with simple algebraic polynomials as the admissible function, is used for the solution. The convergence study and the comparison of numerical results with those of Mei (1973) and Rao et. al (1976) are included in this short paper.

Procedure. A shell having its middle surface bounded by a quadrilateral region is considered in this paper. Coordinates of the four corner points are expressed by (x_j , y_j), where $j = 1, 2, 3$ and 4 in a sequential counter clockwise sense. The displacement and strain components at an arbitrary point in the shell are identified by the primed (') symbols.

$$\begin{array}{lll} u' = u + z\beta_1 & v' = v + z\beta_2 & w' = w \\ \varepsilon'_x = \varepsilon_x + z\kappa_x & \varepsilon'_y = \varepsilon_y + z\kappa_y & \varepsilon'_z = 0 \\ \varepsilon'_{xy} = \varepsilon_{xy} + z\kappa_{xy} & \varepsilon'_{yz} = \varepsilon_{yz} & \varepsilon'_{zx} = \varepsilon_{zx} \end{array} \qquad (1)$$

Terms on the right hand side of equation (1) correspond to the middle surface of the shell. For example: u, v and w are the displacement components along x, y and z axes respectively. Similarly, $\beta_1$and β_2 denote the components of rotation of the normal to the middle surface of the shell and z is the distance measured along the normal. The geometrically nonlinear strain components are expressed in terms of the displacement components as follows.

$$\begin{array}{l} \varepsilon_x = \partial u/\partial x + w/R_1 + f_1\,\partial w/\partial x; \quad \varepsilon_y = \partial v/\partial y + w/R_2 + f_2\,\partial w/\partial y; \\ \varepsilon_{xy} = \partial u/\partial y + \partial v/\partial x + f_2\,\partial w/\partial x + f_1\,\partial w/\partial y; \\ \varepsilon_{zx} = \beta_1 - (u/R_1) + \partial w/\partial x; \quad \varepsilon_{yz} = \beta_2 - (v/R_2) + \partial w/\partial y; \\ \kappa_x = \partial\beta_1/\partial x; \quad \kappa_y = \partial\beta_2/\partial y \text{ and } \quad \kappa_{xy} = \partial\beta_1/\partial y + \partial\beta_2/\partial x \end{array} \qquad (2)$$

It can be noted here that the nonlinearity is associated with the in-plane (membrane) strain components only. The transverse shear strains and curvature terms retain the recognised form from the linear theory.

Furthermore, in equation (2) strain equations are linearized by introducing two functional parameters: $f_1 = \frac{1}{2}(\partial w/\partial x)$ and $f_2 = \frac{1}{2}(\partial w/\partial y)$. To obtain the matrix equation of motion, the following strain energy expression is used.

$$U = \frac{1}{2} \int_{AREA} \int_{-h/2}^{+h/2} \{\varepsilon'\}^T [E] \{\varepsilon'\} \, dz \, dx \, dy \tag{3}$$

In the above, the strain components at an arbitrary point in the shell are represented by the vector: $\{\varepsilon'\}^T = \{\varepsilon'_x \quad \varepsilon'_y \quad \varepsilon'_{xy} \quad \varepsilon'_{yz} \quad \varepsilon'_{zx}\}$. Matrix [E] of order five is composed of the Young's modulus of elasticity and the Poisson's ratio of the material. Similarly, the kinetic energy expression is taken from the basic relationship as

$$K = \frac{1}{2} \int_{AREA} \int_{-h/2}^{+h/2} \rho \{(\partial u'/\partial t)^2 + (\partial v'/\partial t)^2 + (\partial w'/\partial t)^2\} \, dz \, dx \, dy \tag{4}$$

The procedure makes use of the parametric coordinates ξ and η which map the quadrilateral region into a square bounded by $-1 \le (\xi \text{ and } \eta) \le +1$. The Jacobian matrix $[J(\xi,\eta)]$ and its determinant $|J(\xi,\eta)|$ are used while integrating the energy expressions over the given domain. For infinitesimal area, we use: $dx\,dy = |J(\xi,\eta)| \, d\xi \, d\eta$. The solution procedure developed in this work is based on the Ritz method, which requires properly defined displacement fields. Therefore, the following polynomial form is selected to represent the displacement component u.

$$u = \sum_{j=1}^{n} \sum_{k=1}^{n} \underline{a}_{jk} f_k(\xi) \, f_j(\eta) \, \sin \omega t \tag{5}$$

Similar double summation series are used for v, w, β_1 and β_2. The values of j and k are assigned to be $1, 2, \ldots, n+1$; where n = the order of the polynomials $f_k(\xi)$ and $f_j(\eta)$ in each of ξ and η directions respectively; $\underline{a}_{jk}$ is a two dimensional array of the coefficients; ω = circular frequency in radian/second; and t denotes the time variable. The parametric polynomial used in this case is

$$f_j(\xi) = (1+\xi)^{j-1} (1-\xi)^{n-j+1}; \quad \text{for } j = 1, 2, 3, \ldots, (n+1). \tag{6}$$

The coefficients are the unknown quantities at this point of the solution stage and have the same unit as the displacement components they are associated with.

Numerical Results. The formulation is developed for quadrilateral shaped doubly curved shallow shells bounded by four straight edges. This allows us to examine the nonlinear free vibration of shallow shells of various shapes like rectangular, triangular, rhombic and trapezoidal. Value of the fundamental frequency parameter $\Omega = \sqrt{(\rho \omega^2 a^2 / E)}$ is calculated and compared with results from other sources available in the literature. Convergence is examined for this method and compared with the FEM by using the number of unknowns for which the matrix equation of motion has been solved, as the parameter. A square plate with all sides fully clamped is analysed for this purpose. Due to the geometric symmetry, only one quarter of the plate is examined. Five FE models, consisting of 4, 9, 16, 25 and 36 eight node quadrilateral (QUAD8) shallow shell elements respectively, are considered. The degrees-of-freedom for these models are found to be: 105, 200, 325, 480 and 665 respectively. Convergence test for the Ritz method is carried with the values of n being 4, 5, 6, 7, 8 and 9 and the corresponding numbers of degrees-of-freedom 80, 125, 180 245, 320 and 405 respectively. As shown in the figure, rapid convergence is found for both the Ritz and FE methods. The Ritz method provides reasonably accurate results with relatively small number of unknowns. Results from the present study are also compared with the works of other researchers by investigating a fully clamped square plate using sixth order polynomial with $n = 7$. Table below shows the period ratios (T_{NL} / T_L) obtained from various sources viz. the Ritz method, FEM using QUAD8 element, FEA by Mei (1973) and Rao et. al (1976). Here, w_0 represents the maximum deflection at the centre of the plate. More results for other types of geometry and curvatures are also available in the work by Lan (1998).

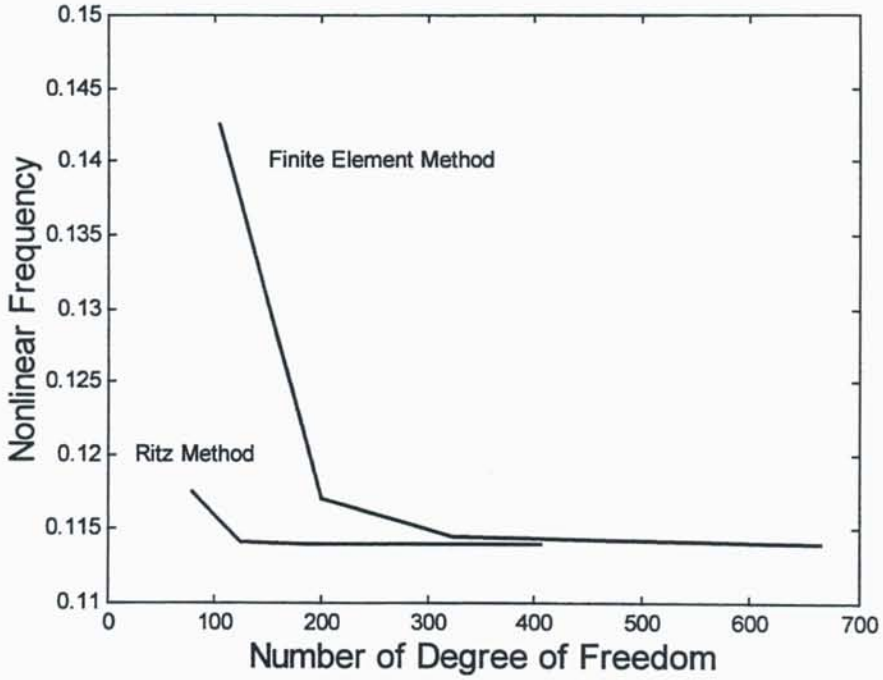

Figure . Convergence Study of the Ritz and Finite Element Methods.

Table. The period ratio (T_{NL}/T_L) for the fully clamped square plate having: $b/a = c/a = 1.0$, $a/R_1 = a/R_2 = 0.0$, $h/a = 0.01$. $\Omega_L = 0.10879$ (Ritz method) and $\Omega_L = 0.10926$ (FEM)

w_0/h	Ritz Method (T_{NL}/T_L)	FE Method (T_{NL}/T_L)	Mei(1973) (T_{NL}/T_L)	Rao(1976) (T_{NL}/T_L)
0.2	0.9949	0.9941	0.9930	0.9930
0.4	0.9803	0.9788	0.9780	0.9731
0.6	0.9574	0.9546	0.9550	0.9427
0.8	0.9282	0.9236	0.9320	0.9052
1.0	0.8945	0.8876	0.8960	0.8637

References

1. Kang, Lan, 1998, "Linear and nonlinear free vibration analysis of plates and shallow shells", M.E.Sc. Thesis, Faculty of Engineering Science, The University of Western Ontario.
2. Mei, C., 1973, "Finite element displacement method for large amplitude free flexural vibrations of beams and plates", Computers and Structures, vol. 3, p.163-174.
3. Satyamoorthy, M., 1983, "Nonlinear vibrations of plates: A review", Shock and Vibration Digest, vol.15, p. 3-16.
4. Satyamoorthy, M., 1987, "Nonlinear vibration analysis of plates: A review and survey of current developments", Appl. Mech. Rev., vol. 40(11), p. 1553-1561.
5. Satyamoorthy, M., 1997, Nonlinear Analysis of Structures, CRC Press, Boca Ratan, U.S.A.
6. Venkateswara Rao, G., Raju, I. S., and Kanaka Raju, K, 1976, "A finite element formulation for large amplitude flexural vibrations of thin rectangular plates", Computers and Structures, vol. 6, p.163-167.
7. Weaver, W. Jr and Johnston, P. R., 1984, Finite Elements for Structural Analysis, Prentice Hall, Inc., NJ, USA.

Vibrations of Elastic Cylindrical Shells with Non-circular Cross-Section: A Survey

Kostas P. Soldatos

Department of Theoretical Mechanics,
University of Nottingham, Nottingham NG7 2RD, UK.

Shell-type structures are used by modern industry (aerospace, marine, power, oil, offshore, nuclear, etc) in very many varieties, shapes and configurations. A circular cylindrical surface can form the middle surface of the geometrically simplest shell structure. On the other hand, thin walled circular cylinders are used extensively in very common as well as in many advanced engineering applications (pipelines, pressure vessels, cylindrical tanks, roof panels, etc). It is therefore not surprising that the elastic cylinder of revolution has been the basic and most popular model for the theoretical and the experimental investigation of the mechanical behaviour of thin-walled curved structural elements.

The vast literature that surrounds the two- and three-dimensional analysis of thin- and thick-walled elastic circular cylindrical shells encounters many hundreds of papers, books and monographs. These deal with all aspects of the mechanical behaviour of circular cylinders including their static behaviour and dynamic response as well as their stability and thermoelastic analysis. Relatively early reviews dealing with the dynamic behaviour of thin walled circular cylindrical shells were presented in the second and third chapters of Leissa's relevant monograph (Leissa, 1973). Since then, however, there were vast further developments in the subject, mainly due to the extensive implementation and use of composite materials. Such developments, in all of the afore-mentioned aspects of the mechanical behaviour of circular cylindrical shells, may be found in more recent relevant review articles (e.g., Bushnell, 1981; Simitses, 1986; Noor, 1990; Noor and Burton, 1990, 1992a,b; Qatu, 1992; Thorton, 1993; Soldatos, 1994; Noor *et al*, 1996; Teng, 1996).

The level of the geometrical difficulty is increasing substantially when the effects of some kind of eccentricity are encountered on the cross-section of a cylindrical surface, thus implying that the plane curve considered is a part or the whole of a closed non-circular arch. The amount of the additional difficulty and complexity involved can be illustrated by simply underlying the fact that eccentricity can be imposed on a circular arch in many different ways. Thus an essentially infinite number of possible non-circular arches (elliptical, parabolic, hyperbolic, etc) can be produced and, therefore, a similarly infinite number of potential non-circular cylindrical cross-sections can be given rise to.

In dealing with the theoretical modelling of non-circular cylindrical shells, that additional difficulty can be confined into the fact that the cross sectional radius of curvature is a function of an arch co-ordinate parameter and is, therefore, not constant. As a result, the governing differential equations of an elastic non-circular cylindrical shell have variable coefficients and become relatively difficult to solve. It then becomes rather evident why the number of the studies that deal with the behaviour of non-circular elastic cylinders, although constantly increasing over the years, is rather limited as it compares with the vast literature related to corresponding cylinders of revolution.

Non-circular cylindrical shells of small or large eccentricity are also used extensively in aerospace and mechanical engineering applications, due either to special external shapes or to internal storage requirements. It should not be ignored in this context that non-circularity of the middle surface cross-section may occur as an

imperfection (small or big) during the manufacturing process of a circular cylindrical shell. This is often considered as an additional reason for studying the mechanics of non-circular cylindrical shells, particularly when dealing with their stability behaviour under external loading. It appears, indeed, that the first publications in this subject studied the stability characteristics of non-circular cylindrical shells (Heck, 1937; Marguerre, 1942; 1951). Despite that the first relevant dynamic investigation appeared quite later (Herrmann and Mirsky, 1957), the vibration studies of non-circular elastic cylinders are, currently, more than twice as many as the corresponding stability investigations.

With the purpose to elevate further developments in the subject, this paper presents a review of the research work related to the dynamic behaviour of non-circular cylindrical shells and shell segments. In this respect, it initially outlines the basic nomenclature, the theoretical models as well as the governing equations employed in this subject. It proceeds with the basic characteristics of the vibration pattern of closed non-circular cylindrical shells with doubly symmetric cross-section (e.g., elliptical, oval) and initially reviews all relevant articles based on classical shell theories. It then covers all papers based on shear deformable shell theories and, where appropriate, it evaluates them critically and underlines the most important results and conclusions. This review pattern is next followed for all articles that dealt with the dynamic analysis of cylindrical shells having an open non-circular profile. The survey finishes by addressing some untouched relevant problems as well as possible future research directions in the subject.

REFERENCES

Bushnell, D. (1981) Buckling of shells - Pitfall for designers, *AIAA J* **19**, 1183-1226.

Heck, O.S. (1937) *The Stability of Orthotropic Elliptic Cylinders in Pure Bending*, NACA TM no 834.

Herrmann, G. and Mirsky, I. (1957) *On Vibrations of Cylindrical Shells of Elliptic Cross-Section*, Tech Rept No 5, Columbia Univ., Contract No AF 18(600)-1247.

Leissa, A.W. (1973) *Vibrations of Shells*, NASA SP-288. Reprinted, 1994, by the Acoustical Society of America.

Marguerre, K. (1942) *Stabilitate der Zylinderschale veranderlicher Krummung*, Zentrale fur wissenschaftliches Berichtswesen der Luft-fahrtforschung des Generalluftzeugmeisters (ZWB), Berlin-Adlershof, Forschungsbericht No 1671.

Marguerre, K. (1951) *Stability of the Cylindrical Shell of Variable Curvature*, NACA TM No 1302.

Noor, A.K. (1990) Bibliography of monographs and surveys on shells, *Appl Mech Rev* **43**, 223-234.

Noor, A.K. and Burton, W.S. (1990) Assessment of computational models of multilayered composite shells, *Appl Mech Rev* **43**, 67-97.

Noor, A.K. and Burton, W.S. (1992a) Mechanics of anisotropic plates and shells - a new look at an old subject, *Comput & Struct* **44**, 499-514.

Noor, A.K. and Burton, W.S. (1992b) Computational models for high-temperature multilayered composite plates and shells, *Appl Mech Rev* **45**, 419-446.

Noor, A.K., Burton, W.S. and Bert, C.W (1996) Computational models for sandwich panels and shells, *Appl Mech Rev* **49**, 155-198.

Qatu, M.S. (1992) Review of shallow shell vibration research, *Shock Vib Dig* **24**, 3-15.

Simitses, G.J. (1986) Buckling and postbuckling of imperfect cylindrical shells: A review, *Appl Mech Rev* **39**, 1517-1524.

Soldatos, K.P. (1994) Review of three-dimensional dynamic analyses of circular cylinders and cylindrical shells, *Appl Mech Rev* **47**, 501-516.

Teng, J.G. (1996) Buckling of shells: Recent advances and trends, *Appl Mech Rev* **49**, 263-506.

Thorton, E.A. (1993) Thermal buckling of plates and shells, *Appl Mech Rev* **46**, 485-274.

Vibration Analysis of a Rotating Laminated Composite Vessel

by

Katsuyoshi Suzuki,Genji Shikanai and Jiqun Hu

Department of Mechanical Systems Engineering
Faculty of Engineering , Yamagata University
4-3-16 Jyonan,Yonezawa,992-8510,Japan

1. INTRODUCTION

There exists a number of investigations dealing with the free vibrations of rotating anisotropic or laminated composite circular cylindrical shells and general shells of revolution [1-11]. But they are not for practical combined shells or vessels but are mostly for simple shells. Suzuki et al.[12] analyzed the vibrations of composite circular cylindrical vessels(nonrotating vessel) by using the Lagrangian minimizing method. The vibration analysis of combined shell structures is very complicated and troublesome, and so many approximate methods such as the finite element method and the substructure synthesis method are used.

In this paper, an analytical solution procedure is presented for the free vibrations of a rotating vessel consisting of a thin laminated composite shell of revolution with a constant meridional curvature and thin laminated composite circular cylindrical shells. The equations of motion and the boundary conditions for the rotating shell of revolution and circular cylindrical shell are obtained from the stationary conditions of each Lagrangian of vibration , of the shell of revolution and the circular cylindrical shell. The equations of motion are solved exactly by using a power series expansion for symmetrically laminated cross-ply shells. The Lagrangian of the rotating vessel is expressed by the sum of each Lagrangian of the shell of revolution and the circular cylindrical shell. The natural conditions of continuity between the shell of revolution and the circular cylindrical shell are obtained from the stationary conditions of the Lagrangian of the vessel considering the geometrical conditions of continuity. The frequency equations are obtained after considering both the boundary conditions and the conditions of continuity at the connection for the solutions. Numerical studies are made for vessels with both ends clamped. The natural frequencies and the mode shapes are presented showing their variations with rotating angular velocity,number of laminae and other parameters.

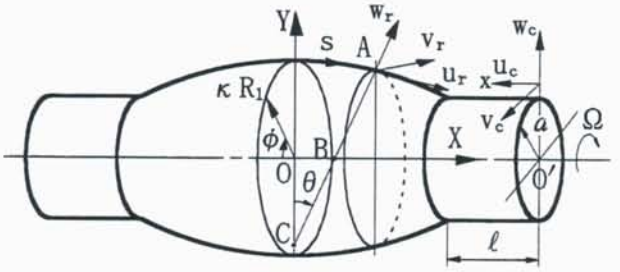

Fig. 1 Analytical model and coordinate system

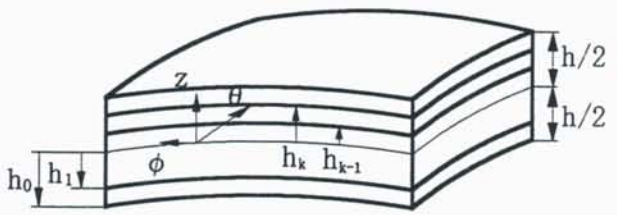

Fig. 2 Cross-sectional view of shell

2. ANALYTICAL MODEL AND CO-ORDINATE SYSTEM

Let us consider the vibrations of a vessel rotating at the angular velocity Ω . The vessel is composed of a thin laminated composite shell of revolution with a constant meridional curvature and two thin laminated composite circular cylindrical shells.

In Figure 1 are shown the middle surface of the vessel and the co-ordinate system. The origin of the shell of revolution is taken to be at the center O on the middle cross-section, with (X,Y) being the orthogonal co-ordinates, θ the angle between the normal to an arbitrary point A on the middle surface and the Y axis, ϕ the circumferential co-ordinate parameter, while Z axis is in the direction of the normal to the point on the meridian with positive outward. By assuming the principal radius of curvature of the meridian as R_1 ($=\overline{AC}$)= const., the principal radius of curvature of the parallel circle R_2 can be expressed as

$$R_2 = (\overline{AB}) = R_1/\Phi, \quad \Phi = \cos\theta/(\cos\theta + \kappa - 1) \tag{1}$$

where κ is the ratio of the principal radius of curvature of the parallel circle to that of the meridian R_1. Let the thickness of the shell be h and the displacements in the θ, ϕ and z directions be u_r, v_r and w_r.

For the circular cylindrical shell, the origin is taken to be at the center O' on the end cross-section, with x being the axial, ϕ the circumferential and z (positive outward) the radial co-ordinate parameters. The length,mean radius and thickness are denoted by ℓ (= μa), a and h, respectively. Employ a nondimensional co-ordinate $\xi = x/a$ and denote the displacements in the x, ϕ and z directions by u_c, v_c and w_c, respectively. Figure 2 shows the cross-sectional view of the shell, in which h_k and h_{k-1} are the values of the normal co-ordinate, measured from the middle surface, at the outer and inner surfaces of the kth laminate, respectively.

3.NUMERICAL RESULTS

Numerical studies are made for vessels of N symmetric cross-ply laminates. As composite materials,graphite fiber reinforced epoxy are considered. All the layers are taken to have equal thickness. The moduli of elasticity of the materials used are taken from Vinson and Sierakowski[13]:E_{11}=138(GPa),E_{22}=8.96(GPa), G_{12}=7.1(GPa), ν_{12}=0.30. Here E_{11} is the modulus of elasticity of the lamina in the direction of the fibers and E_{22} is the transverse modulus; G_{12} is the shear modulus; and ν_{12} is the Poisson's ratio. When the fibers are directed to the meridional direction in the shell of revolution and to the axial direction (x direction) in the circular cylindrical shell, the angle of fiber is called zero degree,on the contrary,is called 90° when the fibers are directed to the circumferential direction(ϕ direction). To show the characteristics of the vibration, the nondimensional frequency parameter α_r and the nondimensional rotating angular velocity parameter α_{r0} are used, where

$$\begin{aligned}
&\alpha_r{}^4 = \rho_0 p^2 R_1{}^4 / E_0 h^2 \\
&\alpha_{r0}{}^4 = \rho_0 \Omega^2 R_1{}^4 / E_0 h^2 \\
&E_0 = E_{11} / \left[12\left(1-\nu_{12}\nu_{21}\right)\right] \\
&\beta_r = R_1 / h \\
&\alpha_c = \alpha_r \Phi'' \\
&\alpha_{c0} = \alpha_{r0} \Phi''' \\
&\beta_c = a/h = \beta_r \Phi''' \\
&\Phi''' = \cos\theta_0 + \kappa - 1
\end{aligned} \tag{2}$$

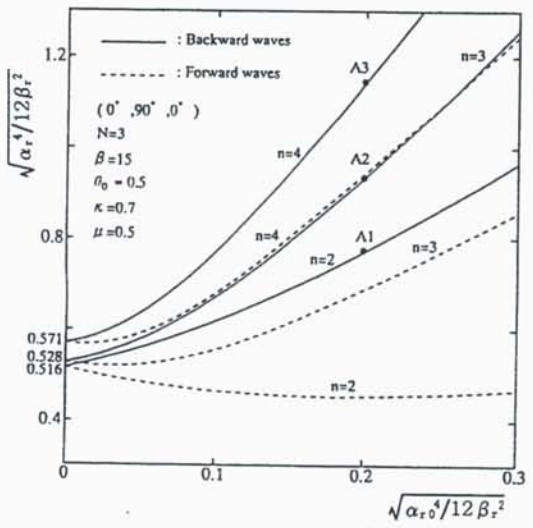

Fig.3 Frequency curves of a rotating vessel (Both ends clamped, symmetric vibration)

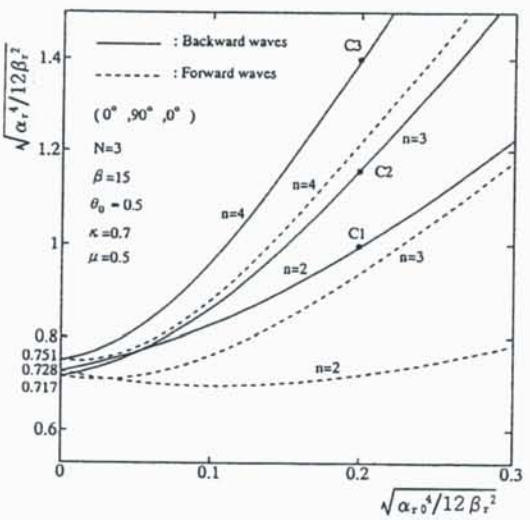

Fig.4 Frequency curves of a rotating vessel (Both ends clamped, antisymmetric vibration)

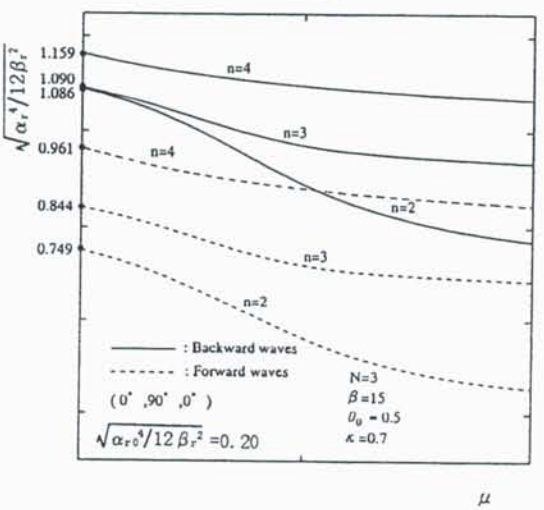

Fig.5 Frequency curves of a rotating vessel (Both ends clamped, symmetric vibration)

and ρ_0, p and h are the density of each lamina, the circular frequency and the total shell thickness.In the calculations for the results shown hereafter, β_r, N, κ, n (circumferential wave number), θ_0 (value of θ at the connection), μ ($=\ell/a$) and $\sqrt{\alpha_{r0}^4/12\beta_r^2}$ were first chosen and then a search was conducted for the values of $\sqrt{\alpha_r^4/12\beta_r^2}$ which satisfied the frequency equations.

Figures 3 and 4 show the frequency curves of a rotating vessel with the stacking sequence (0°, 90°, 0°) in the case where the number of laminae N=3, β_r=15, θ_0=0.5, κ=0.7 and μ=0.5. The marks A1 ~ A3 and C1 ~ C3 on the curves denote the points at which the mode shapes will be shown. The frequencies increase with an increasing number of n or rotating velocity of the vessel.

Figures 5 and 6 show the nondimensional frequencies versus μ. The values of $\sqrt{\alpha_r^4/12\beta_r^2}$ at μ=0 correspond to the eigenvalues for a shell of revolution with both ends clamped. As seen from the figure, the frequencies of the vessel gradually approach the ones of the shell of revolution as the length of the cylinder becomes shorter.

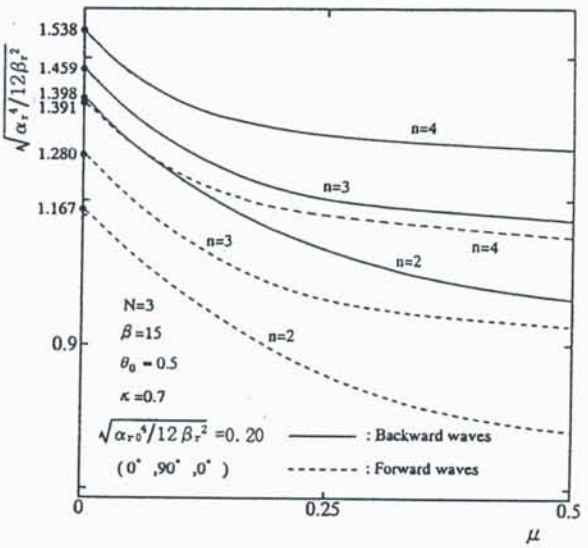

Fig.6 Frequency curves of a rotating vessel (Both ends clamped, antisymmetric vibration)

REFERENCES

(1) Padovan J.,Traveling waves vibration and buckling of rotating anisotropic shells of revolution by finite elements, Int.J.Solids Structures, 11(1975),1367-1380.

(2) Rand O. and Stavsky Y., Free vibrations of spinning composite cylindrical shells, Int.J. Solids Structures, 28-7(1991),831-843.

(3) Chen Y.,Zhao H.B. and Shen Z.P., Vibrations of high speed rotating shells with calculations for cylindrical shells,J.Sound Vib., 160-1(1993),137-160.

(4) Igawa H. and Endo M., Free vibration and buckling of rotating prestressed anisotropic cylindrical shells, Trans.JSME.,61-587,C(1995),2761-2768.

(5) Lam K.Y. and Loy C.T., Free vibrations of a rotating multi-layered cylindrical shell, Int.J. Solids Structures, 32-5(1995),647-663.

(6) Jiqun H.,Suzuki K. and Shikanai G., Vibration analysis of rotating thin laminated composite circular cylindrical shell, Trans. JSME,62-599, C(1996),2549-2555.

(7) Suzuki K., Takayama K. and Shikanai G., Vibration analysis of rotating thin laminated composite shell of revolution , Trans.JSME., 62-600,C(1996),2990-2997.

(8) Igawa H., Yamazawa D. and Endo M.,Forced vibration of rotating anisotropic cylindrical shells, Trans.JSME.,62-600,C(1996),2998-3004.

(9) Igawa H., Yamashita Y. and Endo M., Free vibration of thick rotating prestressed an isotropic cylindrical shells, Trans. JSME., 62-600, C(1996), 3005-3012.

(10)Jiqun H., Suzuki K. and Shikanai G., Vibration analysis of rotating thick laminated composite circular cylindrical shell, Trans. JSME., 63-614, C(1997), 3327-3334.

(11)Jiqun H., Suzuki K. and Shikanai G., Vibration analysis of rotating thin laminated composite circular cylindrical shell having different boundary conditions at both ends, Proc D&D'98 in Hokkaido, No.98-8(1998),

(12)Suzuki K., Shikanai G. and Chino T., Vibrations of composite circular cylindrical vessels, Int. J, Solids Structures, 35-22(1998), 2877- 2899.

(13)Vinson,J.R. and Sierakowski,R.L., The behavior of structures composed of composite materials, (1987) Martinus Nijhoff Publishers, Dordrecht, The Netherlands.

SPATIAL COHERENT STRUCTURES IN THE FORCED DYNAMICS OF A FLEXIBLE MULTI-BAY TRUSS

Xianghong Ma
Graduate Research Assistant, xma@uiuc.edu
and
Alexander F. Vakakis
Associate Professor, avakakis@uiuc.edu
Department of Mechanical & Industrial Engineering
University of Illinois at Urbana - Champaign
Urbana, IL 61801

SUMMARY

Lightweight flexible multi-bay truss structures are often encountered in civil engineering and aerospace applications. The dynamic analysis of such trusses poses interesting technical challenges. This is due to the fact that such structures generally possess high modal densities, with 'clusters' of densely packed modes existing even at relatively low frequencies. In addition, in multi-coupled trusses mode conversions occur that produce closely spaced modes corresponding to different forms of truss vibration, such as predominantly-bending, near-shear, etc. As a result, system identification (modal analysis) of flexible trusses is a challenging task, and accurate low-order models of the truss dynamics are difficult to obtain. Such low dimensional models are essential for controlling disturbance propagation in these systems, or for performing substructure synthesis and structural modification studies.

Even the task of numerically simulating the transient dynamics of extended flexible trusses introduces serious technical difficulties. These are due to the presence of exponential dichotomy in the corresponding transfer matrices, since they possess eigenvalues of very large or small magnitude; this leads to numerical instabilities when straightforward transfer matrix multiplications are performed. The use of the finite element method for computing the transient dynamics has other limitations related to the large number of elements required for the computation of the transient response. At most, this method can provide the transient response of the truss at early times.

The aim of this work is two-fold. First, we aim to develop a numerically stable computational approach for computing the exact transient dynamics of a flexible truss, by employing the direct global matrix (DGM) technique developed by Schmidt and Jensen. This method is based on numerically inverting a global transfer matrix of large dimension, instead of performing error-prone lower dimensional transfer matrix manipulations.

Once the transient responses of the truss are reliably simulated, we proceed to the second aim of the work, namely, to perform nonparametric system identification of the truss dynamics by means of Karhunen-Loeve (K-L) decomposition. This technique is used to extract spatial coherent structures (or proper orthogonal modes - POMs) from a set of time-series of the responses at different points of the truss. In addition to computing the POMs of the truss dynamics, the K-L method provides an estimate of the energy of each identified POM (and, thus, a measure of each POM's importance), a feature that enables the quantitative assessment of the accuracy of the system identification of the truss. Our aim is to demonstrate that by using K-L decomposition we can extract the POMs of a flexible truss with high modal densities; these can then be used to create accurate low-dimensional models of this structure.

VIBRATIONS OF A FLUID–SOLID COLUMN

Jörg Wauer
Institut für Technische Mechanik, Universität Karlsruhe
Kaiserstraße 12, D–76128 Karlsruhe, Germany
E–mail: wauer@itm.uni-karlsruhe.de

ABSTRACT

The coupled extentional vibrations of a column composed of a slender (visco–)elastic bar and an attached chamber filled with a compressible (viscid) fluid are examined. After formulating the governing boundary value problem in its nonlinear form, attention is focused on free vibrations under different assumptions. The classical case of small vibrations without viscosity influences are analyzed first. Complicating effects as finite magnitudes and viscosity (including thermal processes) are analyzed next. Finally, forced vibrations are briefly addressed.

INTRODUCTION

Mixed–domain systems and their vibrational behavior attracted more and more attention during the recent past. Fluid–structure interaction is a problem class for such multifield systems, in fact with boundary coupling: The field equations within the separate domains are decoupled and the coupling appears in the kinematical and dynamic transition conditions at the interface between the fluid and the solid domains. In the present contribution, a prototypical representative for such a system with boundary coupling will be studied where all field quantities depend from one space coordinate only.

GOVERNING BOUNDARY VALUE PROBLEM

Consider a slender bar (mass distribution μ, extentional stiffness EA, non–deformed equilibrium length L, internal damping coefficient d_i) along the x axis of an Cartesian inertial reference frame and an attached chamber with rigid, perfectly smooth walls (see Fig. 1). The face of the bar perfectly closes the chamber (original length H) and can move alonge its side–walls without friction, the opposite end is fixed. The slender

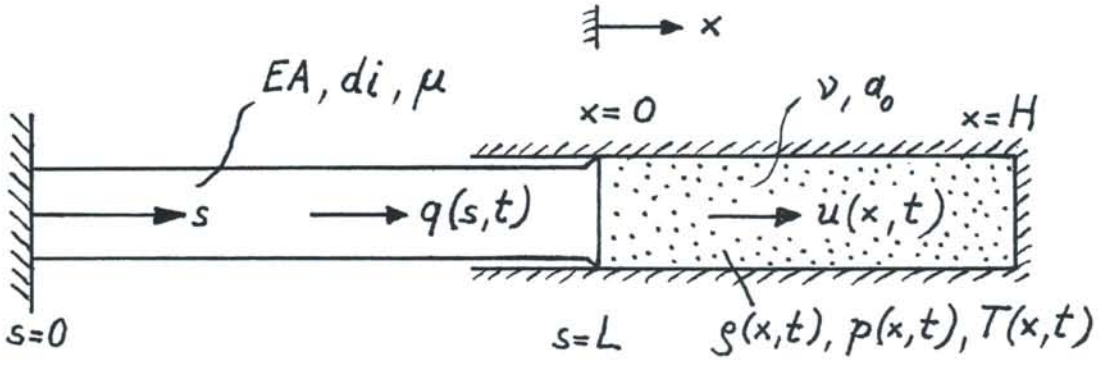

Figure 1: Geometry of the system

chamber is filled with a compressible Newtonian fluid (equilibrium density ρ_0, pressure p_0, temperature T_0,

speed of sound a_0 and viscosity ν). Due to the mentioned properties of the side walls of the chamber, there is a frictionless motion of the fluid along these walls (and no boundary layer can develop).

Of interest are space– and time–dependent longitudinal oscillations $q(s,t)$ of the bar (s denotes its undeformed arc–length) coupled with the axial velocity $u(x,t)$ and the fluctuations of pressure $p(x,t)$, density $\rho(x,t)$ and temperature $T(x,t)$ of the fluid. The temperature of the bar is assumed to remain unchanged. If forced vibrations are considered, a load per unit length $p(s,t)$ at the bar will be introduced.

In general, a non-linear wave equation modified by viscous effects (and under certain circumstances an external excitation) for the bar, the one–dimensional Navier–Stokes equations together with an energy balance and a state equation for the fluid and appropriate boundary conditions at the outer ends of the column (i.e. one for the bar, the other one for the fluid) and finally two transition conditions at the interface between bar and fluid (where one of them is of kinematical and the other one of dynamical nature) describe the dynamic interaction of the two subsystems. An important feature within the nonlinear formulation is that there is a moving interface (described by the end displacement $u(L,t)$ of the bar).

SMALL FREE VIBRATIONS WITHOUT DISSIPATION

Viscous effects are neglected and only linear terms in the boundary value problem are taken into consideration. A consequence for an ideal fluid considered in this section is that temperature changes do not occur. It is straightforward to derive the corresponding eigenvalue problem for the space–dependent amplitudes $Q(s)$ and $U(x)$ of the bar displacements $q(s,t)$ and axial fluid velocity $u(x,t)$, respectively (under elimination of density and pressure) with the square of the natural frequency as the eigenvalue. Following [1], the exact eigenvalue equation can be derived to be solved by a computer–aided evaluation. The eigenvalues can be represented as a function of a stiffness ratio of fluid and bar with a certain coupling parameter which essentially represents the density ratio of fluid and bar. It turns out that there is a significant coupling of the acoustical and the structural modes in the region where the eigenvalues of the decoupled substructures coincide. For practical values of the coupling parameter, there is a curve "veering" between acoustical and structural branches of solutions of the eigenvalue equation. In these rigions of curve veering there is the strongest coupling, outside of these regions, the eigenvalues (and modes) asymptotically approach the characteristics of the decoupled subsystems. Since both subsystems are able to vibrate, there is no clear added mass effect: not in all parameter ranges, the eigenfrequencies corresponding to the structural modes increase due to the additional mass of the fluid.

COMPLICATING EFFECTS

As a first complication, finite–magnitude vibrations (but still for the elastic bar and an inviscid fluid) will be examined. A perturbation analysis is suggested to calculate the corrections due to the inherent nonlinearites of the vibroacoustic problem. For that purpose, the bar oscillations are assumed to be of the order of a small parameter ε. To take into consideration that the dynamic characteristics, in particular the eigenfrequencies, will also be corrected by the nonlinearties, a new time variable is introduced. Then, the vibration variables and also the circular frequency are expanded in powers of ε. Substituting into the governing boundary value problem and equating terms of equal powers of ε, a set of perturbation boundary value problems of successive order is obtained. There is a first–order problem which is identically the same as discussed before and a second–order problem which can also be evaluated analytically [2]. The nonlinearities lead to a softening characteristic of the system, i.e., with increasing vibrational amplitudes, there is a monotonic decrease of the the natural frequencies.

The second generalization which will be discussed is the inclusion of the viscosity (both for fluid and bar) and in general, the appearance of temperature fluctuations (in the fluid), shown here within the linear formulation.

The isothermic case for an elastic (one–degree–of–freedom) structural member was analyzed in all details in [1], too, the more complicated problem including the internal damping of the bar and a non–isothermic behavior of fluid will be dealt with in the present contribution. In all cases, the original real–valued eigenvalues become complex where the imaginary part is responsible for the decay of the coupled vibrations. Since there result an eigenvalue problem with space–independent coefficients once more, the exact eigenvalue equation can be derived to be evaluated straightforwardly. Because the dissipation is small and the thermal activities are low, the decay of the oscillations is weak and the vibrational frequencies remain practically unchanged.

FORCED VIBRATIONS

There is no problem to include the viscous effects for calculating the steady–state response for a harmonic excitation of the bar, for instance. It will be addressed for small vibrations only so that no surprising phenomena happen: There is a pronounced resonance when the driving frequency coincides with the natural frequencies of the coupled system. A modal expansion technique can handle the problem without difficulties because the internal damping of the bar is proportional to the stiffness of the bar and the viscous fluid forces are proportional to the fluid density.

In the non–linaer case, the familiar Duffing phenomena may happen and for a large length of the fluid chamber, shock effects in the fluid are possible [3].

CONCLUSIONS

As an interesting example of mixed–domain systems with boundary coupling, the dynamic interaction of a one–dimensional fluid–solid column has been examined in all essential details. The advantage of the considered problem is that most of the results can be calculated in an analytical form without any discretization. All results and effects described by them, therefore, become very clear and obvious.

REFERENCES

1. Seemann, W. and Wauer, J. 1996. Fluid–Structural Coupling of Vibrating Bodies in a Surrounding Confined Liquid, *Z. Angew. Math. Mech.* **76**, 67–79.
2. Wauer J. 1999. Nonlinear Waves in a Fluid–Filled Planar Duct with a Flexible Wall, *Proc. IUTAM–Sympos. on Recent Developments in Nonlinear Oscillations of Mechanical Systems*, to be published.
3. Nayfeh, A. H. and Kelly, S. G. 1978. Non–linear Interactions of Acoustic Fields with Plates under Harmonic Excitation, *J. Sound Vibr.* **60**, 371–377.

Remarks on the Three-Dimensional Vibration of Disks and Cylinders

Jonathan Wickert
Department of Mechanical Engineering
Carnegie Mellon University
Pittsburgh, PA 15213-3890
Email: wickert@cmu.edu Tel: (412) 268-2494

1. Introduction

Thick annular disks and cylinders are common structural elements, and the study of their vibration forms a classical area within elastodynamics. Vibration of an arbitrarily thick annular disk is investigated here by Ritz discretization of the Rayleigh quotient in terms of the three-dimensional kinetic and strain energy expressions. Application of this standard technique yields natural frequencies and mode shapes for coupled axial, radial, and circumferential vibration. This treatment is applied to "disks" of arbitrary dimension, and so the analysis can encompass models for annular plates, bars, rods, rings, and shells. The solutions so obtained converge in the limiting cases to the values expected from the respective classical theories, and ones that account for shear deformation and rotary inertia. In this paper, several interesting findings on the vibration of axisymmetric disks and cylinders are discussed with a view towards three-dimensional phenomena that are not expected on the basis of the classical theories alone.

2. In-Plane Vibration Modes of Arbitrarily Thick Disks

In automotive disk brakes, squeal noise and vibration are commonly attributed to motion of the disk out of its equilibrium plane. In particular, sound is radiated efficiently from a disk during bending. However, to the extent that frictional stresses are oriented within the plane of the disk, radial and circumferential motions can also be excited. Laboratory experiments on commercial brake rotors demonstrate that in-plane modes exist at frequencies comparable to those of out-of-plane bending, motivating an examination of the relationships among those two classes of modes.

For an annular disk having ratio 50% between the inner and outer diameters, the non-dimensionalized natural frequency spectrum is shown in Figure 1 as a function of h^*, the ratio of thickness to outer diameter [1]. As the structure evolves from a thin plate ($h^* \approx 0.01$) to a long cylinder ($h^* \approx 100$), the mode shapes and frequency loci undergo continuous transition. For instance, the predominant displacement for the highlighted fundamental two nodal diameter plate mode changes from axial at small h^* into coupled radial and circumferential displacements for large values. Motions for this and similar modes become fully three-dimensional over the intermediate thickness range. In addition to the beam and plate asymptotes evident in the figure, the model also predicts modes that are asymptotic to those of classical theories for the torsion of shafts and for the longitudinal vibration of rods. The various asymptotes are identified by their slopes at limiting values of h^*.

Loci which are insensitive to h^* over the full range, such as the second highlighted locus in Figure 1, correspond to in-plane modes. For $h^* > 1$, loci converge with increasing h^* to asymptotes near 0.53 and 1.24. At $h^* = 100$, those values agree to within 3% with frequencies predicted for the radial modes of infinitely long annular cylinders as predicted by Gazis in the late 1950's. Loci which are sensibly independent of h^* at large values, such as those at a frequency of 0.72, represent higher-order longitudinal modes and agree to within 1% of frequency predictions for the longitudinal shear modes of infinite cylinders. They are discussed further below. Of particular interest are the circumstances in which frequencies for specific in-plane and out-of-plane modes are commensurate, offering opportunity for energy transfer from in-plane to bending vibration. Several such intersections of loci occur in the thickness range $0.04 < h^* < 0.2$, which is typical of commercial brake rotors.

The transition of the lowest bending and in-plane modes with increasing thickness is depicted in Figure 2. In mode "a", for example, the axial displacement has zero nodal cylinders, two nodal diameters, and no axial nodal planes; radial and circumferential displacements, on the other hand, both have an

axial nodal plane. This nodal pattern distribution is maintained throughout the entire range of h*, although the primary displacement component does change from axial to radial at large h*. In contrast, the shape of in-plane mode "b" is relatively unaffected by increases in h*. At h* = 4.0, modes "a" and "b" are both radial cylinder modes having two nodal diameters, and differ only by the presence of the additional axial nodal plane which is present in mode "a".

3. Frequency Clusters in Finite Length Cylinders

The formation of "clusters" in the natural frequency spectrum of long cylinders is examined next [2] with emphasis on the cylinder's radial (R) and longitudinal shear (LS) classes of modes. Unlike modes seen in classical longitudinal vibration problems, the axial displacement in a longitudinal shear mode varies with angular position over a given cross-section.

As the length of a traction-free annular cylinder is increased, distinct members within any family of radial (R) or longitudinal shear (LS) modes have natural frequencies that asymptotically approach a common non-zero value. Such modes, potentially having significantly different numbers of nodes along the cylinder's generator, can have natural frequencies that are indistinguishable from one another within the resolution of test equipment or numerical simulation. The three-dimensional vibration model discussed here predicts the formation of narrow "frequency clusters" with the cylinder's increasing length, the converged value of which bounds from below the frequencies of all modes within a particular family.

With disk thickness now being interpreted more appropriately as the cylinder's length L* in Figure 3, the frequency spectrum is shown as a function of length, illustratively for aluminum material properties and an inner-outer diameter ratio of 0.87. The natural frequencies for the bending, torsion, and longitudinal vibration modes are shown as dotted lines, and those values agree with their respective classical theories for appropriate values of L*. Of particular interest are the vibration modes for which the natural frequencies converge to nearly a constant value at large L*. Their loci are drawn with solid lines, and the labels identifying the R or LS families are shown near each frequency cluster. Here the index "m" denotes the number of nodal planes along the generator, and the second index "n" represents the number of azimuthal planes. Each family of modes is distinguished by a particular frequency to which its members converge. For instance, radial modes having any value of m and n = 2, 3, or 4 cluster at frequencies near 0.101, 0.282, or 0.528, respectively. Although bending waves in an infinite cylinder have cutoff frequency of zero, radial and longitudinal shear waves have finite-valued, non-zero, cutoff frequencies. Indeed, the cutoff frequencies for those families of waves are the same as the asymptotes in L* established by the frequency clusters. Figure 4 shows a measured collocated point transfer function of a steel cylinder with L* = 52. The beam bending modes dominate the low frequency range, while both bending and (m,2) radial modes are present in the 1.2-3.2 kHz range. The spectrum is dense at the 1.225 kHz cluster with the nine radial modes m = 0, ..., 8 being concentrated there. The frequencies of those modes, each having a different number of nodes along the generator, are indistinguishable at this level of measurement resolution.

The isometric views in Figure 5 depict the number and location of axial nodal planes for the lowest four members of the (m,2)-R family at L* = 10. The nondimensional frequencies for these modes are 0.101, 0.101, 0.103, and 0.108, so that at this level of precision, the frequencies for the lowest two modes are "repeated." Likewise, the frequency of the third mode is only some 3% higher than the frequency of the (0,2)-R and (1,2)-R cluster, but it has two additional nodal planes. At L* > 22, the frequency of (2,2)-R also reaches 0.101, and at L* > 49, all four modes shown have the same frequency at this level of precision.

References

1. K.I. Tzou, J.A. Wickert, and A. Akay, "In-Plane Vibration Modes of Arbitrarily Thick Disks," *ASME Journal of Vibration and Acoustics*, **120**(2), pp 384-391, 1998.

2. K.I. Tzou, J.A. Wickert, and A. Akay, "Frequency Clusters in the Spectrum of Annular Cylinders," *ASME Journal of Applied Mechanics*, in press.

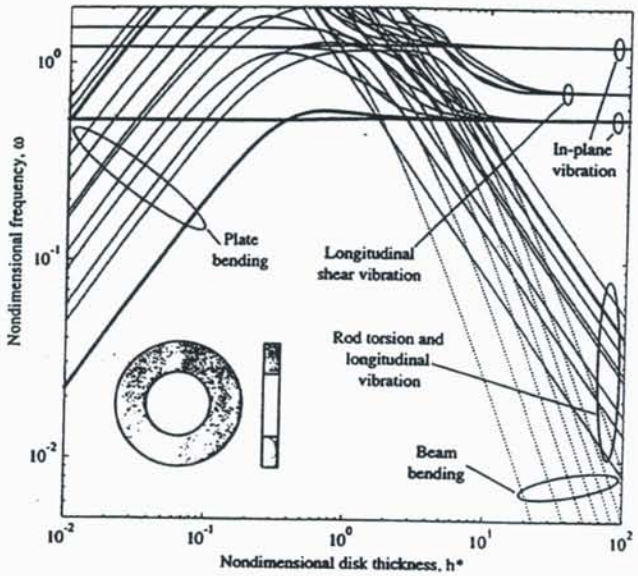

Figure 1: Spectrum of a free annular disk.

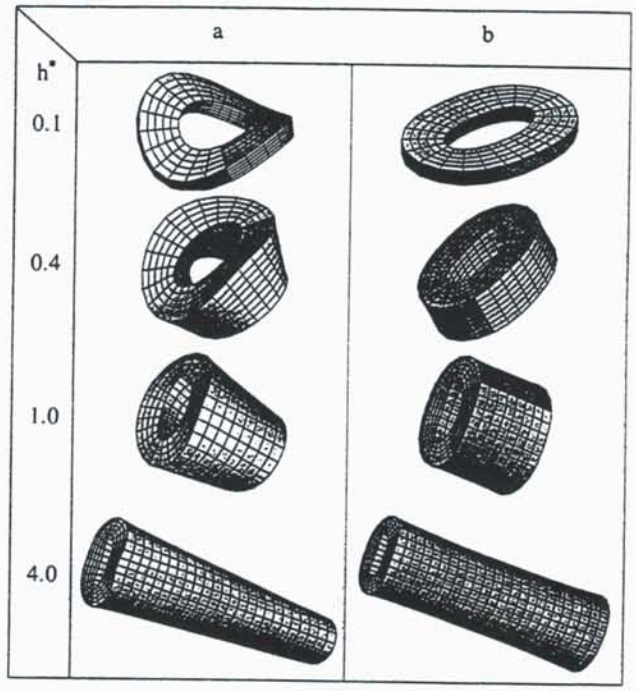

Figure 2: Transition of selected modes from plate to cylinder geometries with increasing thickness.

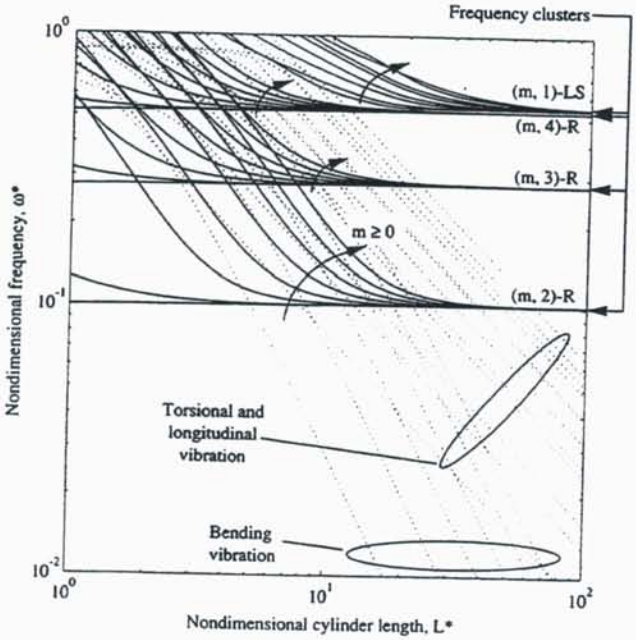

Figure 3: Spectrum of a free annular cylinder.

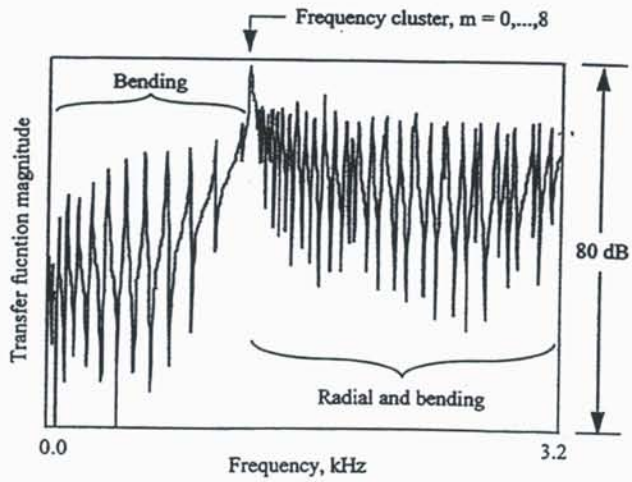

Figure 4: Measured transfer function and cluster.

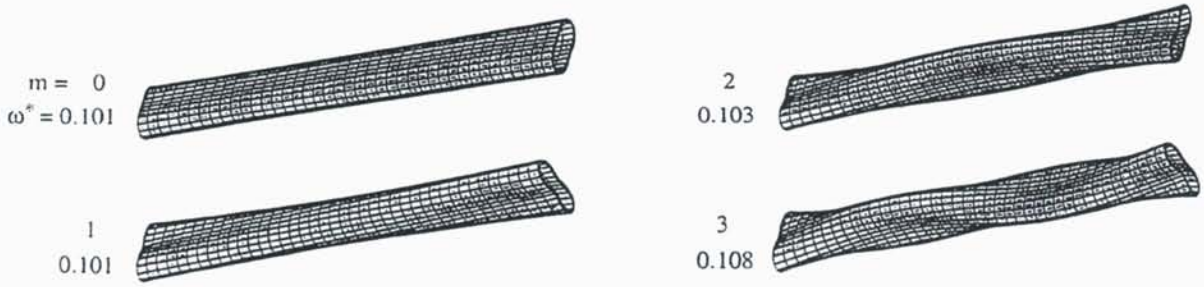

Figure 5: First four mode shapes and their natural frequencies in the (m,2)-R cluster of Figure 3.

ON OBTAINING MODES FROM DYNAMIC STIFFNESS MATRIX ANALYSIS OF PIECEWISE CONTINUOUS STRUCTURES

F.W. Williams

Cardiff School of Engineering, Cardiff University, Cardiff CF24 3TB, UK

INTRODUCTION

The Wittrick-Williams (W-W) algorithm[1,2] gives all required eigenvalues of a structure with certainty when using exact theory. These are natural frequencies of vibration, buckling loads[3] or frequencies of wave propagation[4]. The present contribution considers mode finding for all of these cases.

Exact member theory yields exact member stiffness matrices by solving member differential eqns (DE's), including mass per unit length μ and axial force P. The usual FE rules give the overall stiffness matrix **K** from these member matrices. Hence the elements of **K** are transcendental functions of the frequency ω and/or the μ and P of members. Therefore the eigenvalue problem is transcendental and so usual FE linear eigensolvers are inapplicable and instead the W-W algorithm

$$J = \sum J_s + \sum J_m + s\{\mathbf{K}\} \qquad (1)$$

must be used, where multi-level substructuring is permitted[5] and : J = no. of eigenvalues of the structure exceeded by a trial eigenparameter; $J_s(J_m)$ = no. of eigenvalues of a substructure (member) exceeded if its attachments to its parent structure are clamped; the summations cover, respectively, all substructures and members; **K** = overall stiffness matrix obtained after substructuring; and $s\{\mathbf{K}\}$ = no. of negative leading diagonal elements after Gauss elimination has reduced **K** to the upper triangular $\mathbf{K}^{\Delta}$. When Eqn. 1 is applied to a *substructure* to finds its J_s, the first summation covers all substructures it contains *directly* and the second one covers all members it contains *directly*. 85 papers covering extensions and applications of the algorithm are cited elsewhere[6]. Several, e.g. extension to rotationally periodic structures[7] or substructures[8], can involve **K** being Hermitian, such that the natural frequencies often appear in pairs.

CRITERIA SUGGESTED AND USED FOR JUDGING MODE FINDING METHODS

Computer programs should ideally solve *all* problems within the family for which they are written, but all too frequently they fail for problems which are exceptionally complex or excessively simple, e.g. limiting cases such as **K** being a scalar because substructuring removes all the degrees of freedom except one from **D**, the displacement vector to which **K** corresponds. Therefore some relevant criteria are suggested in Table 1(a). The first is that it should not be assumed that the final diagonal element of $\mathbf{K}^{\Delta}$ approaches zero as ω approaches the eigenvalue. This is because if the last h-1 elements of **D** are null in the correct mode, the last h-1 elements of the diagonal of $\mathbf{K}^{\Delta}$ are finite and the h-th element from the bottom of $\mathbf{K}^{\Delta}$ approaches zero. This occurs quite frequently, e.g. because the modes of symmetric structures are symmetric or anti-symmetric, or for structures with uncoupled in- and out-of-plane behaviour. The second criterion is that the method must be able to calculate the modes with **D=0** that occur for many simple problems[2]. The third criterion is the ability to find r independent

modes when the W-W algorithm has shown there to be r ($\geq$2) coincident eigenvalues and the fourth criterion is that these modes should be strictly[9] mutually orthogonal. The remaining criteria in Table 1(a) are self-explanatory and involve subjective judgements by the authors. They are used to assess the five early mode finding methods[10] presented below to give Table 1(b), where $\surd(\times)$ denotes satisfied (not satisfied) and A to C denote degrees of satisfaction, with A being best.

The first method is simply to set the last element of **D** to an arbitrary value and to solve $\mathbf{K}^{\Delta}\,\mathbf{D} = \mathbf{0}$. The second method finds where the lowest diagonal zero is in $\mathbf{K}^{\Delta}$ and, if it is the h-th element from the bottom, back substitutes into $\mathbf{K}^{\Delta}\,\mathbf{D} = \mathbf{0}$ with the last h–1 elements of **D** set to zero and the element next above these given an arbitrary value. The third method modifies this to find r independent modes when r eigenvalues coincide, by finding the last r diagonal elements of $\mathbf{K}^{\Delta}$ which go from +ve to –ve between the lower and upper bounds on these eigenvalues The fourth method uses the fact that the response of any structure excited close to an eigenvalue is dominated by the associated mode. It solves $\mathbf{K}\,\mathbf{D} = \mathbf{P}$ for a randomly chosen **P**, with **K** evaluated at the closest available approximation to the eigenvalue. The fifth method repeats this method r times for problems with r coincident eigenvalues. All five methods usually give modes which are typically three orders less accurate than are the eigenvalue approximations from which they are calculated.

TABLE 1

(a)

No.	Criterion	No.	Criterion
1	Works if last element of **D** is zero	6	Fast
2	Works when correct **D** is null	7	Cheap
3	Finds independent 'coincident' modes	8	Accurate
4	'coincident' modes are orthogonal	9	Reliable
5	Simple		

(b)

Method		Performance for criterion no.								
No.	Description	1	2	3	4	5	6	7	8	9
1	Arbitrary last element for **D**	×	×	×	×	A	A	A	A–	C
2	Arbitrary other element for **D**	√	×	×	×	A–	A	A	A–	C+
3	Method 2 for 'coincident' modes	√	×	√	×	B	A–	A–	A–	B–
4	Random force vector, i.e. **P**	√	(×)	×	×	B+	B+	A–	A–	B+
5	Method 4 repeated r times	√	(×)	√	×	B	B	B	B	B
6	Random **P** with extra joints	√	√	√	×	B–	B+	B+	A–	A–
7	Expanded **K** and pivoting	√	√	√	×	C	C	C	A	A
8	'Inverse iteration'	√	×	√	×	B	A	A	A–	A–

RECENT ADVANCES

Ronagh *et al*[11] introduced an elegant addition to the fourth and fifth methods, to find modes for which **D**=**0** while also giving mode accuracy which more closely approaches (e.g. to one order) that of the eigenvalue approximation used. This is method 6 in Table 1(b) and consists of adding an extra randomly situated joint within the length of any member which was found, *after convergence on the eigenvalue*, to have a clamped-ended member eigenvalue close to or (apparently) at this eigenvalue.

A major effort is now being made to re-evaluate and modify these previous mode finding methods and hence to develop new methods which ideally should satisfy the first four criteria of Table 1(a) and perform well for the remaining criteria. To date, only a few preliminary results and brief statements of the associated theory have been published[12,13]. Two such methods are methods 7 and 8. Method 7 involves expanding **K** to include extra rows and columns corresponding to the constants which occur in the solutions of the DE's of the members and employs full pivoting when obtaining $\mathbf{K}^{\Delta}$ from **K**. Method 8 seems very promising. It solves the 'inverse iteration' problem $\mathbf{K}\ \mathbf{D}^{i+1} = \mu\ \mathbf{D}^{i}$, where i denotes the i-th estimate of the mode and μ is a normalization parameter. An ultimate goal is to establish all the relationships between it and the excellent iterative work of Melosh and Smith[14].

REFERENCES

1. F.W. Williams and W.H. Wittrick, An automatic computational procedure for calculating natural frequencies of skeletal structures, *Int. J. Mech. Sci.*, **12:9**, 1970, 781-791.
2. W.H. Wittrick and F.W. Williams, A general algorithm for computing natural frequencies of elastic structures, *Q. J. Mech. Appl. Math.*, **24:3**, 1971, 263-284.
3. W.H. Wittrick and F.W. Williams, An algorithm for computing critical buckling loads of elastic structures, *J. Struct. Mech.*, **1:4**, 1973, 497-518.
4. H.J. Ouyang, F.W. Williams and D. Kennedy, A general method for analyzing wave propagation along longitudinally periodic structures, *J. Sound Vib.*, **177:2**, 1994, 277-281.
5. F.W. Williams, Natural frequencies of repetitive structures, *Q. J. Mech. Appl. Math.*, **24:3**, 1971, 285-310.
6. F.W. Williams, Review of exact buckling and frequency calculations with optional multi-level substructuring, *Computers & Structures*, **48:3**, 1993, 547-552.
7. F.W. Williams, An algorithm for exact eigenvalue calculations for rotationally periodic structures, *Int. J. Num. Meth. Engng.*, **23:4**, 1986, 609-622.
8. F.W. Williams, Exact eigenvalue calculations for structures with rotationally periodic substructures, *Int. J. Num. Meth. Engng.*, **23:4**, 1986, 695-706.
9. K.L. Chan and F.W. Williams, Orthogonality of modes for piecewise continuous structures, *Proc. of Int. Conf. on Vibration Engng*, Dalian, China, Aug., 1998. Northeastern University Press, China, 20-24.
10. C.T. Hopper and F.W. Williams, Mode finding in non-linear structural eigenvalue calculations, *J. Struct. Mech.*, **5:3,** 1977, 255-278.
11. H.R. Ronagh, R. Lawther and F.W. Williams, Calculation of eigenvectors with uniform accuracy, *J. Engng. Mech. (of ASCE),* **121:9**, 1995, 948-955.
12. S. Yuan, K.S. Ye and F.W. Williams, Towards exact computation of vibration modes in dynamic stiffness matrix methods, *5th Int. Symp. on Structural Engineering for Young Experts : Theories and Practices of Structural Engineering*, Shenyang, China, Aug., 1998. Seismological Press, Beijing, China, 11-19.
13. S. Yuan, K.S. Ye and F.W. Williams, From "random" to "precise" : On exact computation of vibration modes in dynamic stiffness matrix methods, *2nd Symp. for Univs of Mainland China, Taiwan and Hong Kong area on Civil and Structural Engineering*, Taipei, Taiwan, Aug., 1998. Civil and Cultural Foundation of National Taiwan University, Taiwan, 9-17.
14. H.A. Smith, D.C. Sorensen and R.K. Singh, A Lanczos-based technique for exact vibration analysis of skeletal structures, *Int. J. Num. Meth. Engng.*, **36**, 1993, 1987-2000.

On a novel approach to solving for the natural frequencies of a class of doubly curved shells including closed shells.

P.G. Young,

School of Engineering, University of Exeter, Exeter, Devon, UK

Abstract:

A three dimensional shell theory is presented which is applicable to doubly curved open shells which are arbitrarily deep in one principal direction but shallow in the other. The strain-displacement equations are expressed in Cartesian coordinates and the limits of applicability of these equations are discussed. These equations are then used in a Ritz variational formulation with algebraic polynomials as trial functions to solve for the natural frequencies of a number of doubly curved shell problems. By introducing penalty functions to enforce continuity of displacements at two opposite ends of a shell of rectangular planform, closed shells, such as cylinders, barrels, cooling tower type structures, toroids and rings, can be treated.

Strain-Displacement Equations:

Consider a homogeneous isotropic shell described in orthogonal curvilinear coordinates α_1, α_2 lying along the neutral surface and a coordinate α_3 normal to the neutral surface. If we assume the principal curvatures R_1 and R_2 lie along the coordinates α_1 and α_2 and the thickness a_3 to radius of curvature ratios are small, that is a_3/R_1 and a_3/R_2 <<1, the three dimensional linear strain displacement equations are given by (cf. Soedel [1], pp 25-26, Leissa [2], pp. 7)

$$\varepsilon_{11} = \frac{1}{A_1}\left[\frac{\partial U_1}{\partial \alpha_1} + \frac{U_2}{A_2}\frac{\partial A_1}{\partial \alpha_2} + U_3\frac{A_1}{R_1}\right], \qquad \varepsilon_{12} = \frac{A_1}{A_2}\frac{\partial}{\partial \alpha_2}\left[\frac{U_1}{A_1}\right] + \frac{A_2}{A_1}\frac{\partial}{\partial \alpha_1}\left[\frac{U_2}{A_2}\right],$$

$$\varepsilon_{22} = \frac{1}{A_2}\left[\frac{\partial U_2}{\partial \alpha_2} + \frac{U_1}{A_1}\frac{\partial A_2}{\partial \alpha_1} + U_3\frac{A_2}{R_2}\right], \qquad \varepsilon_{13} = A_1\frac{\partial}{\partial \alpha_3}\left[\frac{U_1}{A_1}\right] + \frac{1}{A_1}\frac{\partial U_3}{\partial \alpha_1}, \qquad (1)$$

$$\varepsilon_{33} = \frac{\partial U_3}{\partial \alpha_3}, \qquad \varepsilon_{23} = A_2\frac{\partial}{\partial \alpha_3}\left[\frac{U_2}{A_2}\right] + \frac{1}{A_2}\frac{\partial U_3}{\partial \alpha_2},$$

where ε_{11}, ε_{22}, ε_{33} are the normal strains, ε_{12}, ε_{13} and ε_{23} the shear strains, and U_1, U_2 and U_3 the displacements in the α_1, α_2 and α_3 directions respectively, and where A_1 and A_2 are the first fundamental quantities or Lamé parameters.

The strain displacement equations given by (1) can be simplified if we assume that either ratio a_1/R_1 or a_2/R_2 is small (<<1), or in other words the shell is shallow in either the α_1 or α_2 direction (in the following analysis it will be assumed that a_2/R_2<<1) and that the principal radii of curvature R_1 and R_2 are constant. The shell can then be approximately described in Cartesian coordinates by letting $x = R_1\, d\theta = \alpha_1$, $y = \alpha_2$, $z = \alpha_3$, $R_x = R_1$ and $R_y = R_2$ from which we obtain side-lengths $a = R_1\,\theta = a_1$ and $b = R_1 \sin\phi \cong a_2$ and thickness $c = a_3$. The fundamental quantities are then given by $A_1 = 1$ and $A_2 = 1$ and the strain-displacement equations can be expressed in terms of the displacements u, v and w in the x, y and z coordinates respectively as,

$$\varepsilon_{xx} = \frac{\partial u}{\partial x} + \frac{w}{R_x} \qquad \varepsilon_{xy} = \frac{\partial u}{\partial y} + \frac{\partial v}{\partial x}$$

$$\varepsilon_{yy} = \frac{\partial v}{\partial y} + \frac{w}{R_y} \qquad \varepsilon_{xy} = \frac{\partial u}{\partial z} + \frac{\partial w}{\partial x} - \frac{u}{R_x} \qquad (2)$$

$$\varepsilon_{zz} = \frac{\partial w}{\partial z} \qquad \varepsilon_{yz} = \frac{\partial v}{\partial z} + \frac{\partial w}{\partial y} - \frac{v}{R_y}$$

The shell is effectively "unwrapped" or "unravelled" in the deep direction (instead of using the more typical projection onto the x-y plane) which extends the applicability of the strain-displacement equations (2) to shells which are arbitrarily deep in one direction. In fact shells may even be wrapped end to end ($a = 2\Pi R_x$) or coiled ($a > 2\Pi R_x$) (although for coiled shells the interference of one surface on another is not taken into account). For shells of rectangular planform wrapped end to end ($a = 2\Pi R_x$), closed shells can be modelled by enforcing continuity at $x = 0$ and at $x = a$. However, for these shells the radius of curvature R_x will not, in general, be constant but will vary along the axial length b (except for the special case of a cylinder where $1/R_y = 0$). It can be shown that, in addition to the previously stated assumptions, the proposed equations will only apply for closed shells providing $b^2/(2R_xR_y)<<1$.

Application of strain-displacement equations to free vibrations using a Ritz approach

If we assume simple harmonic motion at radian natural frequency ω, the displacements u, v and w in the x, y and z directions respectively, can be expressed as: $u(x,y,z,t) = U(x,y,z) \sin \omega t$; $v(x,y,z,t) = V(x,y,z) \sin \omega t$ and $w(x,y,z,t) = W(x,y,z) \sin \omega t$. The displacements U, V and W for a thick shell of rectangular planform can be approximated using algebraic polynomials as follows

$$
\begin{aligned}
U(x,\,y,\,z) &= \sum_{i=0}^{n_x}\sum_{j=0}^{n_y}\sum_{k=0}^{n_z} A_{ijk}\, x^{i+l^u_{x=0}}\, y^{j+l^u_{y=0}}\, z^{k+l^u_{z=0}}\, (a-x)^{l^u_{x=a}}\, (b-y)^{l^u_{y=b}}\, (c-z)^{l^u_{z=c}} \\
V(x,\,y,\,z) &= \sum_{i=0}^{n_x}\sum_{j=0}^{n_y}\sum_{k=0}^{n_z} B_{ijk}\, x^{i+l^v_{x=0}}\, y^{j+l^v_{y=0}}\, z^{k+l^v_{z=0}}\, (a-x)^{l^v_{x=a}}\, (b-y)^{l^v_{y=b}}\, (c-z)^{l^v_{z=c}} \\
W(x,\,y,\,z) &= \sum_{i=0}^{n_x}\sum_{j=0}^{n_y}\sum_{k=0}^{n_z} C_{ijk}\, x^{i+l^w_{x=0}}\, y^{j+l^w_{y=0}}\, z^{k+l^w_{z=0}}\, (a-x)^{l^w_{x=a}}\, (b-y)^{l^w_{y=b}}\, (c-z)^{l^w_{z=c}}
\end{aligned}
\qquad (3)
$$

where the indices $l^u_{x=0}, l^v_{x=0}, l^w_{x=0}, l^u_{x=a}, l^v_{x=a}, l^w_{x=a}$ etc depend on the constraints placed on the displacements U, V and W on the six faces of the solid shell (x=0, x=a, y=0, y=b, z=0 and z=c).

The maximum strain energy V_{max} can be expressed straightforwardly in terms of the normal and shear strains:

$$
V_{\max} = \frac{1}{2}\iiint \left[\lambda \left(\varepsilon_{xx} + \varepsilon_{yy} + \varepsilon_{zz}\right)^2 + 2G\left(\varepsilon_{xx}^2 + \varepsilon_{yy}^2 + \varepsilon_{zz}^2\right) + G\left(\gamma_{xy}^2 + \gamma_{yz}^2 + \gamma_{zx}^2\right) \right] \mathrm{dx\ dy\ dz}
\qquad (4)
$$

where $\lambda = \dfrac{\nu E}{(1+\nu)(1-2\nu)}$ and $G = \dfrac{E}{2(1+\nu)}$ are the Lame parameters.

By substituting equations (2) into equation (4), V_{max} can be expressed in terms of the middle surface displacements integrated over the volume of the solid.

The maximum kinetic energy T_{max} can also be expressed in terms of the middle surface displacements as

$$
T_{\max} = \left(\frac{\rho w^2}{2}\right)\iiint \left(U^2 + V^2 + W^2\right) dx\ \mathrm{dy\ dz}
\qquad (5)
$$

where ρ is the density of the element material and the integration is again performed over the volume of the solid.

Finally, the trial function series (3) are substituted for U, V and W in the maximum kinetic and strain energy expressions and the Lagrangian functional $L_{max} = (T_{max} - V_{max})$ is minimized with respect to the undetermined linear coefficients A_{ijk}, B_{ijk} and C_{ijk} to give a homogeneous linear system of equations. Eigenvalues and corresponding eigenvectors can then be obtained by a number of methods (in the present paper using subspace iteration).

Enforcement of continuity conditions to model shells of revolution.

The approach described above can be used to treat cylindrically shaped closed shells by creating a fictitious seam or cut in the shell along the axial length. The shell can then be unwrapped into the Cartesian coordinate system so long as continuity of geometric boundary conditions along the cut edge is ensured. For a closed cylindrical shell with axial coordinate in the y direction and with $x = 2\Pi R_x = a$, these continuity conditions are given by $U_{x=0}=U_{x=a}$, $V_{x=0}=V_{x=a}$ and $W_{x=0}=W_{x=a}$. In the present paper the continuity conditions are satisfied by using connecting springs of very high stiffness value K_u, K_v and K_w to enforce continuity of displacement U, V and W at x = 0 and x = a. The strain energy contribution V_u, V_v and V_w of these springs is then simply added to the strain energy V_{max} of the shell

$$V_u = \frac{1}{2} K_u \iiint \left(U_{x=0} - U_{x=a}\right)^2 dydz, V_v = \frac{1}{2} K_v \iiint \left(V_{x=0} - V_{x=a}\right)^2 dydz, and V_w = \frac{1}{2} K_w \iiint \left(W_{x=0} - W_{x=a}\right)^2 dydz \quad (6)$$

Results and discussion:

In Table 1, the lowest seven non-dimensional frequency parameters $\Omega = \omega R \sqrt{(\rho / G)}$ are given for a cylinder of thickness to radius ratio $c/R_x = 0.3$ and thickness to length ratio c/b = 0.3 with shear diaphragm boundary conditions on each end as obtained by modelling: (i) a quarter of the cylinder as a 90° shell panel and applying all distinct combinations of symmetry and anti-symmetry conditions at x = 0 and at $x = \Pi/2\ R_x = a$; (ii) half the cylinder as a 180° shell panel applying all combinations of symmetry and anti-symmetry conditions at x = 0 and at $x = \Pi\ R_x = a$; (iii) a full cylinder ensuring continuity of displacements at x = 0 and at $x = 2\Pi\ R_x = a$ by using artificial springs (penalty functions) with very high stiffness parameters. Results obtained using the present approach are compared with those obtained by Armenakas et al.[3] using an exact solution and agreement can be seen to be excellent.

Table 1: Frequency Parameters Ω for a cylindrical shell for c / R_x = c/b = 0.3 and with $\nu = 0.3$.

		MODE NUMBER							
	$N_x x N_y x N_z$	1	2	3	4	5	6	7	8
90°	6x6x3	1.173	1.185	1.247	1.353	1.711	1.948	2.094	2.176
	9x9x6	1.162	1.179	1.242	1.333	1.673	1.948	2.094	2.120
180°	8x8x5	1.162	1.179	1.242	1.333	1.714	1.948	2.094	2.223
	12x4x4	1.162	1.179	1.242	1.333	1.674	1.948	2.094	
360°	12x4x4	1.162	1.179	1.242	1.341	1.923	1.948	2.094	*
	14x4x4	1.162	1.179	1.242	1.334	1.715	1.948	2.094	*
	Exact	1.161	1.173	1.232	1.340	1.690	1.948	2.085	2.146#
%Error*		0.1	0.5	0.8	-0.5	-1.0	0.0	0.4	-1.2

* Error = 100 x ([9x9x6 result 90°] - Exact) / Exact

\# Results obtained by Soldatos et al. [4]

References:

1. W. Soedel, *Vibrations of Shells and Plates*, Marcel Dekker, New York, USA (1981).
2. A. Leissa, *Vibration of Shells*, Acoustical Society of America, USA, 1993.
3. A.E Armenakas, D.C. Gazia and G Herrmann, *Free Vibrations of Circular Cylindrical Shells*, Pergamon Press, Oxford, 1969.
4. K.P. Soldatos and V.P. Hadjigeorgiou, *Three-Dimensional Solution of the Free Vibration Problem of Homogeneous Isotropic Shells and Panels*, Journal of Sound and Vibration, **137** (3), 369-384, 1990.